課程博士

2022 年 3 月

関西大学審査学位論文

Relationship between Polymer Network Structure and Thermomechanical Properties of Epoxy Thermosets Containing Schiff-base Mesogenic Moieties

シッフ塩基含有メソゲン骨格エポキシ樹脂の ネットワーク構造と熱機械物性の相関性

理工学研究科　総合理工学専攻

高分子化学

19D6013　太田　早紀

博士論文要旨

理工学研究科総合理工学専攻
高分子化学
19D6013
太田　早紀

Relationship between Polymer Network Structure and Thermomechanical Properties of Epoxy Thermosets Containing Schiff-base Mesogenic Moieties

シッフ塩基含有メソゲン骨格エポキシ樹脂のネットワーク構造と熱機械物性の相関性

エポキシ樹脂は、硬化剤や触媒存在下でモノマーの開環付加反応が進行し、三次元ネットワーク構造を形成する。電気絶縁性や接着性に優れるエポキシ樹脂は、半導体封止材、電子部品用接着剤、複合材料のマトリックス樹脂に用いられている。近年、電子機器の高性能化・軽薄化に伴い、機器内部で発生する熱量は著しく増加しているため、周辺部品に使用されるエポキシ樹脂の熱物性の一層の改善が重要な課題となっている。

しかしながら、エポキシ樹脂のガラス転移温度(T_g)はシアネートエステル樹脂やポリイミド樹脂と比較して低いうえ、その熱物性・力学物性は T_g 以上の高温領域で著しく低下する。また、線膨張係数は T_g 以上で一桁以上増加するため、複合材料の界面剥離や反りを引き起こす。このために、次世代電子機器の要求特性を満たした樹脂材料の開発には、エポキシ樹脂の T_g 向上が重要な課題となっている。ネットワークポリマーの T_g 向上には、架橋密度の増加および剛直構造の導入により、ネットワーク鎖のミクロブラウン運動を効率的に抑制する必要がある。更にこの問題の解決手法の一つとして、ガラス状態からゴム状態への明確な転移を示さない T_g-less 材料が注目されている。

また、三次元ネットワーク構造内の不均一性のため、エポキシ樹脂はフォノン散乱が生じやすく、熱伝導率が低い。このために、金属やセラミック等の無機フィラーが充填されるが、熱伝導性の低いマトリックス樹脂が複合材料の熱伝達を阻害することが問題となっている。一方、無機フィラーの高充填化は熱伝導性の改善には有効である反面、密度増加や電気物性・力学物性の低下を引き起こす。したがって、複合材料の高熱伝導化には、エポキシ樹脂自身の熱伝導性の向上が求められている。

分子骨格内にメソゲン基を有するエポキシ樹脂は、メソゲン基の自己組織化により、三次元ネットワーク構造内に秩序性の高い液晶ドメイン構造を形成する。更に、ネットワーク構造に内在する剛直なメソゲン基により、メソゲン骨格エポキシ樹脂は、汎用エポキシ樹脂と比較して、優れた熱伝導性や耐熱性を示す。

本論文は、シッフ塩基含有メソゲン骨格エポキシ樹脂の自己重合性と配列性に基づく、ネットワークポリマーの構造制御により、材料の熱物性を飛躍的に向上させたものである。

本論文の内容は以下の 3 部から構成されている。

(1) メソゲン骨格内に架橋点を導入したネットワークポリマーの構造解析と熱物性評価

(2) 高秩序配列構造を有するネットワークポリマーの構造解析と熱伝導性評価

(3) 複合材料マトリックスの構造解析と高熱伝導材料の創製

(1) メソゲン骨格内に架橋点を導入したネットワークポリマーの構造解析と熱物性評価

第 1 章では、無触媒条件下でシッフ塩基含有メソゲン骨格エポキシの自己重合反応を進行させることで、剛直なメソゲン基に架橋点を導入したネットワーク構造を形成した。その結果、剛直なメソゲン骨格への架橋点導入効果により、ネットワーク鎖のミクロブラウンは効率的に抑制され、300℃以下の高温領域においても明確なガラス転移を示さない T_g-less 挙動が見いだされた。

第 2 章では、イミダゾール潜在性触媒の添加量が自己重合系のネットワーク構造および熱物性に及ぼす影響を検討した。その結果、イミダゾール触媒の少量添加は硬化反応性向上に有効であり、材料の物理的耐熱性の向上を達成した。しかしながら、イミダゾール触媒の過剰添加はメソゲン骨格内への架橋点導入率を低下させ、材料の耐熱性低下を引き起こすことを明らかにした。

第 3 章では、イミダゾール潜在性触媒を併用した場合、硬化温度コントロールにより、同組成硬化物の T_g を約 60℃変化させられることを明らかにした。また、陽電子消滅寿命測定(PALS)および Xe-フラッシュ法により、高温硬化系ではネットワーク鎖の充填密度は低下するものの、その熱伝導率は低温硬化系の 1.3 倍向上することを報告した。

これらの結果は、極めて容易な手法で、エポキシ樹脂の T_g-less 化を達成するとともに、材料の熱物性を意図的に制御可能であること明らかにした。

(2) 高秩序配列構造を有するネットワークポリマーの構造解析と熱伝導性評価

第 4 章では、硬化反応性の異なる 2 種の硬化剤の混合使用により、メソゲン骨格エポキシ樹脂の配列制御が可能であることを明らかにした。最適配合比で調製した硬化物では、液晶ドメインのサイズ拡大および高秩序性スメクチック相構造の形成が確認された。また、Xe-フラッシュ法による熱伝導率測定を行ったところ、最適配合比で調製した硬化物の熱伝導率(0.31 W/(m･K))は、他系(0.27～0.30 (W/(m･K)))と比較してわずかに高い値を示した。更に、周期加熱放射測温法により作成した熱伝導マップは、硬化物中の明瞭な熱伝導分布の存在を示した。これらの熱伝導性評価法から、硬化物中の局所的な低熱伝導領域の存在が材料の飛躍的な高熱伝導化を妨げる可能性を示した。

(3) 複合材料マトリックスの構造解析と高熱伝導材料の創製

第 5 章では、液晶性エポキシ樹脂に MgO フィラーを充填することにより、材料の高熱伝導化を達成した。

第 6 章では、MgO フィラー表面のメソゲン骨格エポキシ吸着層形成が、ネットワーク鎖のスメクチック相形成に寄与していることを明らかにした。得られた硬化物の熱伝導率は、未吸着処理系と比較して約 1.6 倍増加したことから、フィラー表面処理層の最適化により、複合材料の高熱伝導化を達成した。更に、本硬化系は、同フィラー充填量の汎用エポキシ複合材料と比較しても、非常に優れた熱伝導性を示した。

以上

CONTENTS

GENERAL INTRODUCTION

With the rapid development of intelligent electrical devices, heat generation has significantly increased year upon year. Polymer materials are used in various industrial fields because of their excellent processability and lightweight. Epoxy resins are among the most common thermosetting resins and form three-dimensional crosslinking structures when epoxy monomers proceed with the ring-opening addition reaction. Their curing reactions are generally classified into two types. One is additional polymerization with curing agents of active hydrogen compounds, such as amine, phenol, anhydride, and thiol compounds. The other one is anionic/cationic polymerization with catalysts such as tertiary amine and Lewis's acid. Due to their low price, excellent electrical insulating, and adhesive properties, epoxy resins are used as composite materials, particularly semiconductors, IC packaging, and printed circuit boards. Therefore, it has been challenging to improve the epoxy resin's thermal properties for long-term reliability and high-performance of electronic devices.

However, the drawbacks of conventional epoxy resins such as diglycidyl ether of bisphenol A (DGEBA) are their relatively lower glass-transition temperatures (T_gs) of ~200°C than those of cyanate ester resins and polyimide resins. Moreover, the mechanical and thermal properties of network polymers are drastically deteriorated above their T_g. Furthermore, compared with the inorganic fillers, the matrix resins exhibit a substantial increase in their coefficient of thermal expansion (CTE) with increasing temperature. The rubbery CTEs of epoxy resins are more than an order of magnitude greater than their glassy CTEs. These differences in CTEs can cause severe damage, such as cracking and peeling at the filler–matrix interfaces of the composite material.

To overcome these problems, *T_g-less* or high T_g materials have gained much attention recently. "*T_g-less*" refers to an apparent disappearance of a T_g. Specifically, negligible transition behavior is observed between the rubbery region and the glassy region as a result of greatly restraining the micro-Brownian motion of polymer chains. One advantage of the T_g-less materials is their ability to maintain good thermal and mechanical properties over a wide temperature range. Thus far, numerous researchers have reported that the micro-Brownian motion of polymer chains can be greatly restrained by the formation of organic–inorganic hybrids [1-19], although the inorganic components lead to brittleness and poor processability of the materials.

In terms of the molecular design of network polymers, (i) increasing the crosslinking density and (ii) introducing rigid chemical structure and polar functionalities into the epoxy network are practical approaches to inhibit the thermal motion of network polymer chains [20-44]. According to our previous study [31], we synthesized a tetrafunctional mesogenic epoxy monomer (TGEPTA) and prepared a T_g-less epoxy thermoset by curing TGEPTA with 4,4′-diaminodiphenylmethane (DDM) (Figure 1). Moreover, the TGEPTA/DDM system exhibited T_g-less behavior over a broad temperature region below 250°C and maintained good thermal conductivity and tensile properties even at high temperatures. We attributed these features to an effective restriction of the thermal motion of the network polymer chains as a result of the rigid mesogenic moieties in the highly crosslinked network structures. Numerous studies revealed that the orientation of network polymer chains strongly influences the thermal and mechanical properties of mesogenic epoxy resins.

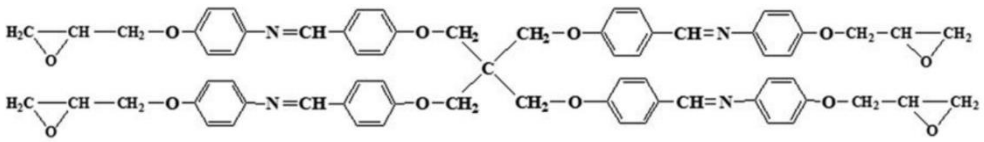

TGEPTA

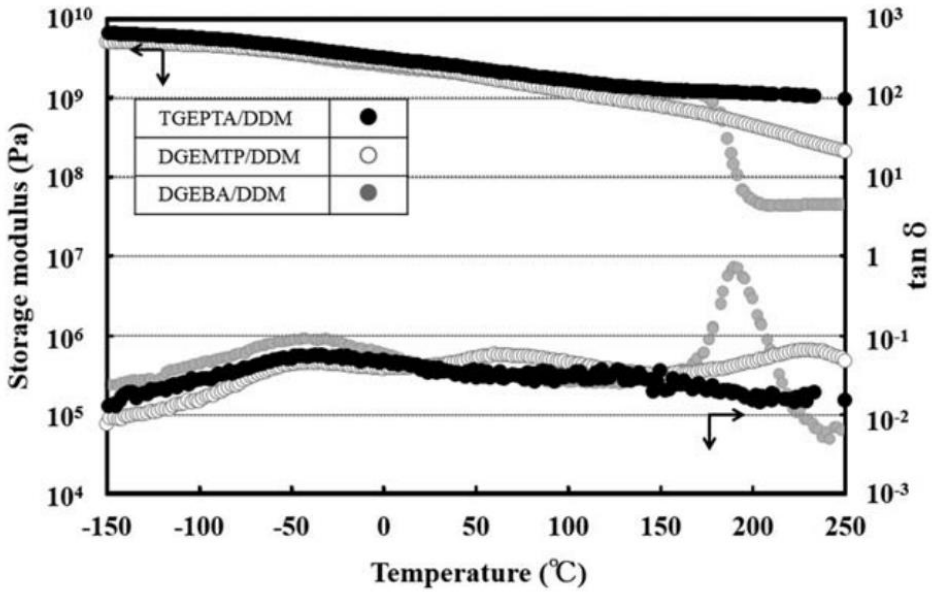

Figure 1 Dynamic mechanical properties of TGEPTA, DGEMTP, and DGEBA/DDM systems.

On the other hand, the thermal conductivity of the conventional epoxy resins (0.1-0.2W/(m・K)) is relatively low since there are many defects in the amorphous structures of networked chains, increasing phonon scattering in the materials. One solution for this problem is the percolation formation of high thermal conductive fillers such as silica, alumina (Al_2O_3), boron nitride (BN), and carbon materials. Moreover, the thermal conductivities of the composite materials are strongly influenced by many factors including the loading contents, shapes, surface-modifications of filler particles [45-68]. Ganguli *et al.* [47] reported that the thermal conductivity of the graphite/epoxy composite significantly increased by the chemical modification using a silane coupling agent (Figure 2). However, a higher filler loading increased a material's density and deteriorated electrical and mechanical properties. In addition, the heat transport in the composite could be inhibited by matrix resin and heat resistance at the filler-matrix interface.

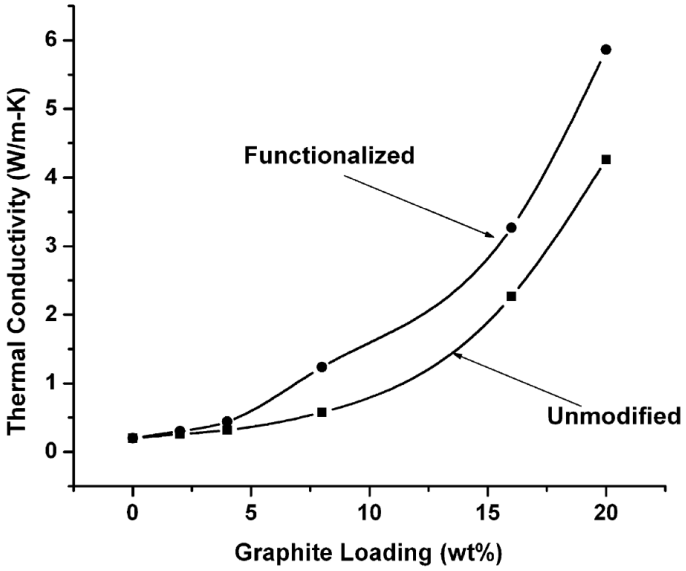

Figure 2 Thermal conductivity plot of the graphite-epoxy composite.

Another solution is improving the instinct thermal conductivity of epoxy resin. Mesogenic moieties are conjugated and rigid structures to form mesophase via the self-assembly of mesogenic moieties under a suitable temperature condition. It is well-known that mesogenic epoxy resins form highly ordered liquid crystalline (LC) domains in the networked polymer chains. Mesogenic epoxy resins also exhibit outstanding performance, such as higher thermal conductivity, higher fracture toughness, and excellent heat

resistance [69-99]. Owing to such excellent thermal conductivity, various inorganic fillers have been dispersed in mesogenic epoxy resins to develop high thermal conductivity composites [100-111]. According to our previous study [100], we controlled the LC phase structures of mesogenic epoxy thermosets by changing temperatures (Figure 3). As a result, it was found that the thermal conductivity of a highly ordered LC epoxy/BN composite was 2.2 W/(m·K) at 30 vol% loading, which was dramatically higher than that of an isotropic system (1.5 W/(m·K)) at the same filler loading (Figure 4).

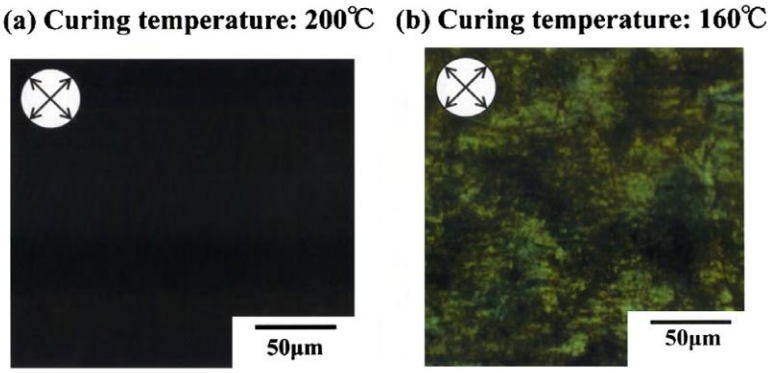

Figure 3 Polarized optical micrographs of the DGETAM/*m*-PDA systems. Curing temperature: (a)200℃ and (b) 160℃.

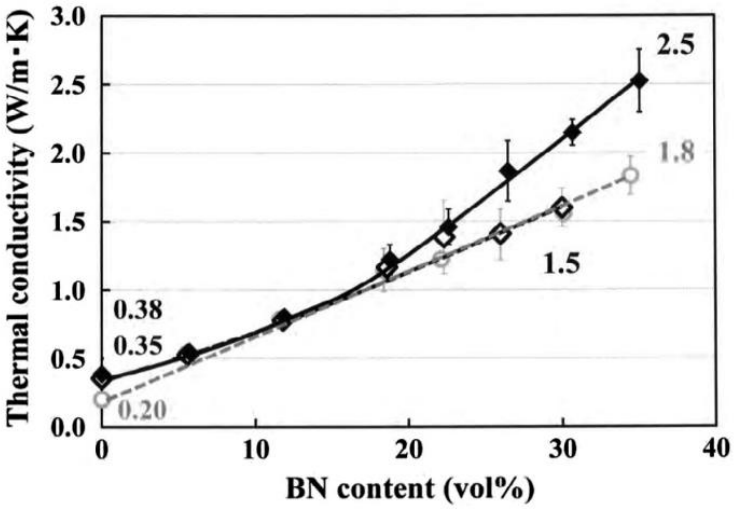

Figure 4 Thermal conductivity of the DGEBA/*m*-PDA/BN composites (○) and DGETAM/*m*-PDA/BN composites ((◇) isotropic, (◆) LC)).

Nevertheless, it is more difficult and complicated to control the LC phase structure of the matrix resin in the presence of inorganic fillers. In general, the self-assembly behavior of LC molecules is strongly affected by interfacial interactions such as hydrogen bonding and dipole–dipole interactions between the filler surface and the mesogenic moieties [112-115]. For instance, Jang *et al.* showed that the formation of the LC phase structure of a mesogenic epoxy resin can be induced by the interfacial interaction of mesogenic moieties with polar functional groups such as the hydroxyl and carbonyl groups on the carbon nanotube surface. In addition, Tanaka *et al.* [115] revealed that the alignment behavior of the mesogenic epoxy network polymer chains strongly depends on the surface free energy of the substrate surface using a Microbeam Small-Angle X-ray Scattering. The results demonstrated that the mesogenic epoxy thermoset formed a homeotropically aligned mono domain-like SmA structure in the vicinity of a substrate with high surface free energy (Figure 5).

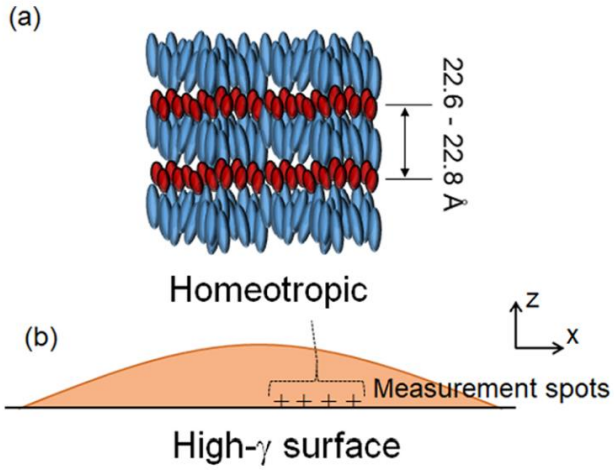

Figure 5 Models of (a) polydomain SmA structure in the vicinity of the G_L substrate and (b) *μ*SAXS measurement spots.

Thus, the series of studies aims to improve the thermal property of epoxy thermosets. To achieve this goal, the studies focused on the characteristics of Schiff base-derived self-polymerization and liquid crystalline (LC) phase formation of mesogenic epoxy resins. In addition, our primary objectives are to demonstrate the structure-property relationship of epoxy thermosets by structural analysis from microscopic to nanoscopic.

A summary of this series of studies about the network structures and thermal properties of Schiff base type mesogenic epoxy resin is as follows;

Part I (Chapter 1, 2, 3) describes the Schiff base-derived self-polymerization and the thermomechanical properties of mesogenic epoxy/imidazole cured systems.

Part II (Chapter 4) describes the LC phase structure and thermal conductivity of mesogenic epoxy resins cured by binary mixed curing agents.

Part III (Chapter 5, 6) describes the application as matrix resin and surface-treatment effect of mesogenic epoxy/magnesium oxide (MgO) composites.

Chapter 1.

Self-polymerization Mechanism and Thermomechanical Properties of Schiff Base Type Mesogenic Epoxy Thermosets

In this chapter, novel glass-transition-temperature-less (T_g-less) epoxy thermosets were developed by a non-catalytic method based on a Schiff base (CH=N)-derived self-polymerization of mesogenic epoxy. The self-polymerization mechanism was verified by differential scanning calorimetry (DSC), Fourier transform infrared spectroscopy (FTIR), and X-ray photoelectron spectroscopy (XPS). It was found that the epoxy–CH=N addition reaction formed a new tertiary amine, introducing a crosslinking point into the rigid mesogenic moiety. Dynamic mechanical analysis (DMA) of the cured system showed a slight α-relaxation in tanδ, and a high storage modulus was maintained at >250°C. Also, no drastic increase in the coefficient of thermal expansion (CTE) related to the glass-transition behavior was observed in this cured system. The DMA and TMA results revealed that such a distinctive crosslinking structure could effectively suppress the thermal motion of networked chains, resulting in T_g-less behavior.

Chapter 2.

Thermomechanical Properties and Network Structures of Schiff Base Type Mesogenic Epoxy Thermosets Cured by Imidazole Catalyst

In this chapter, an imidazole catalyst was used to enhance the self-polymerization reactivity of Schiff base type mesogenic epoxy resin. The structure-property relationship

of the imidazole-cured systems was investigated by DMA, TMA, positron annihilation lifetime spectrometry (PALS). The results suggested that the crosslinking points in the rigid mesogenic moiety could result in T_g-less behavior in the lower imidazole system, similar to the non-imidazole system. By contrast, the higher imidazole content system proceeded with epoxy–imidazole adduct formation rather than CH=N-derived self-polymerization. Consequently, the number of crosslinking points in the rigid mesogenic moiety significantly decreased, deteriorating the thermomechanical properties of final products. Moreover, it is found that the addition of excess imidazole forms the lower-density domain.

Chapter 3.

Glass Transition Temperature and Packing Density of Schiff Base Type Mesogenic Epoxy/Imidazole Systems Cured at Different Temperatures

In this chapter, the effect of curing temperatures on their T_gs and packing densities were investigated by DMA and PALS. Schiff base type mesogenic epoxy resins were cured by the same content of imidazole catalyst at different temperatures. At lower curing temperatures, epoxy mainly proceeds with the imidazole-derived polymerization, forming a highly ordered nematic phase structure via self-assembly of mesogenic moieties. On the other hand, at higher curing temperatures, epoxy could proceed with a CH=N-derived self-polymerization, in addition to the imidazole-derived ones. As a result, this cured system exhibited higher T_g than the lower temperature curing system although it showed relatively lower packing density. This result indicated that the crosslinking points into the rigid mesogenic moiety effectively suppressed network polymer chains' thermal motion.

Chapter 4.

Thermal Conductivity and Liquid Crystalline Phase Structure of Schiff Base Type Mesogenic Epoxy Thermosets Cured by Binary Mixed Curing Agent

In this chapter, Schiff base type mesogenic epoxy resin (DGETAM) was cured by the

binary mixed curing agent with different chemical structures, *m*-phenylenediamine (*m*-PDA) and 4, 4'-bis (4-aminobenzoyloxy) dodecane (12BAB). The optimal composition ratio in binary mixed curing agent to form highly ordered network structure was determined by polarized optical microscopy (POM), X-ray diffractometry (XRD), and a polarized IR mapping measurement. The results revealed that the DGETAM/*m*-PDA/12BAB_20 mol% system forms larger size of LC domain structure with a highly ordered smectic phase. According to the laser flash method, the thermal conductivity of DGETAM/*m*-PDA/12BAB_20 mol% system(0.31 W/(m・K)) is slightly higher compared to those of the other DGETAM and bisphenol A type epoxy (DGEBA) systems (0.27～0.30 (W/(m・K))). However, the thermal conductive map drawn by the periodic heating radiation-temperature measuring method indicated a clear thermal conductivity distribution in the DGETAM/*m*-PDA/12BAB_20 mol% system. These results suggest that the effective phonon conductivity may be suppressed by the locally low thermal conductive regions derived from the amorphous polymer chains, although this cured system formed a highly ordered network structure.

Chapter 5.

Thermal Conductivity and Liquid Crystalline Phase Structure of Schiff Base Type Mesogenic Epoxy/MgO Composites

In this chapter, an MgO filler was incorporated into Schiff base type mesogenic epoxy resin (DGETAM). The thermal conductivity of the DGETAM/MgO composite was 1.41 W/(m·K) at 33 vol% content, which was remarkably higher than the value predicted using Bruggeman's model. To investigate the reason for this significant enhancement of the thermal conductivity in the LC epoxy composites, the LC phase structure of the composite was analyzed by a POM, an XRD and a polarized IR mapping measurement. An XRD analysis indicated the local formation of a highly ordered smectic phase structure, even in the high-loading composite. This result indicated the promotion of the self-assembly of the mesogenic network polymer chains by the MgO filler loading. We considered that this highly ordered structural formation can lead to an increase in the matrix resin's thermal conductivity, which can result in the effective enhancement of the thermal

conductivity in the LC epoxy/MgO composite.

Chapter 6.

The Effect of Filler Surface Treatment on Thermal Conductivity and Liquid Crystalline Phase Structure of Schiff Base Type Mesogenic Epoxy/MgO Composites

In this chapter, mesogenic epoxies were adsorbed onto the surface of an MgO filler treated with an amino-silane coupling agent and the epoxy-adsorbed MgO filler was dispersed into the LC epoxy matrix resin to develop a high thermal conductivity composite. The effect on the interfacial interaction and the free volume of the LC epoxy composite was investigated by XPS, XRD, and PALS. The thermal conductivity of the obtained composite (3.16 W/(m·K)) was remarkably higher than that of the nonadsorbed MgO system (1.93 W/(m·K)) at almost the same content of 44-45 vol%. This significant improvement of the thermal conductivity can be attributed to the highly ordered structural formation that was induced by the π-π interaction effect of the mesogenic moieties between the adsorbed epoxies and the matrix resin.

REFERENCES

1. Q. Hu, E. Marand, *Polymer*, **1999**, 40, 4833-4843
2. L. Matejka, O. Dukh, J. Kolarik, *Polymer*, **2000**, 41, 4, 1449–1459
3. S. Kang, S. II Hong, C. R. Choe, M. Park, S. Rim, J. Kim, *Polymer*, **2001**, 42, 3, 879-887
4. G. Z. Li, L. Wang, H. Toghiani, T. L. Daulton, K. Koyama, C. U. Pittman, Jr., *Macromolecules*, **2001**, 34, 25, 8686-8693
5. J. Choi, J. Harcup, A. F. Yee, Q. Zhu, R. M. Laine, *Journal of the American Chemical Society*, **2001**, 123, 46, 11420-11430
6. T. Matsumura, M. Ochi, *Journal of the Society of Rubber Science and Technology, Japan*, **2003**, 76, 9, 329-333
7. M. J. Abad, L. Barral, D. P. Fasce, R. J. J. Williams, *Macromolecules*, **2003**, 36, 9, 3128-3135
8. B. X. Fu, M. Namani, A. Lee, *Polymer*, **2003**, 44, 7739-7747
9. Y. Ni, S. Zheng, K. Nie, *Polymer*, **2004**, 45, 16, 5557-5568
10. J. Choi, A. F. Yee, R. M. Laine, *Macromolecules*, **2004**, 37, 9, 3267-3276
11. F. Xiao, Y. Sun, Y. Xiu, C. P. Wong, *Journal of Applied Polymer Science*, **2007**, 104, 4, 2113-2121
12. L. M. McGrath, R. S. Parnas, S. H. King, J. L. Schroeder, D. A. Fischer, J. L. Lenhart, *Polymer,* **2008**, 49, 999-1014
13. S. Ma, W. Liu, Z. Wang, C. Hu, C. Tang, *Polymer-Plastics Technology and Engineering*, **2010**, 49, 467-473
14. J. S. Jang, J. Varischetti, G. W. Lee, J. Suhr, *Composites: Part A: Applied Science and Manufacturing*, **2011**, 42, 1, 98-103
15. F. Jin, S. Park, *Polymer Degradation and Stability*, **2012**, 97, 11, 2148-2153
16. Y. Ma, L. He, *Materials Chemistry and Physics*, **2017**, 201, 120-129
17. G. Zhu, D. Han, Y. Yuan, F. Chen, Q. Fu, *Chinese Journal of Polymer Science*, **2018**, 36, 1297-1302
18. Y. Kim, H. Chun, S. Park, S. Park, C. H. Oh, *Polymer*, **2018**, 147, 81-94
19. H. Yi, M. Zhang, D. Yao, W. Gong, *Polymer Engineering and Science*, **2021**, 61, 3, 780-792

20. M. Kaji, T. Endo, *Journal of Polymer Science Part A: Polymer Chemistry*, **1999**, 37, 16, 3063-3069
21. C. Wang, M. Lee, *Journal of Applied Polymer Science*, **1999**, 73, 9, 1611-1622
22. M. Kaji, K. Ogami, T. Endo, *Journal of Applied Polymer Science*, **1999**, 72, 7, 953-959
23. M. Kaji, K. Nakahara, T. Endo, *Journal of Applied Polymer Science*, **1999**, 74, 3, 690-698
24. M. Kaji, K. Nakahara, K. Ogami, T. Endo, *Journal of Applied Polymer Science*, **2000**, 75, 4, 528-535
25. X. Su, X. Jing, *Journal of Applied Polymer Science*, **2007**, 106, 737-742
26. G. Pan, Z. Du, C. Zhang, C. Li, X. Yang, H. Li, *Polymer*, **2007**, 48, 13, 3686-3693
27. H. Nishida, H. Ueda, S. Matsuda, H. Kishi, A. Murakami, *Asia-Pacific Journal of Chemical Engineering,* **2007**, 2, 63–69
28. K. Arita, T. Oyama, *Journal of Applied Polymer Science*, **2016**, 133, 17 DOI: 10.1002/app.43339
29. J. Wan, J. Zhao, B. Gan, C. Li, J. Molina-Aldareguia, Y. Zhao, Y. Pan, D. Wang, *ACS Sustainable Chemistry and Engineering*, **2016**, 4, 5, 2869-2880
30. D. Liu, H. Wang, H. Jiang, D. Zhou, *Journal of Applied Polymer Science*, **2016,** 133, 4
31. M. Harada, D. Morioka, M. Ochi, *Journal of Applied Polymer Science*, **2018**, 135, 16, 46181
32. X. Xu, S. Ma, J. Wu, J. Yang, B. Wang, S. Wang, Q. Li, J. Feng, S. You, J. Zhu, *Journal of Materials Chemistry A,* **2019,** 7, 15420-15431
33. Y. Zu, L. Zong, J. Wang, X. Jian, *Polymer*, **2019**, 172, 372-381
34. Y. Tian, Q. Wang, L. Shen, Z. Cui, L. Kou, J. Cheng, J. Zhang, *Chemical Engineering Journal*, **2020**, 123124
35. M. Zhang, X. Miao, J. Fu, F. Bao, X. An, L. He, X. Li, Y. Meng, *Polymer International*, **2020**, 69, 867-875
36. Y. Qi, Z. Weng, K. Zhang, J. Wang, S. Zhang, C. Liu, X. Jian, *Chemical Engineering Journal*, **2020**, 387, 124115
37. X. Chen, J. Hou, Q. Gu, Q. Wang, J. Gao, J. Sun, Q. Fang, *Polymer*, **2020**, 195,

122443

38. X. Xiong, A. Han, R. Ren, J. Wei, P. Chen, *Polymer Testing*, **2020**, 81, 106167
39. W. Xie, S. Huang, D. Tang, S. Liu, J. Zhao, *Chemical Engineering Journal*, **2020**, 394, 123667
40. Y. Qi, Z. Weng, Y. Kou, J. Li, Q. Cao, J. Wang, S. Zhang, X. Jian, *Composites Part B*, **2021**, 214, 108749
41. D. Sivanesan, B. Seo, C. Lim, S. Kim, H. Kim, *Polymer*, **2021**, 220, 123568
42. M. O. Ghallemohamadi, H. Behniafar, *Materials Today Communications*, **2021**, 26, 101984
43. F. Zhang, Y. Li, Z. Weng, T. Zhang, Z. Wang, J. Wang, X. Jian, *Journal of Materials Science*, **2021**, 56, 9079-9092
44. Y. Tian, M. Ke, X. Wang, G. Wu, J. Zhang, J. Cheng, *European Polymer Journal*, **2021**, 147, 110282
45. Y. Xu, D. D. L. Chung, *Composite Interfaces*, 2000, 7, 4, 243-256
46. R. Haggenmueller, C. Guthy, J. R. Lukes, J. E. Fischer, K. I. Winey, *Macromolecules*, **2007**, 40, 2417-2421
47. S. Ganguli, A. K. Roy, D. P. Anderson, *Carbon*, **2008**, 46, 806-817
48. S. Yang, C. M. Ma, C. Teng, Y. Huang, S. Liao, Y. Huang, H. Tien, T. Lee, K. Chiou, *Carbon*, **2010**, 48, 592-603
49. K. Wattanakul, H. Manuspiya, N. Yanumet, *Colloids and Surfaces A: Physicohem, Eng. Aspects*, **2010**, 369, 203-210
50. K. Yang, M. Gu, *Composites: Part A*, **2010**, 41, 215-221
51. Y. Zhang, S. Xiao, Q. Wang, S. Liu, Z. Qiao, Z. Chi, J. Xu, J. Economy, *Journal of Materials Chemistry*, **2011**, 21, 14563
52. C. Teng, C. M. Ma, C. Lu, S. Yang, S. Lee, M. Hsiao, M. Yen, K. Chiou, T. Lee, *Carbon*, **2011**, 49, 5107-5116
53. H. Im, J. Kim, *Carbon*, **2012**, 50, 5429-5440
54. U. S. Jeong, Y. J. Lee, D. G. Shin, H. M. Lim, S. Y. Mun, W. T. Kwon, S. R. Kim, Y. H. Kim, *Transactions on Electrical and Electronic Materials*, **2015**, 16, 351–354
55. F. Luo, K. Wu, S. Wang, M. Lu, *Composites Science and Technology*, **2017,** 144, 100-106

56. D. Kang, N. Kim, M. Park, C. Nah, J. S. Kim, C. Lee, Y. Kim, C. B. Kim, M. Goh, K. Jeong, *ACS Applied Materials and Interfaces*, **2018**, 10, 315-3159
57. B. M. Maira, K. Tekuchi, P. Chammingkwan, M. Terano, T. Taniike, *Composites Science and Technology*, **2018**, 165, 259-265
58. Y. Guo, J. He, H. Wang, Z. Su, Q. Qu, R. Tian, X. Tian, X. Li, *Polymer Composites*, **2019**, 40, 1600-1611
59. V. Mai, D. Lee, J. Park, D. Lee, *Polymers*, **2019**, 11, 579
60. C. Liu, T. Zhang, F. Daneshvar, S. Feng, Z. Zhu, M. Kotaki. M. Mullins, H. Sue, *Polymer*, **2020**, 207, 122913
61. Z. Liu, X. Liu, *ACS Applied Materials and Interfaces*, **2020**, 12, 6503-6515
62. D. Liang, P. Ren, F. Ren, Y. Jin, J. Wang, C. Feng, Q. Duan, *Journal of Polymer Research*, **2020**, 27, 212
63. J. Wie, M. Kim, J. Kim, *Applied Surface Science*, **2020**, 529, 147091
64. F. Su, L. Zhang, C. Li, *Polymer Composites*, **2021**, 42, 3562-3571
65. W. A. L. Sanchez, C. Huang, J. Chen, Y. Soong, Y. Chan, K. Chiou, T. Lee, C. Cheng, C. Chiu, *Polymers*, **2021**, 13, 147
66. J. M. Kim, D. Jung, L. S. Kim, M. Kim, S. Jeong, S. Lee, S. Chang, J. Y. Cho, S. H. Kim, J. Y. Park, K. Choi, G. Yi, K. M. Nam, G. Lee, *Materials Today Communications*, **2021**, 27, 102230
67. Y. Hu, C. Chen, Y. Wen, Z. Xue, X. Zhou, D. Shi, G. Hu, X. Xie, *Composites Science and Technology*, **2021**, 209, 108760
68. Y. Liang, B. Liu, B. Zhang, Z. Liu, W. Liu, *International Journal of Heat and Mass Transfer*, **2021**, 164, 120533
69. A. Shiota, C. K. Ober, *Journal of Polymer Science: Part A: Polymer Chemistry*, **1996**, 34, 1291-1303
70. Q. Lin, A. F. Yee, H. J. Sue, J. D. Earls, R. E. Hefner, Jr., J*ournal of Polymer Science: Part B : Polymer Physics*, **1997,** 35, 2363-2378
71. M. Ochi, Y. Shimizu, N. Nakanishi, Y. Murata, *Journal of Polymer Science: Part B: Polymer Physics*, **1997**, 35, 397-405
72. C. Ortiz, R. Kim, E. Rodighiero, C. K. Ober, E. J. Kramer, *Macromolecules*, **1998**, 31, 4074-4088

73. J. Y. Lee, J. Jang, *Journal of Polymer Science: Part A: Polymer Chemistry*, **1999**. 37, 419-425
74. W. F. A. Su, K. C. Chen, S. Y. Tseng, *Journal of Applied Polymer Science*, **2000**, 78, 446-451
75. D. Ribera, A. Mantecon, A. Serra, *Journal of Polymer Science: Part A: Polymer Chemistry*, **2002**, 40, 3916-3926
76. M. Ochi, H. Takashima, *Polymer*, **2001**, 42, 2379-2385
77. M. Akatsuka, Y. Takezawa, *Journal of Applied Polymer Science*, **2003**, 89, 2464-2467
78. M. Harada, M. Ochi, M. Tobita, T. Kimura, T. Ishigaki, N. Shimoyama, H. Aoki, *Journal of Polymer Science: Part B: Polymer Physics*, **2003**, 41, 1739-1743
79. P. Castell, A. Serra, M. Galia, *Journal of Polymer Science: Part A: Polymer Chemistry*, **2004**, 42, 3631-3643
80. S. R. Lu, X. W. Yang, C. Wei, *Plastics, Rubber and Composites*, **2010**, 39, 2
81. S. Song, H. Katagi, Y. Takezawa, *Polymer*, **2012**, 53, 4489-4492
82. H. Guo, J. Zheng, J. Gan, L. Liang, K. Wu, M. Lu, *J. Mater. Sci.: Mater. Electron*, **2016**, 27, 2754–2759
83. F. Chen, Y. Cong, B. Zhang, *Liquid Crystals*, **2016**, 43, 8, 1100-1109
84. S. Kawamoto, H. Fujiwara, S. Nishimura, *International Journal of Hydrogen Energy*, **2016**, 41, 7500-7510
85. M. Harada, N. Okamoto, M. Ochi, *Journal of Applied Polymer Science*, **2016**, 133, 47
86. Y. Kim, H. Yeo, N. You, S. G. Jang, S. Ahn, K. Jeong, S. H. Lee, M. Goh, *Polymer Chemistry*, **2017**, 8, 2806-2814
87. A. M. Islam, H. Lim, N. You, S. Ahn, M. Goh, J. R. Hahn, H. Yeo, *ACS Macro Letters*, **2018**, 7, 1180-1185
88. M. Harada, M. Hirotani, M. Ochi, *Journal of Applied Polymer Science*, **2019**, 136, 34
89. Z. Lin, Y. Cong, B, Zhang, H. Huang, *Liquid Crystals*, **2019**, 46, 10
90. I. Jeong, C. B. Kim, D. Kang, K. Jeong, S. G. Jang, N. You, S. Ahn, D. Lee, M. Goh, *Journal of Polymer Science: Part A: Polymer Chemistry*, **2019**, 57, 708-715

91. Q. Zhang, G. Chen, K. Wu, J. Shi, L. Liang, M. Lu, *Journal of Applied Polymer Science*, **2020**, 137, 38
92. G. Lv, E. Jensen, C. M. Evans, D. G. Cahill, *ACS Applied Polymer Materials*, **2021**, 3, 4430-4435
93. Y. Lin, S. L. Hsu, T. Ho, L. Jheng, Y. Hsiao, *Journal of Polymer Research*, **2021**, 28
94. A. Olamilekan, H. Yeo, *ACS Applied Polymer Materials*, **2021**, 3, 4147-4155
95. M. S. Windberger, E. Dimitriou, S. Rendl, K. Wewerka, F. Wiesbrock, *Polymers,* **2021**, 13, 65
96. M. Harada, Y. Yokoyama, M. Ochi, *High Performance Polymers*, **2021**, 33, 1, 3-11
97. M. Harada, Y. Kosuke, *Journal of Applied Polymer Science*, **2021**, 138, 25, 50593
98. N. Tang, S. Tanaka, Y. Takezawa, K. Kanie, *Journal of Applied Polymer Science*, **2021**, 138, 47
99. X. Yang, X. Zhong, J. Gu, *Journal of Materials Science and Technology*, **2021**, 68, 209-215
100. M. Harada, N. Hamaura, M. Ochi, Y. Agari, *Composites: Part B*, **2013**, 55, 306-313
101. H. Guo, M. Lu, L. Lianh, J. Zheng, Y. Zhang, Y. Li, Z. Li, C. Yang, *Journal of Applied Polymer Science*, **2014**, 131, 12
102. T. Giang, J. Kim, *Journal of Industrial and Engineering Chemistry*, **2015**, 30, 77-84
103. F. Luo, K. Wu, H. Guo, Q. Zhao, M. Lu, *Composites Science and Technology*, **2016**, 132, 1-8
104. F. Luo, K. Wu, H. Guo, Q. Zhao, M. Lu, *Polymer International*, **2016**, 66, 1, 98-107
105. F. Luo, K. Wu, X. Huang, W. Hu, M. Lu, *Industrial and Engineering Chemistry Research*, **2017**, 56, 489-494
106. S. Tanaka, F. Hojo, Y. Takezawa, K. Kanie, A. Muramatsu, *Polymer-Plastics Technology and Engineering*, **2018**, 57, 269-275
107. S. Tanaka, F. Hojo, Y. Takezawa, K. Kanie, A. Muramatsu, *ACS Omega*, **2018**, 3, 3562−3570
108. S. Ota, K. Yamaguchi, M. Harada, *Journal of network polymer, Japan*, **2019**, 40, 278-286
109. G. Chen, Q. Zhang, Z. Hu, S. Wang, K. Wu, J. Shi, L. Liang, M. Lu, *Journal of Macromolecular Science, Part A : Pure and Applied Chemistry*, **2019**, 5, 56, 484-495

110. F. Luo, P. Yan, H. Li, Q. Qian, B. Huang, Q. Chen, K. Wu, M. Lu, *Composites Science and Technology*, **2020**, 200, 108473

111. Y. Lin, S. Hsu, T. Ho, L. Jheng, Y. Hsiao, *Polymers*, **2020**, 12, 1913

112. T. Uchida, K. Ishikawa, M. Wada, *Molecular Crystals and Liquid Crystals*, **1980**, 60, 37-52

113. J. J. Mallon, P. M. Adams, *Molecular Crystals and Liquid Crystals Science and Technology*, **1992**, 213, 173-186

114. J. Jang, J. Bae, S. Yoon, *Journal of Materials Chemistry*, **2003**, 13, 676-6813

115. S. Tanaka, Y. Takezawa, K. Kanie, A. Muramatsu, *ACS Omega*, **2020**, 5, 33, 20792–20799

Part I

Thermomechanical Properties of Epoxy Thermosets by Introducing Crosslinking Points into Rigid Mesogenic Moiety via Schiff Base-derived Self-polymerization

Chapter 1.

Self-polymerization Mechanism and Thermomechanical Properties of Schiff Base Type Mesogenic Epoxy Thermosets

I-1-1. INTRODUCTION

Recently, T_g-less materials have gained tremendous attention, aiming to improve the physical heat resistance of network polymer materials. One advantage of the T_g-less materials is their ability to maintain good thermal and mechanical properties over a wide temperature range. Therefore, T_g-less epoxy materials should be developed to ensure the long-term reliability and high performance of electronic devices. Thus far, numerous researchers have reported that the micro-Brownian motion of polymer chains can be greatly restrained by the formation of organic–inorganic hybrids [1-6], although the inorganic components lead to brittleness and poor processability of the materials. On the other hand, numerous studies have been conducted to improve the thermal properties of epoxy resins by incorporating various rigid structures or increasing crosslinking densities [7-15]. According to our previous study [16], a tetrafunctional mesogenic epoxy monomer (TGEPTA) was synthesized and cured with 4,4′-diaminodiphenylmethane (DDM) to a high-heat-resistant epoxy thermoset. Moreover, the TGEPTA/DDM system exhibited T_g-less behavior over a broad temperature region below 250°C and maintained good thermal conductivity and tensile properties even at high temperatures. We attributed these features to an effective restriction of the thermal motion of the network polymer chains as a result of the rigid mesogenic moieties in the highly crosslinked network structures.

Mormann *et al.* [17, 18] were the first to report that a Schiff base (CH=N)-containing mesogenic epoxy could proceed via self-polymerization in the absence of an initiator. Lee *et al.* [19] proposed a self-polymerization mechanism in which (i) the self-polymerization is triggered by nucleophilic addition of a CH=N group to an epoxy group, followed by (ii) the obtained alkoxide reacting with another epoxy group to induce anionic polymerization. However, Lee *et al.* [19] provided no experimental evidence for this self-polymerization mechanism from a chemical structural perspective; thus, further

investigation is needed. In addition, most of the previous related studies have focused only on the curing behavior; little attention has been devoted to the network structure and properties of thermosets obtained by this CH=N-derived self-polymerization.

Thus, in this chapter, we verified the CH=N-derived self-polymerization mechanism of mesogenic epoxy resin on the basis of differential scanning calorimetry (DSC), Fourier transform infrared (FTIR) spectroscopy, and X-ray photoelectron spectroscopy (XPS) analyses. In addition, we attempted to develop a new class of T_g-less epoxy thermoset using this CH=N-derived polymerization. We expected this polymerization to form crosslinking points in the rigid mesogenic moiety and to effectively suppress the chain thermal motion.

I-1-2. EXPERIMENTAL

I-1-2-1. Synthesis method of diglycidyl ether of terephthalylidene-bis-(4-amino-3-methylphenol) (DGETAM)

Diglycidyl ether of terephthalylidene-bis-(4-amino-3-methylphenol) (DGETAM) was synthesized based on our previous paper [20]. As the first step, terephthalaldehyde (40 g, 0.30 mol, Sigma-Aldrich Co.), 4-amino-3-methyl-phenol (73 g, 0.60 mol, Fujifilm Wako Pure Chemical Co., Ltd.), and zinc chloride (Fujifilm Wako Pure Chemical Co., Ltd.) as a catalyst were dissolved in 600 ml of EtOH. The solution was stirred for 2 h under a reflux condition to proceed with a dehydration-condensation reaction between amine and aldehyde groups. After cooling at 8°C for 12 h, the yellow precipitation was collected by filtration and washed with EtOH (50 mL × 7 times). Finally, the obtained product was dried under vacuum pressure at 100°C for 2 h. The first step product was yellow powder (83 g, 0.24 mol), and the yield was 80%.

As the second step, the first step product (80 g, 0.23 mol), an excess amount of 1-chloro-2, 3-epoxypropane (255 g, 2.76 mol, Fujifilm Wako Pure Chemical Co., Ltd.), and a tetra-n-butylammonium chloride (Sigma-Aldrich Co.) as a catalyst were dissolved in 90 mL of DMSO and stirred at 80ºC for 1 h. Subsequently, a 50% aqueous NaOH (15 g, 0.38 mol) solution was slowly added at 80ºC for 0.5 h, and the obtained mixture was stirred at 80°C for 3 h to complete the ring closure reaction of epoxy groups. After cooling at 8°C for 12 h, the yellow precipitation was collected by filtration. Next, the crude

product was recrystallized from 450 mL of chloroform. Finally, the obtained product was dried under vacuum pressure at 100°C for 3 h. The DGETAM was yellow powder (60 g, 0.13 mol), and the yield was 57%. The chemical structure of DGETAM was confirmed by ^{1}H-NMR and FT-IR spectroscopy.

^{1}H-NMR ($CDCl_3$) : 2.61 ppm (s, 6H, methyl). 2.84 ppm (m, 4H, epoxy CH_2), 3.37 ppm (m, 2H, epoxy CH), 4.10 ppm (m, 4H, ether CH_2), 6.79 ppm (d, 4H, aromatic), 6.99 ppm (d, 2H, aromatic), 7.99 ppm (s, 4H, aromatic), 8.43 ppm (s, 2H, CH=N)

IR (KBr) : 1620 cm^{-1} (C=N, imine), 1100 cm^{-1} (C-O, ether), 910 cm^{-1} (C-O, epoxy)

The transition temperature of DGETAM was measured using a differential scanning calorimeter (DSC; DSC7020, Seiko Instruments Inc.) at heating rate of 5°C/min. As a result, the DGETAM exhibited a nematic phase between 170°C and 212°C: C 170 N 212 I.

I-1-2-2. Curing materials

The liquid crystalline (LC) epoxy (DGETAM; C 170 N 212, Mw = 456) was synthesized in-house.

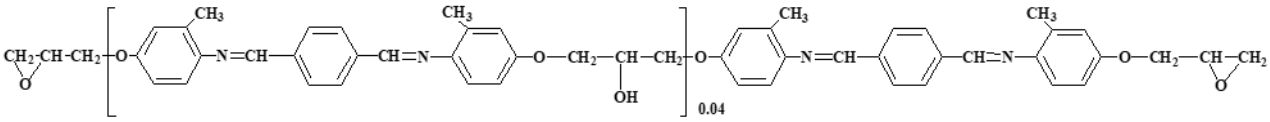

Diglycidyl ether of bisphenol A (DGEBA; JER 828EL, Mw = 370, epoxy equivalent: 185 g/eq.) was available from Mitsubishi Chemical Co., Ltd.

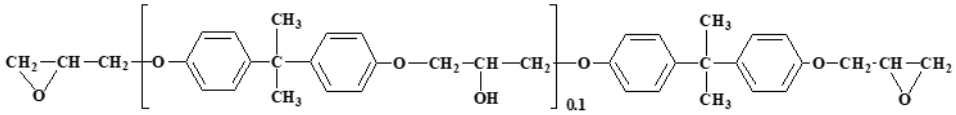

1-(2-Cyanoethyl)-2-undecylimidazole (CEUZ, Mw = 275, m.p. 49-54°C) was purchased from Tokyo Chemical Industry Co., Ltd.

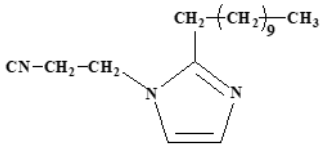

2-Ethyl-4-methylimidazole (2E4MZ, Mw = 110, m.p. 40 ℃, b.p. 164 ℃) was purchased from Fujifilm Wako Pure Chemical Co. All materials were used without further purification.

I-1-2-3. Curing method of DGETAM systems

DGETAM (1.20 g, 2.63 mmol) in an aluminum cup (25×35×15 mm^3) completely melted on a heating plate at 190-200°C for 5 min. Next, it was degassed under a vacuum for 5 min to remove the physically absorbed water and the residual solvent used in the synthesis of DGETAM. Finally, it was cured in an oven at 220°C for 1 h and gradually cooled to ambient temperature. The obtained sample was 25×35 mm^2 with a thickness of about 0.8 mm.

I-1-2-4. Curing method of DGEBA/2E4MZ_3 phr systems

DGEBA in an aluminum cup (45×45×25 mm^3) was degassed under a vacuum at 130°C for 10 min. Subsequently, DGEBA (8.0 g, 21.6 mmol) was mixed with 3 phr 2E4MZ (0.24 g, 2.18 mmol)) and stirred at 130°C for 1 min. Finally, it was cured in an oven at 130°C for 2h + 180°C for 2 h + 210°C for 1 h and gradually cooled. The obtained sample was 45×45 mm^2 with a thickness of about 3 mm.

I-1-2-5. Measurement and analysis

Thermal behaviors of epoxy monomers were identified using a differential scanning calorimeter (DSC; DSC7020, Seiko Instruments Inc.) from 50°C to 320°C at a heating rate of 5°C/min. The sample (about 3 mg) was filled into an aluminum pan.

The phase transition behavior of epoxy monomers was observed using polarized optical microscopy under crossed Nicols (POM; BX53 LED-33P-OC, Olympus Corp.) equipped with a hot stage (TPC-2000; ULVAC) from 50°C to 250°C at a heating rate of 5°C/min.

The chemical structure of cured systems was investigated using a Fourier transform infrared spectroscopy (FTIR; Spectrum 100, Perkin-Elmer Inc.). The sample was incorporated into a KBr pellet (Merck) and molded by a tableting machine (Shimadzu Corp.). The resolution of the IR spectrum was 4 cm^{-1}, and the spectra were collected after 32 scans for each sample. The conversion of the epoxy group was estimated from the reduction rate of the peak area at 910 cm^{-1}. Here, the peak area at 1600 cm^{-1} assigned to the aromatic ring was used as an internal standard.

The gelation degree of the cured system was roughly evaluated by the solubility

test. The sample (about 5 mg) was immersed in 10 mL of THF as a solvent at room temperature.

The molecular weight distribution was analyzed by gel permeation chromatography (GPC, LC20AD, Shimadzu Corp.) with THF as the eluent at 40°C using a refractive index detector (RID-20A, Shimadzu Corp.). The sample (about 5 mg) was completely dissolved in 10 mL of THF.

The chemical structure of the cured system was investigated using an X-ray photoelectron spectroscopy (XPS; ESCA-3400HSE, Shimadzu Corp.). The XPS spectra were measured using MgKα radiation generated at 10 kV and 15 mA. The step energy of the XPS spectrum was 0.05 eV, and the spectra were collected after 64 scans for each sample. All samples were fixed on a sample stage using carbon tape. The disk-shaped sample of the uncured DGETAMs was molded by a tableting machine (Shimadzu Co.) and, the thickness was about 1 mm, which is thick enough to avoid the effect of the carbon tape. The surface of the cured system was polished with sandpaper and a buff polishing machine to obtain a flat, smooth surface. Here, the C1s spectra at 285 eV corresponding to hydrocarbons were used to reference for the energy calibration. The XPS spectra were analyzed by Gaussian function and decomposed into corresponding peaks to investigate the chemical shift in detail.

The coefficient of linear thermal expansion (CTE) of the cured system was evaluated by a thermomechanical analyzer (TMA/SS 7100; Seiko Instruments Inc.). A bar-shaped sample (4.0×30.0×0.5 mm^3) was tested in tension mode and loaded 200 mN. The first and second heating conditions were -50°C to 250°C at 5°C/min. The cooling condition was from 250°C to 25°C at 2°C/min. first and second run results were adopted for the DGETAM system, and only second run result were adopted for the DGETAM/CEUZ_1-10 phr systems.

The dynamic mechanical analysis (DMA) of the cured system was conducted using a non-resonance forced vibration viscoelastometer (Rheogel-E4000, UBM Co.). A bar-shaped sample (4.0×30.0×0.4 mm^3) was tested in tension mode. The test condition was -150°C to 300°C at a heating rate of 5°C/min. The vibration frequency and amplitude were adjusted to 10 Hz and ± 5 μm, respectively.

I-1-3. RESULTS AND DISCUSSION

I-1-3-1 Thermal behavior of the DGETAM system

The thermal behaviors of the Schiff base (CH=N)-containing mesogenic epoxy monomer (DGETAM) were characterized by DSC and POM (Figure I-1-1). The endothermic peaks at 170°C and 212°C in the DSC thermogram of DGETAM correspond to the melting and clearing points. The POM observations confirmed the formation of nematic LC Schlieren textures at 190–220°C. However, broad and sharp exothermic peaks were observed at 220–290°C and 290–310°C, respectively. According to the TG-DTA analysis under air (Figure I-1-2), a drastic reduction of the residual weight began at ~320°C. Therefore, the sharp exothermic peak at 290–310°C corresponds to thermal decomposition. As mentioned in the Introduction, Mormann *et al.* [17, 18] reported that the thermal polymerization of various CH=N-containing mesogenic epoxies can occur without any catalysts or curing agents. On the basis of their work, we speculated that the broad exothermic peak at 220–290°C originated from self-polymerization. Nevertheless, Mormann *et al.* [17, 18] focused primarily on the curing behavior in their DSC study and did not examine whether this self-polymerization proceeded in the actual thermosets.

Here, DGETAM was isothermally cured at various temperatures (160–240°C) without any catalysts to investigate the self-polymerization behavior in detail. The epoxy conversion was found to be 60% or less at 160–200°C, whereas it was substantially increased to greater than 90% at 220–240°C. Moreover, the gelation degree of the cured systems was roughly evaluated on the basis of solubility tests (Figure I-1-3). The system cured at 200°C for 1 h (epoxy conversion: 57%) was soluble in THF, although some insoluble substance remained. The system cured at 220°C for 0.5 h (epoxy conversion: 41%) was fully soluble in THF. The gel-permeation chromatogram of the uncured DGETAM showed two peaks related to the epoxy monomer (96%) and the oligomer (4%). In addition to these peaks, the chromatogram of the 220°C, 0.5 h-cured system showed a broad peak at 16–20 min elution time, which we ascribed to high-molecular-weight components. The 220°C, 1 h-cured system (epoxy conversion: 93%) was entirely insoluble in THF, indicating network polymer formation. Consequently, the optimal curing conditions of the DGETAM system were determined to be 220°C and 1 h.

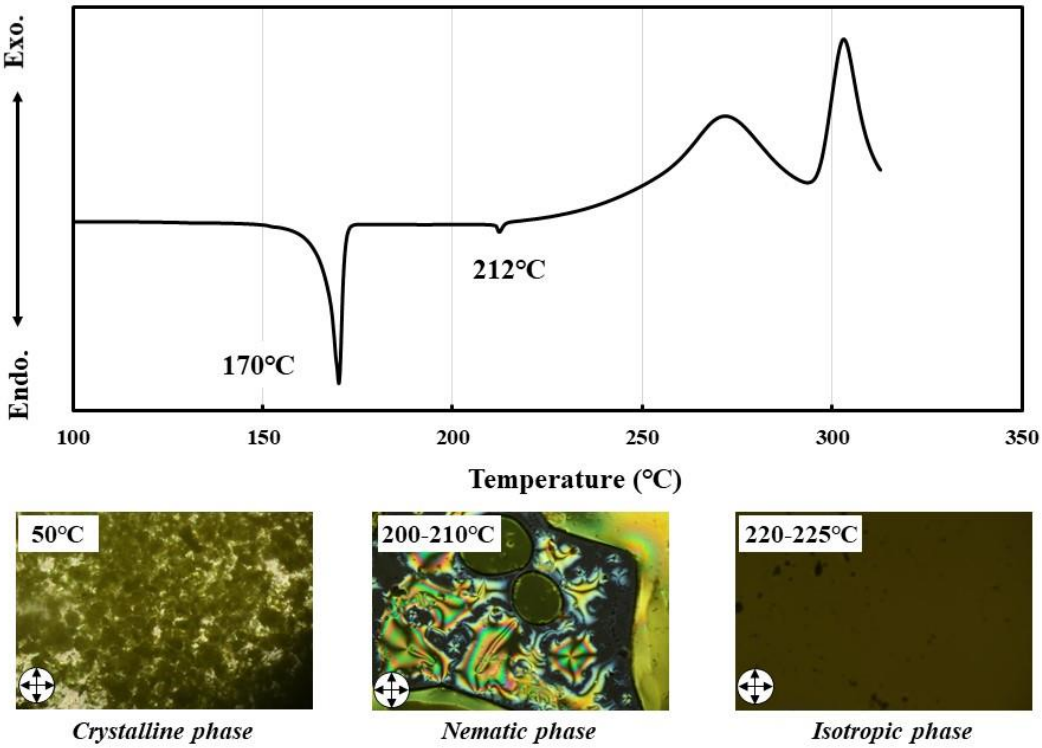

Figure I-1-1 DSC chart and polarized optical micrographs of uncured DGETAM.

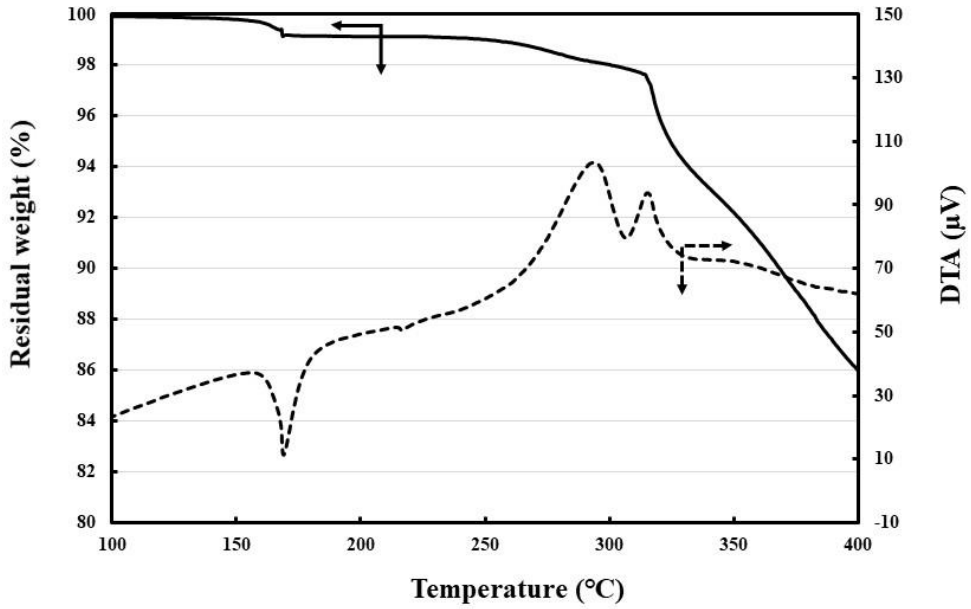

Figure I-1-2 TG-DTA chart of DGETAM (under air atmosphere, heating rate : 10℃/min).

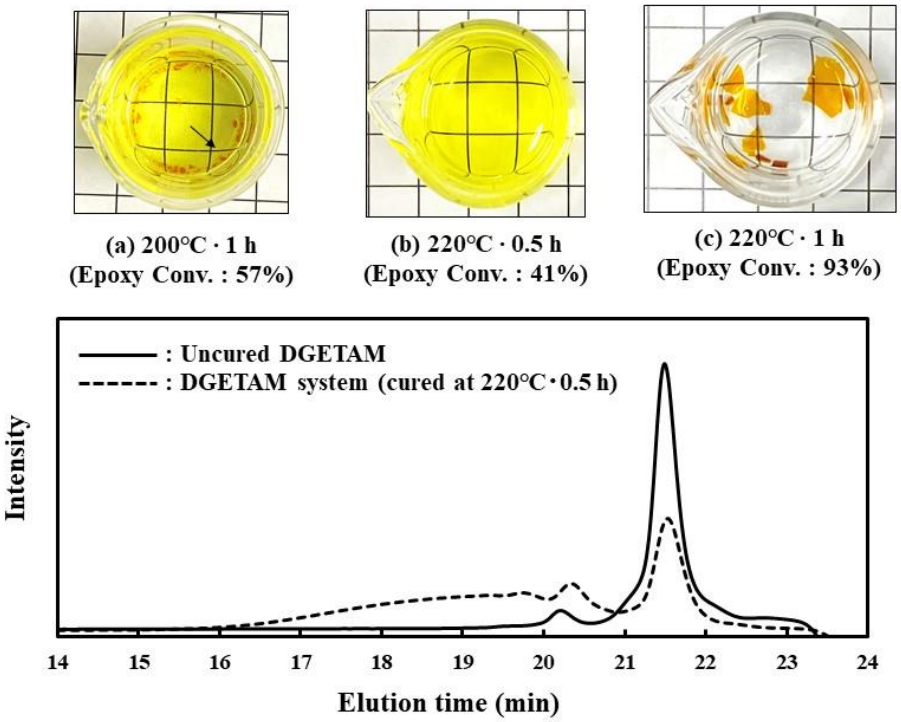

Figure. I-1-3 Optical photographs, conversion of epoxy group and GPC charts of DGETAM systems cured under different curing conditions.

I-1-3-2 Chemical structure of the DGETAM system

The chemical structure of the DGETAM system cured at 220°C for 1 h was studied by FTIR spectroscopy (Figure I-1-4). Compared with the absorption peak of the epoxy group (910 cm^{-1}) in the FTIR spectrum of the uncured DGETAM, that in the spectrum of the DGETAM system almost disappeared. As shown in Table 1, the epoxy conversion of this system was 93%. In addition, a small peak of a C=O group appeared at 1700 cm^{-1}, implying local thermal degradation of the network polymer chains under a relatively high-temperature curing condition [21-23]. In addition, the spectrum of the DGETAM system showed a broad OH-group peak at 3100–3700 cm^{-1}. More interestingly, after the self-polymerization, the intensity of absorption peak of the CH=N group (1619 cm^{-1}) decreased substantially and a small individual peak of the C–N group (1090 cm^{-1}) in the tertiary amine appeared. However, this C–N peak could not be clearly observed because it was overlapped by other peaks.

XPS analysis was used to investigate the C–N group in the tertiary amine of the

DGETAM system in detail (Figure I-1-5). Compared with the peak in the N1s spectrum of the uncured DGETAM (398.7 eV), that in the N1s spectrum of the DGETAM system appeared at a substantially higher binding energy of 399.7 eV. The obtained N1s spectra were deconvoluted into the peak components of the CH=N group (398.7 eV), the C–N group of the tertiary amine (399.9 eV), and the NH_2 group (401.1 eV) [24]. The binding energy corresponding to the CH=N group (398.7 eV) was determined on the basis of our data for uncured DGETAM. The spectrum of the uncured DGETAM mainly exhibited a single CH=N peak with an area ratio of 85%, whereas that of the DGETAM system contained a small CH=N peak (peak area ratio: 25%) and a substantial C–N peak (peak area ratio: 72%). These results suggest that most of the CH=N groups were consumed, resulting in the formation of a new C–N group.

Both the FT-IR and XPS results are highly consistent with the proposed mechanism of Lee *et al.* [19]. Thus, the following mechanism (Scheme I-1-1) was experimentally confirmed: (i) The initial step involves a nucleophilic addition reaction between the N atom in the CH=N group and the epoxy group. This reaction forms a zwitterion possessing an azomethine cation ($–CH=N^+–$) and an alkoxide ($–O^-$). (ii) The resultant anion reacts with another epoxy group to drive the propagation reaction and form a new active site on another alkoxide. (iii) After the H^+ transfer within the epoxy resins, the tertiary amine and OH groups are formed. There are two CH=N groups for each mesogenic moiety; thus, another CH=N group can also react with the epoxy group.

On the basis of the proposed mechanism, we assumed two types of crosslinking points: One crosslinking point is formed in the rigid mesogenic moiety by the epoxy–CH=N addition reaction. The other is formed between mesogenic moieties by polymerization with an alkoxide. Because of positioning in the rigid mesogenic moiety, we expected the former crosslinking points to suppress the thermal motion of network polymer chains more effectively than the latter regular crosslinking points. Because the CH=N peak in in the FTIR and XPS spectra dramatically changed after the self-polymerization (Figure I-1-4, Figure I-1-5, respectively), the epoxy–CH=N addition reaction proceeded preferentially compared with the polymerization with the alkoxide under this curing temperature.

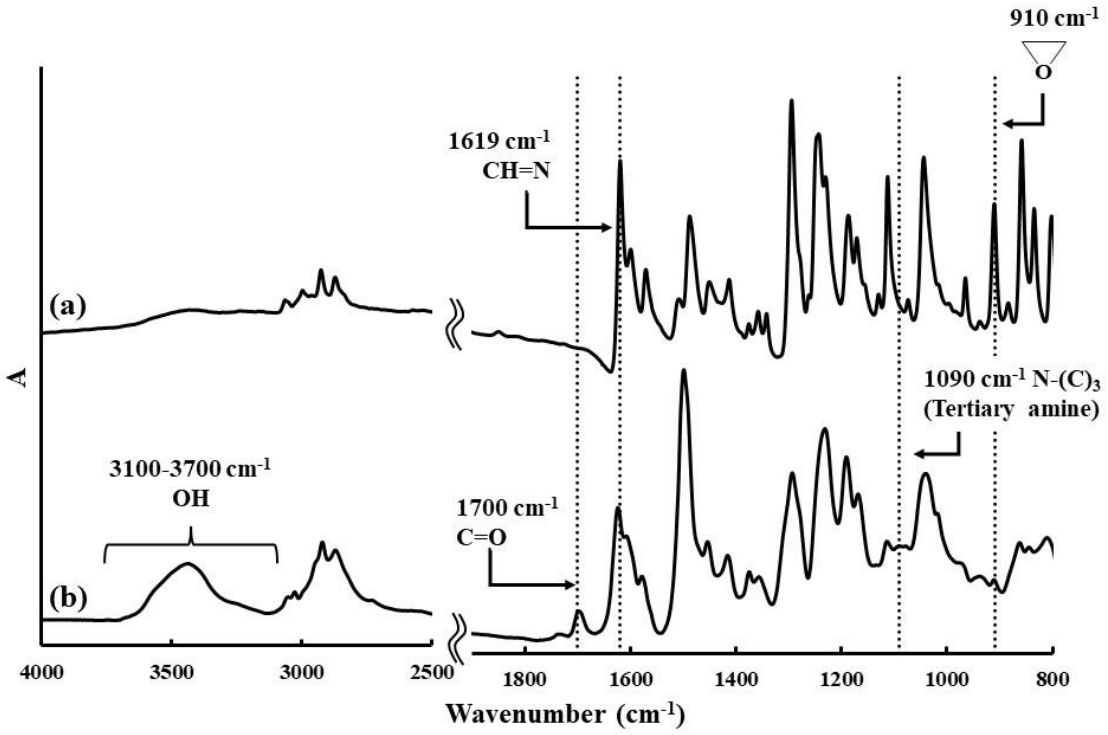

Figure I-1-4 FT-IR spectra of (a) uncured DGETAM and (b) DGETAM system.

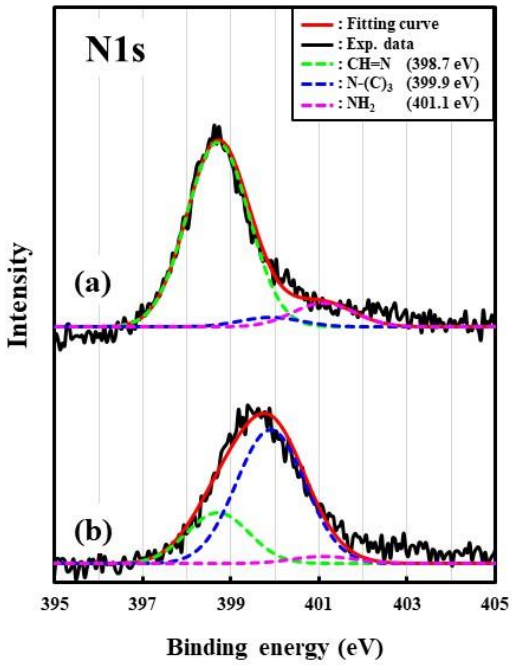

Figure I-1-5 N1s spectra of (a) uncured DGETAM and (b) DGETAM system.

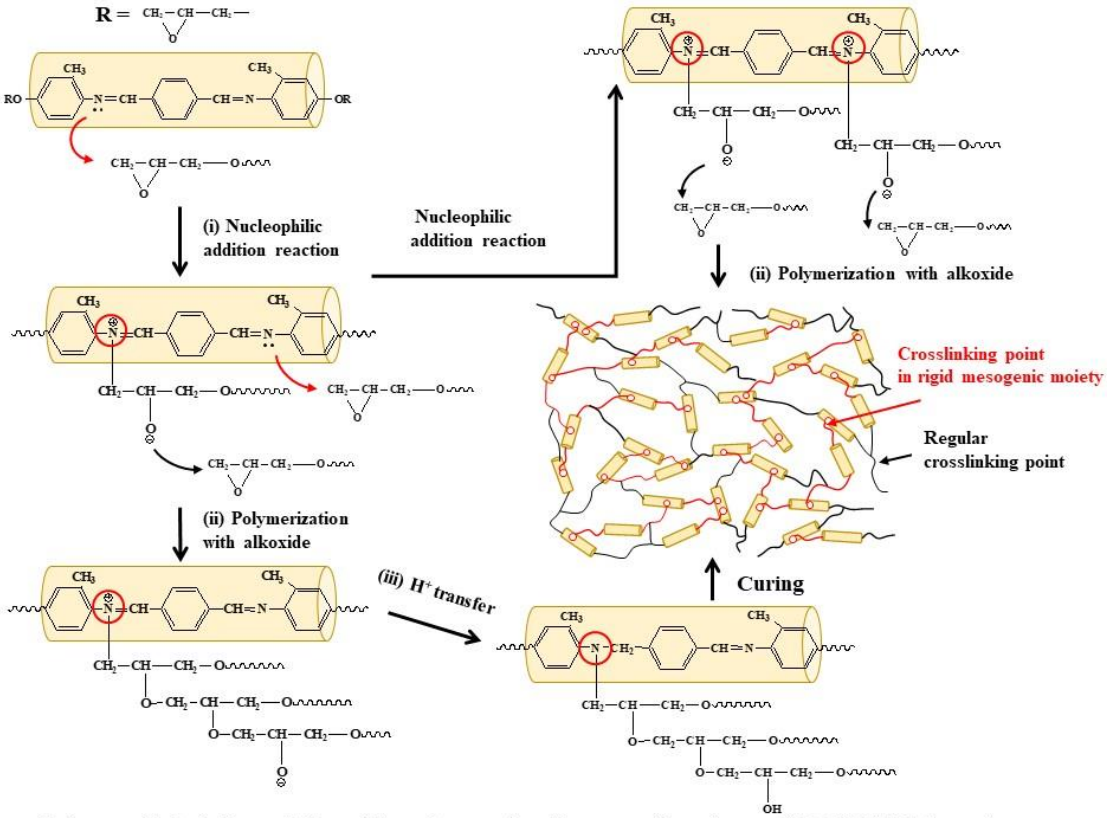

Scheme I-1-1 Possible self-polymerization mechanism of DGETAM system.

I-1-3-3 Thermomechanical properties of the DGETAM systems

The temperature dependence of the CTE of the DGETAM systems was evaluated by TMA (Figure I-1-6). In the first run, the CTE drastically increased at ~150°C and then substantially decreased at >200°C. The epoxy conversion of this system was 93% (Table 1), whereas the absorption peak of the epoxy group (910 cm^{-1}) completely disappeared after the first run (Supporting Information Figure S2). Accordingly, the uncured epoxies underwent post-curing during the heating process of the first run, which suppressed the thermal expansion of the whole network structure. At the same time, the absorption peaks of the C=O group (1700 cm^{-1}) and the C=C group (1630–1660 cm^{-1}) remarkably increased in intensity after the first run. These data indicate that the post-curing and the further thermal decomposition of the network polymer chains occurred simultaneously during the first-run heating. By contrast, the CTE for the second run gradually increased over a wide temperature range. This CTE phenomenon indicates T_g-less behavior. This behavior is attributed to the crosslinking points in the rigid mesogenic moieties strongly

restraining the thermal expansion of the networked chains (Figure I-1-7).

The dynamic mechanical properties of the cured systems were studied by DMA (Figure I-1-8). Here, a bisphenol-A-type epoxy (DGEBA) system cured with an imidazole catalyst (2E4MZ) was used as an exemplar network polymer for comparison. In the DMA thermogram of the DGEBA/2E4MZ system, the storage modulus sharply decreased at ~150°C and the T_g of 174°C was confirmed from the tanδ peak. During the first run of the DGETAM system, the storage modulus substantially decreased at ~160°C and then gradually increased at >220°C. The DMA thermogram of the DGETAM system also showed a broad and intense tanδ peak at 150–290°C. Similar to the behavior observed in the TMA results (Figure 5), this behavior is attributed to the post-curing of unreacted epoxies. By contrast, the second-run results showed only a slight reduction in the storage modulus at >150°C and the storage modulus value was consistently higher than that of the DGEBA/2E4MZ system. These results are attributed to the crosslinking points in the rigid mesogenic moiety (Schene I-1-1). Moreover, the peak height of the α-relaxation behavior became lower and broader than that in the first run because the increase of the crosslinking density effectively inhibited the micro-Brownian motion of the network polymer chains. Given the aforementioned results, such T_g-less materials can be achieved by the crosslinking-point formation in the rigid mesogenic moiety if the CH=N-derived self-polymerization entirely proceeded.

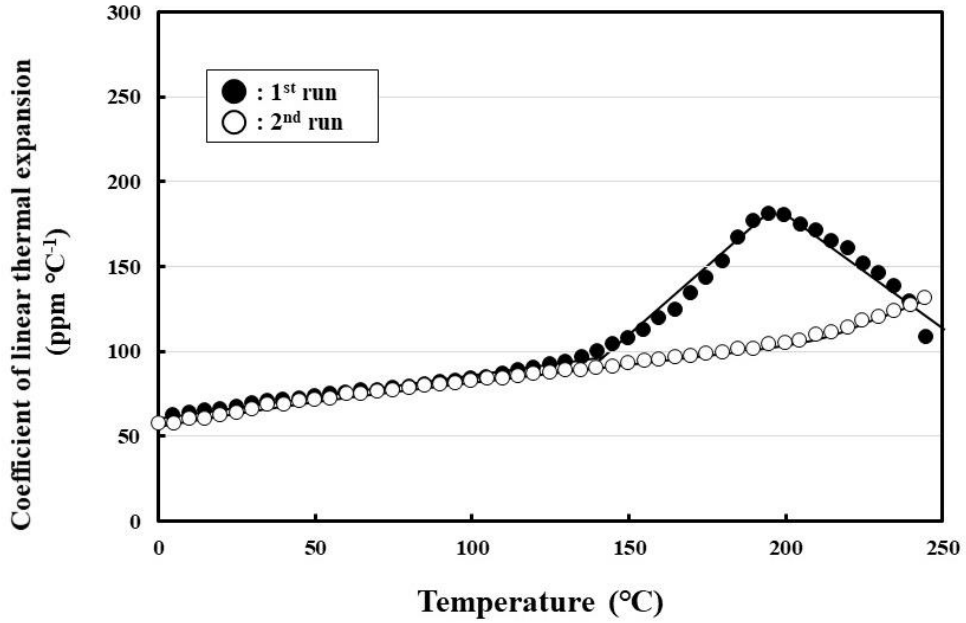

Figure I-1-6 Temperature-dependency of coefficient of linear thermal expansion (CTE) of DGETAM system (1st run and 2nd run).

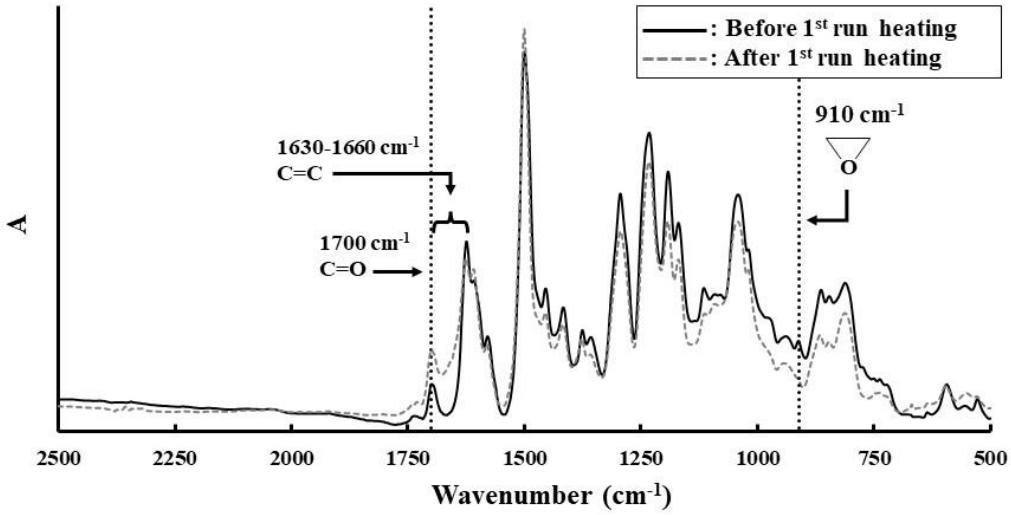

Figure I-1-7 FT-IR spectra of DGETAM system (before and after 1st run heating of TMA).

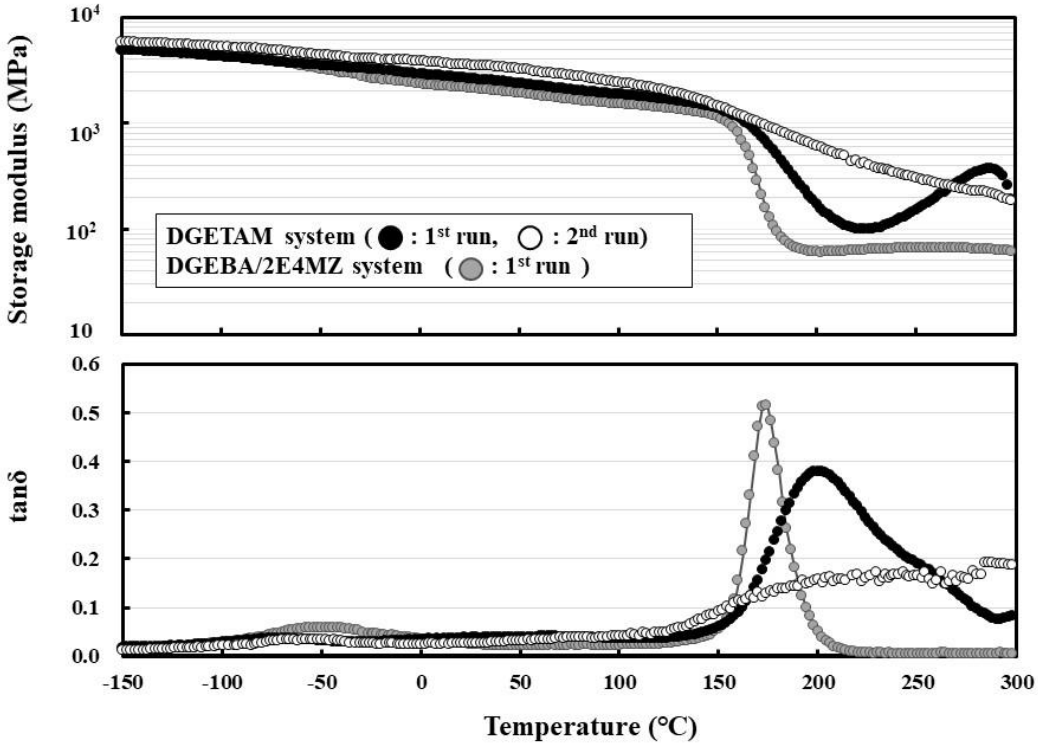

Figure I-1-8 Dynamic mechanical properties of DGETAM system (1st run and 2nd run) and DGEBA/2E4MZ system (1st run).

I-1-4. CONCLUSIONS

In this chapter, novel T_g-less epoxy materials were successfully prepared by a Schiff base (CH=N)-derived self-polymerization of mesogenic epoxy. The self-polymerization mechanism was experimentally verified by DSC, FTIR, and XPS analyses. The epoxy–CH=N addition reaction produced a new tertiary amine, forming a crosslinking point in the rigid mesogenic moiety. The DMA and TMA results indicated that such a distinctive crosslinking structure could effectively suppress the micro-Brownian motion of the network polymer chains.

I-1-5. REFERENCES

1. T. Matsumura, M. Ochi, *Journal of the Society of Rubber Science and Technology*, Japan, **2003**, 76, 9, 329-333
2. L. Matejka, O. Dukh, J. Kolarik, *Polymer*, **2000**, 41,1449–1459
3. Q. Hu, E. Marand, *Polymer*, **1999**, 4833-4843
4. J. S. Jang, J. Varischetti, G. W. Lee, J. Suhr, *Composites: Part A*, **2011**, 42, 98-103
5. F. L. Jin, A. J. Park, *Polymer Degradation and Stability*, **2012**, 97, 2148-2153
6. Y. J. Kim, H. Chun, S. Y. Park, S. J. Park, C. H. Oh, *Polymer*, **2018**, 147, 81-94
7. M. Kaji, T. Endo, *Journal of Polymer Science Part A: Polymer Chemistry*, **1999**, 37, 3063-3069
8. C. S. Wang, M. C. Lee, *Journal of Applied Polymer Science*, **1999**, 73, 1611-1622
9. G. Pan, Z. Du, C. Zhang, C. Li, X. Yang, H. Li, *Polymer*, **2007**, 48, 3686-3693
10. K. Arita, T. Oyama, *Journal of Applied Polymer Science*, **2016**, 133, DOI: 10.1002/app.43339
11. M. Kaji, K. Ogami, T. Endo, *Journal of Applied Polymer Science*, **1999**, 72, 953-959
12. M. Kaji, K. Nakahara, T. Endo, *Journal of Applied Polymer Science*, **1999**, 74, 690-698
13. M. Kaji, K. Nakahara, K. Ogami, T. Endo, *Journal of Applied Polymer Science*, **2000**, 75, 528-535
14. X. Su, X. Jing, *Journal of Applied Polymer Science*, **2007**, 106, 737-742
15. J. Wan, J. Zhao, B. Gan, C. Li, J. M. Aldareguia, Y. Zhao, Y. T. Pan, D. Wang, *ACS Sustainable Chem. Eng.*, **2016**, 4, 2869−2880.
16. M. Harada, D. Morioka, M. Ochi, *Journal of Applied Polymer Science*, **2018**, DOI: 10.1002/app.46181
17. W. Mormann, M. Brocher, *Polymer,* **1998**, 40, 193-198
18. W. Mormann, M. Brocher, *Macromolar Chemistry and Physics*, **1998**, 199, 1935-1938
19. J. Lee, Y. W. Song, M. J. Shim, *Journal of Industrial and Engineering Chemistry.* **2004**, 10, 4, 601-607
20. M. Harada, M. Ochi, M. Tobita, T. Kimura, T. Ishigaki, N. Shimoyama, H. Aoki, *Journal of Polymer Science: Part B: Polymer Physics*, **2004**, 42, 758-765

21. S. G. Hong, *Polymer Degradation and Stability*, **1995**, 48, 211-218
22. B. Mailhot, S. M. Therias, M. Ouahioune, J. Gardette, *Macromolecular Chemistry and Physics*, **2005**, 206, 575-584
23. Y. Zahra, F. Djouani, B. Fayolle, M. Kuntz, J. Verdu, *Progress in Organic Coatings*, **2014**, 77, 380-38
24. A. Yuan, H. Lei, F. Xi, J. Liu, L. Qin, Z. Chen, X. Dong, *Journal of Colloid and Interface Science*, **2019**, 548, 56-65

Chapter 2.

Thermomechanical Properties and Network Structures of Schiff Base Type Mesogenic Epoxy Thermosets Cured by Imidazole Catalyst

I-2-1. INTRODUCTION

Mesogenic epoxy resins have recently attracted tremendous attention for their unique and distinct properties. Due to their rigid and bulky chemical structure, mesogenic epoxy resins exhibit higher glass transition temperatures (T_g) and excellent thermal conductivity compared to those of conventional epoxy resins. According to our previous study [1], a tetrafunctional mesogenic epoxy monomer (TGEPTA) was synthesized and cured with 4,4′-diaminodiphenylmethane (DDM). Moreover, the TGEPTA/DDM system exhibited T_g-less behavior over a broad temperature region below 250°C and maintained good thermal conductivity and tensile properties even at high temperatures. We attributed these features to an effective restriction of the thermal motion of the network polymer chains as a result of the rigid mesogenic moieties in the highly crosslinked network structures. Also, we previously investigated the CH=N-derived self-polymerization mechanism of mesogenic epoxy resin and revealed that the crosslinking points in the rigid mesogenic moiety and to effectively suppress the chain thermal motion.

In this chapter, an imidazole catalyst was used to enhance the self-polymerization reactivity of Schiff base type mesogenic epoxy resin. The structure-property relationship of the imidazole-cured systems was investigated by DMA, TMA, positron annihilation lifetime spectrometry (PALS).

I-2-2. EXPERIMENTAL

I-2-2-1. Curing materials

The liquid crystalline (LC) epoxy (DGETAM; C 170 N 212, Mw = 456) was synthesized in-house.

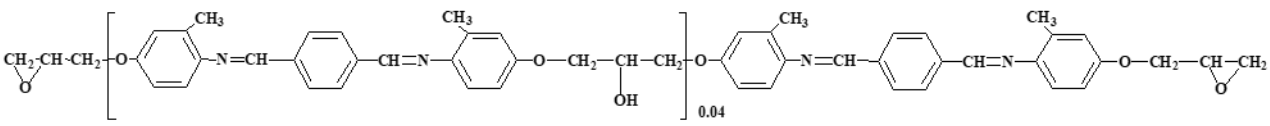

1-(2-Cyanoethyl)-2-undecylimidazole (CEUZ, Mw = 275, m.p. 49-54°C) was

purchased from Tokyo Chemical Industry Co., Ltd. All materials were used without further purification.

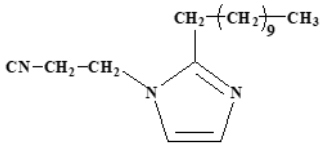

I-2-2-2. Curing method of DGETAM systems

DGETAM (1.20 g, 2.63 mmol) in an aluminum cup (25×35×15 mm^3) completely melted on a heating plate at 190-200°C for 5 min. Next, it was degassed under a vacuum for 5 min to remove the physically absorbed water and the residual solvent used in the synthesis of DGETAM. Finally, it was cured in an oven at 220°C for 1 h and gradually cooled to ambient temperature. The obtained sample was 25×35 mm^2 with a thickness of about 0.8 mm.

I-2-2-3. Curing method of DGETAM/CEUZ_1-10 phr systems

Similar to the DGETAM system above, DGETAM was completely melted at 190-200°C for 5 min and degassed for 5 min. Subsequently, DGETAM (1.20 g, 2.63 mmol) was mixed with 1-10 phr CEUZ (0.012-0.120 g, 0.0436-0.436 mmol)) and stirred at 220-230°C for 1 min. Finally, it was cured in an oven at 220°C for 1 h and gradually cooled. The obtained sample was 25×35 mm^2 with a thickness of about 0.8 mm.

I-2-2-4. Measurement and analysis

Curing behaviors of DGETAM system and DGETAM/CEUZ systems were identified using a differential scanning calorimeter (DSC; DSC7020, Seiko Instruments Inc.) from 50°C to 320°C at a heating rate of 5°C/min. The sample (about 3 mg) was filled into an aluminum pan.

The chemical structure of cured systems was investigated using a Fourier transform infrared spectroscopy (FTIR; Spectrum 100, Perkin-Elmer Inc.). The sample was incorporated into a KBr pellet (Merck) and molded by a tableting machine (Shimadzu Corp.). The resolution of the IR spectrum was 4 cm^{-1}, and the spectra were collected after 32 scans for each sample. The conversion of the epoxy group was estimated from the

reduction rate of the peak area at 910 cm^{-1}. Here, the peak area at 1600 cm^{-1} assigned to the aromatic ring was used as an internal standard.

The thermal decomposition behavior of epoxy monomers and cured systems was studied by thermogravimetric analysis (TGA; TG/DTA 6200, Seiko Instruments Inc.). The test condition was under N_2 atmosphere (gas flow rate: about 350 mL/min) from 100°C to 600°C at a heating rate of 25°C/min using an aluminum pan. The sample weight was about 5 mg.

The LC phase structures of DGETAM system and DGETAM/CEUZ systems was observed using polarized optical microscopy under crossed Nicols (POM; BX53 LED-33P-OC, Olympus Corp.). The sample was polished with sandpaper and a buff polishing machine to prepare a film of approximately 30 μm in thickness.

The chemical structure of cured systems was investigated using a Fourier transform infrared spectroscopy (FTIR; Spectrum 100, Perkin-Elmer Inc.). The sample was incorporated into a KBr pellet (Merck) and molded by a tableting machine (Shimadzu Corp.). The resolution of the IR spectrum was 4 cm^{-1}, and the spectra were collected after 32 scans for each sample. The conversion of the epoxy group was estimated from the reduction rate of the peak area at 910 cm^{-1}. Here, the peak area at 1600 cm^{-1} assigned to the aromatic ring was used as an internal standard.

The dynamic mechanical analysis (DMA) of the cured system was conducted using a non-resonance forced vibration viscoelastometer (Rheogel-E4000, UBM Co.). A bar-shaped sample (4.0×30.0×0.4 mm^3) was tested in tension mode. The test condition was -150°C to 300°C at a heating rate of 5°C/min. The vibration frequency and amplitude were adjusted to 10 Hz and ± 5 μm, respectively.

The coefficient of linear thermal expansion (CTE) of the cured system was evaluated by a thermomechanical analyzer (TMA/SS 7100; Seiko Instruments Inc.). A bar-shaped sample (4.0×30.0×0.5 mm^3) was tested in tension mode and loaded 200 mN. The first and second heating conditions were -50°C to 250°C at 5°C/min. The cooling condition was from 250°C to 25°C at 2°C/min. Second run result were adopted for the all systems.

The mean free volume of the cured system was studied by positron annihilation lifetime spectroscopy (PALS) using a slow positron beam [2] housed at the National

Institute of Advanced Industrial Science and Technology (AIST). A sample with a size of 20×20×0.4 mm^3 was placed on a ceramic heater covered with a graphite sheet and heated for about 20 min at the corresponding temperature. The temperature was monitored within 1℃ resolutions using a thermocouple attached to the heater and was converted to that of the sample's surface by the calibrated coefficient. Positron irradiation was carried out under vacuum (~10^{-3} Pa). The time resolution was 0.26 ns full width at half-maximum (FWHM), and the incident energy was set at 10 keV, which corresponds to a mean implantation depth of 1.2 μm from the sample's top surface with a material density of 1.2 g/cm^3 measured by a pycnometer method at 21-23°C. The total count for positron annihilation events was 2×10^6 for the positron lifetime spectrum of each sample. All PALS spectra were analyzed using the PALSfit program [3] and decomposed into three lifetime components: τ_1, τ_2, τ_3 ($\tau_1 < \tau_2 < \tau_3$). The long-lived component τ_3 corresponds to the *o*-positronium (*o*-Ps) pick-off annihilation lifetime. The mean free volume radius (R) was estimated using a spherical infinite potential well model (Tao–Eldrup model, (Eq. I-2-1)) [4, 5]:

$$\tau_3 = \frac{1}{2}\left[1 - \frac{R}{R_0} + \frac{1}{2\pi}\sin\left(\frac{2\pi R}{R_0}\right)\right]^{-1} , \qquad \text{Eq. I-2-1}$$

where $R_0 = R + \Delta R$ and ΔR is the thickness of an electron layer in the spherical potential well (ΔR = 0.166 nm).

The mean free volume (V_f) was determined using the equation (Eq. I-2-2):

$$V_f = \frac{4}{3}\pi R^3 , \qquad \text{Eq. I-2-2}$$

I-2-3. RESULTS AND DISCUSSION

I-2-3-1 Curing behavior of DGETAM/CEUZ systems

We used an imidazole catalyst (CEUZ) to improve the curing degree of the DGETAM system by means other than post-curing because it avoids thermal degradation. The CEUZ effect on the curing reaction was studied by DSC (Figure I-2-1). As mentioned in Chapter 1, the DSC thermogram of the DGETAM system showed a broad exothermic peak at 220–290°C, which was assigning to the CH=N-derived self-polymerization. In the DGETAM/CEUZ_1 phr system, this peak shifted to a lower temperature by ~10°C. In addition, this peak temperature decreased substantially with increasing CEUZ content,

implying that the addition of an imidazole catalyst accelerated the CH=N-derived self-polymerization. However, when the CEUZ content was greater than 3 phr, another exothermic peak appeared at 150°C in the DSC thermogram, corresponding to the imidazole-derived polymerization. Other researchers [6-9] have already reported the imidazole-derived polymerization mechanism (Scheme I-2-1), where (i) the pyridine-type N atom serves as an initiator and attacks the epoxy group for the ring-opening reaction, followed by (ii) the newly formed alkoxide functioning as a new active site and undergoing anionic polymerization. That is, the adducts form through (i) the addition reaction, and the three-dimensional network polymer structure subsequently forms via (ii) anionic polymerization. By contrast, the peak area related to the CH=N-derived self-polymerization substantially decreased with increasing CEUZ content and finally disappeared in the DSC thermogram of the DGETAM/CEUZ_10 phr system. This result suggests that this CH=N-derived self-polymerization is less likely to occur at a higher CEUZ content. Meanwhile, the DSC thermograms of all of the systems showed an endothermic peak at 169–172°C, which arose from the melting of the residual solid epoxy, which was not involved in the aforementioned melted imidazole-derived reaction. These peak areas gradually decreased with increasing addition of CEUZ. These data indicate that the amount of unreacted epoxy capable of CH=N-derived self-polymerization decreased with increasing CEUZ content. Consequently, the CH=N and the imidazole-derived self-polymerizations were found to occur competitively and the ratio between these two reactions is dependent on the CEUZ content. The CEUZ-derived reaction preferentially occurs in higher-imidazole systems.

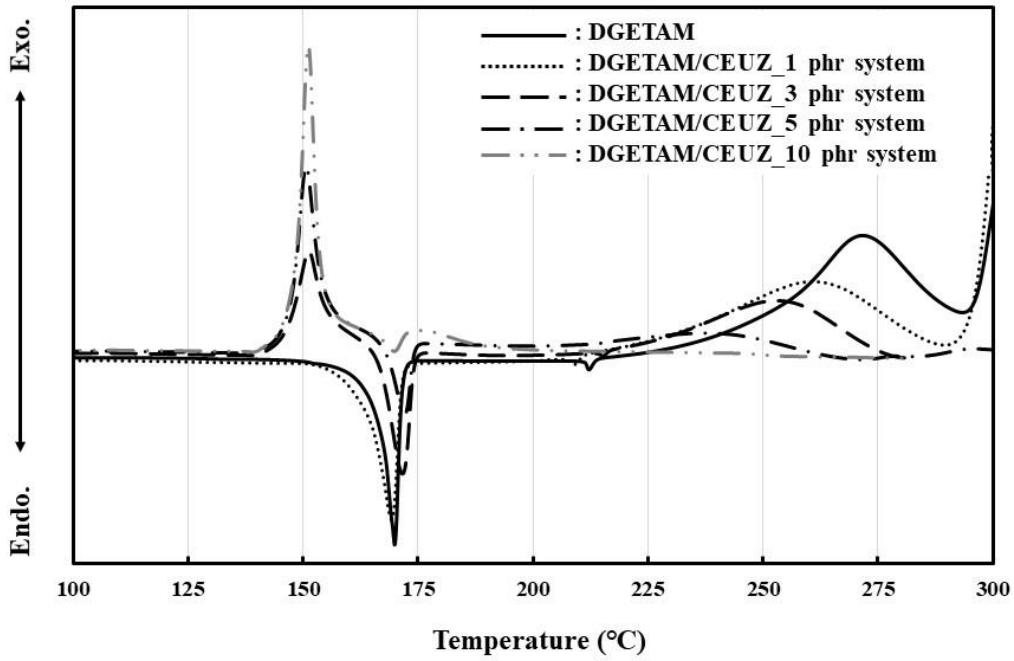

Fig. I-2-1 DSC charts of DGETAM systems with various CEUZ (before curing).

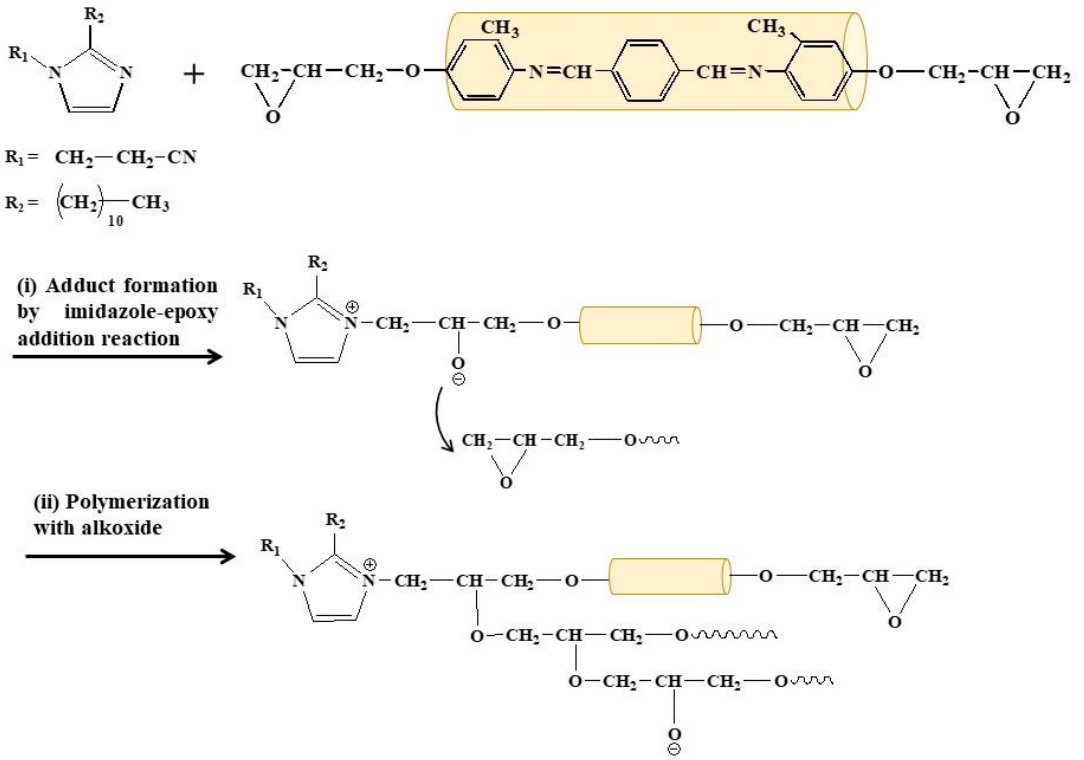

Scheme I-2-1 Possible reaction mechanism of DGETAM/CEUZ system.

I-2-3-2 Chemical structure of the DGETAM/CEUZ systems

The chemical structure of the DGETAM/CEUZ systems was investigated using FTIR spectroscopy (Figure I-2-2). The absorption peak of the epoxy group (910 cm^{-1}) completely disappeared in the spectra of all of the DGETAM/CEUZ_1-10 phr systems, irrespective of the CEUZ content. As summarized in Table I-2-1, the epoxy conversion of the DGETAM/CEUZ systems was higher than that of the DGETAM system (93%). These results suggest that the CEUZ enhanced the curing reactivity of the DGETAM systems. Moreover, similar to the CH=N group peak in the spectrum of the DGETAM system, that in the spectrum of the (b) DGETAM/CEUZ_1 phr system was substantially weaker than the corresponding peaks in the spectra of the DGETAM/CEUZ_3-10 phr systems. In addition, the spectrum of the DGETAM/CEUZ_1 phr system also exhibited a small individual peak associated with the C–N group in the tertiary amine (1090 cm^{-1}). From these results, we considered that the addition of CEUZ_1 phr could generate the C–N group of the tertiary amine via the CH=N–epoxy addition reaction as well as the DGETAM system (Scheme I-1-1), as presented in Chapter 1. Specifically, the DGETAM/CEUZ_1 phr system was assumed to be able to form the crosslinking points in the rigid mesogenic moiety. By contrast, an individual C–N peak was not clearly observed at 1090 cm^{-1} in the DGETAM/CEUZ_3-10 phr systems. The DSC results (Figure I-2-1) reveal that, when the CEUZ content is greater than 3 phr, the imidazole-derived reaction preferentially occurs instead of the CH=N-derived reaction. Therefore, these systems are predicted to contain fewer crosslinking points in their mesogenic moiety compared with the DGETAM system and the DGETAM/CEUZ_1 phr system.

Table I-2-1 shows the 5% weight loss temperature (T_{d5}) of the DGETAM/CEUZ_1-10 phr systems. Notably, the T_{d5} dramatically increased with increasing CEUZ content. In particular, the T_{d5} of the DGETAM/CEUZ_10 phr system (351°C) increased by 20°C compared with that of the DGETAM system (331°C). These results indicate that the addition of CEUZ can suppress the initial thermal degradation of the network polymer chains. This behavior is attributed to the decreased C=N group with higher binding energy (615 kJ/mol) than that of the C–N group (292 kJ/mol) [10].

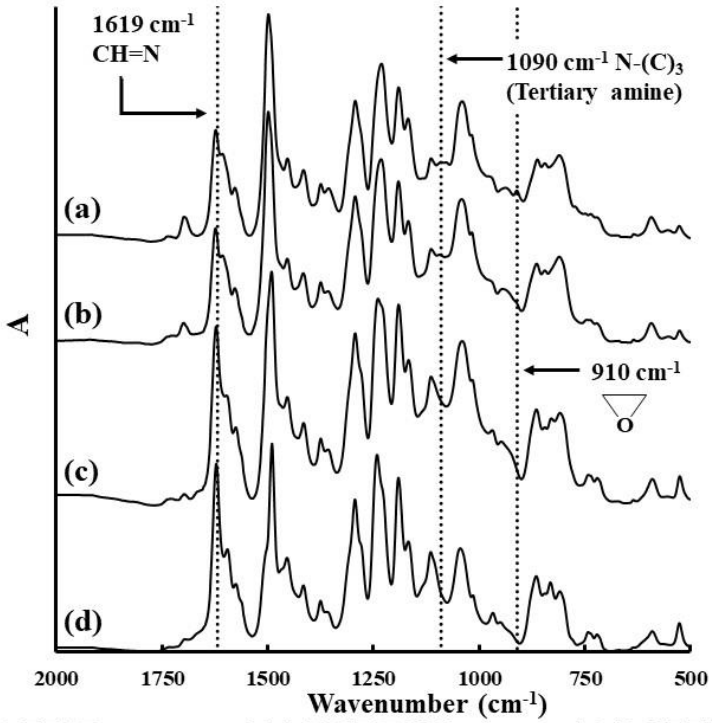

Figure I-2-2 FT-IR spectra of (a) DGETAM system, (b) DGETAM/CEUZ_1 phr system, (c) DGETAM/CEUZ_ 3 phr system, and (d) DGETAM/CEUZ_10 phr system.

Table I-2-1 Conversion of epoxy group and TGA data of cured systems.

Curing system	CEUZ (phr)	Curing condition	Epoxy conversion(%)*1	T_{d5} (°C) *2
DGETAM system	0	220°C · 1 h	93	331
DGETAM/CEUZ_1 phr system	1		99	334
DGETAM/CEUZ_3 phr system	3		98	338
DGETAM/CEUZ_5 phr system	5		99	345
DGETAM/CEUZ_10 phr system	10		99	351

*1 : determined from the reduction rate of FT-IR spectrum of epoxy peak (910 cm^{-1})
*2 : determined by TGA under N_2

I-2-3-3 Network structure of the DGETAM/CEUZ systems

Optical photographs of the DGETAM systems with various CEUZ contents (0–10 phr) are shown in Figure I-2-3. All the systems exhibited a red–brown appearance; however, the transparency remarkably decreased with increasing CEUZ content. This result indicates that substantial CEUZ addition could induce the formation of phase separation structures. In addition, the POM images indicate an enlargement of the birefringence area in the systems with greater CEUZ contents. A large number of small bright dotted patterns were dispersed in the whole observation area of the DGETAM/CEUZ_10 phr system. This observation suggests the partial self-assembly of the mesogenic moieties, which led to the highly stacked LC domain in the network structure. In general, for the imidazole-derived curing, the epoxy–imidazole adduct forms prior to the anionic polymerization. Therefore, more epoxy groups participate in the initial addition reaction with the imidazole compound because of the excess imidazole content. Accordingly, this imidazole–epoxy adduct formation could cause the highly stacked LC domains in systems with a high CEUZ content.

The density of the cured systems at 21-23°C is shown in Table I-2-2. In systems with a CEUZ content lower than 3 phr, no substantial difference was observed in the density. By contrast, the density gradually decreased when the CEUZ content was greater than 5 phr. Notably, the density of the DGETAM/CEUZ_10 phr system was lower by 2% than that of the DGETAM system, even though this system formed the highly stacked LC domains. This result implies that the DGETAM/CEUZ_10 phr system had a network structure with a distribution of packing densities. At high CEUZ contents, more epoxy groups could be consumed by the process of forming the imidazole–epoxy adduct; consequently, fewer epoxies were involved in the etherification crosslinking reaction. Therefore, the density of the surrounding area around the highly stacked LC domains could decrease, resulting in a reduction of the material's density.

On the basis of the aforementioned results, we propose a model for the possible network structure of the DGETAM/CEUZ_1 phr system and the DGETAM/CEUZ_10 phr system (Scheme I-2-2). Similar to the DGETAM system, the DETAM/CEUZ_1 phr system mainly contains the crosslinking points in the rigid mesogenic moiety as a result of the CH=N–epoxy addition reaction. By contrast, the DGETAM/CEUZ_10 phr system

contains highly stacked LC domains domain with low crosslinking density.

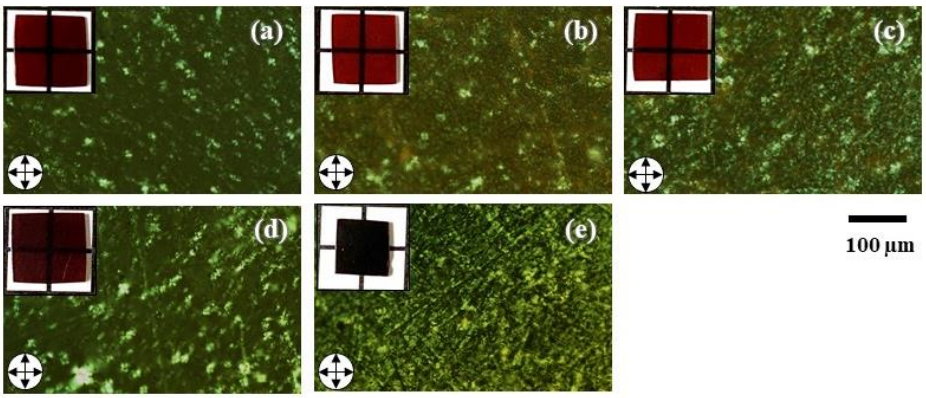

Figure I-2-3 Optical photographs and polarized optical micrographs of (a) DGETAM system, (b) DGETAM/CEUZ_1 phr system, (c) DGETAM/CEUZ_3 phr system, (d) DGETAM/CEUZ_5 phr system, and (e) DGETAM/CEUZ_10 phr system.

Table I-2-2 Density and grass transition temperatures of cured systems.

Curing system	Density at 22°C (g/cm^3)	$T_{g(DMA)}$ (°C)*1	$T_{fg(PALS)}$ (°C)*2	$T_{g(TMA)}$ (°C)*3
DGETAM system	1.208 ± 0.003	204	214	T_g-less
DGETAM/CEUZ_1 phr system	1.203 ± 0.002	254	208	T_g-less
DGETAM/CEUZ_3 phr system	1.201 ± 0.002	254	205	147
DGETAM/CEUZ_5 phr system	1.194 ± 0.003	202	170	130
DGETAM/CEUZ_10 phr system	1.182 ± 0.003	154	–	107

*1 $T_{g(DMA)}$: Glass transition temperature estimated from tanδ by DMA (1st run).
*2 $T_{fg(PALS)}$: Glass transition temperature estimated from mean free volume by PALS (1st run).
*3 $T_{g(TMA)}$: Glass transition temperature estimated from CTE by TMA (2nd run).

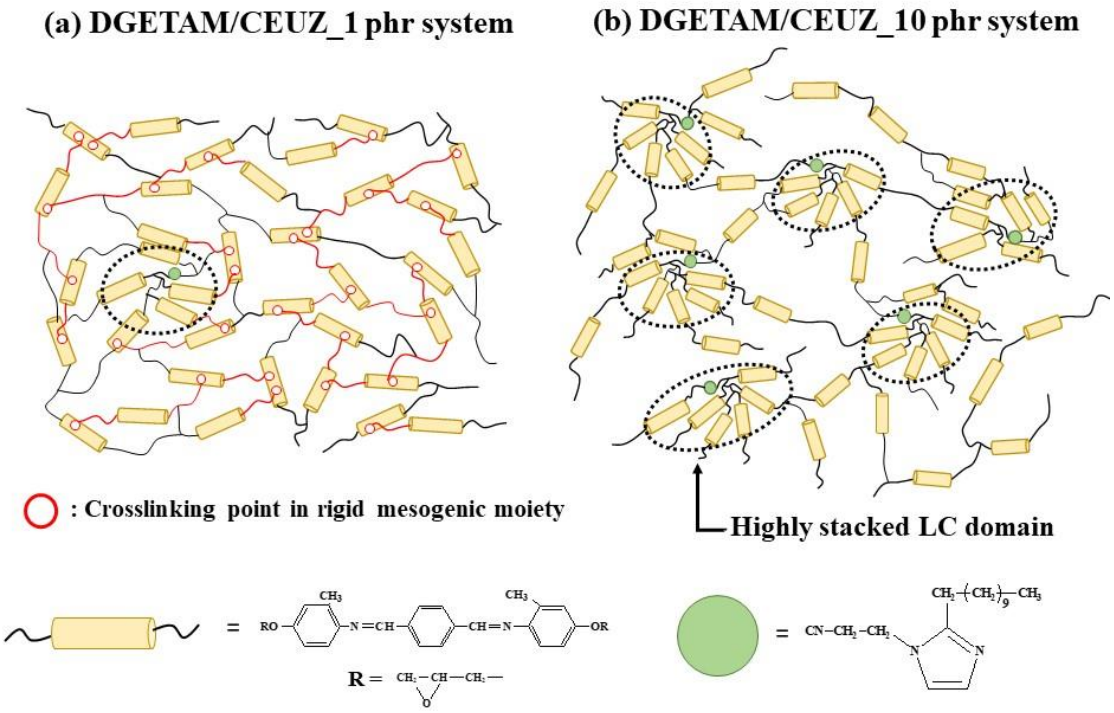

Scheme I-2-2 Proposed network structure of (a) DGETAM/CEUZ_1 phr system and (b) DGETAM/CEUZ_10 phr system.

I-2-3-4 Thermomechanical properties of the DGETAM/CEUZ systems

The dynamic mechanical properties of the cured system were studied by DMA (Figure I-2-4). Compared with the DGETAM system, the DGETAM/CEUZ_1 phr systems exhibited a storage modulus greater than 170°C and negligibly low α-relaxation behavior. This T_g-less behavior is due to the improved curing reactivity (epoxy conversion: 99%, Table I-2-1) caused by the small imidazole catalyst and the formation of crosslinking points in the rigid mesogenic moiety. Although the DMA thermogram of the DGETAM/CEUZ_3 phr system showed a very small and flat tanδ peak, the storage modulus substantially decreased at temperatures greater than 270°C. This behavior is attributed mainly to the DGETAM/CEUZ_3 phr system decreasing the number of crosslinking points in the rigid mesogenic moiety compared with the DGETAM/CEUZ_1 phr system. These data suggest that introducing crosslinking points into rigid mesogenic moieties plays a critical role in the T_g-less epoxy resin. By contrast, at CEUZ contents higher than 5 phr, the storage modulus in the rubbery region was dramatically reduced. In addition, the α-relaxation peak was shifted to a lower temperature and broadened. The

$T_{g(DMA)}$s of the DGETAM/CEUZ_5 phr and DGETAM/CEUZ_10 phr systems were 202°C and 154°C, respectively (Table I-2-2). Such a drastic decrease in T_g cannot be explained only by fewer crosslinking points in the rigid mesogenic moieties; it is likely related to the phase-separation structure with a packing-density distribution and to the micro-Brownian motion of the crosslinking network polymer chains occurring at a relatively lower temperature. More interestingly, the storage modulus from −150°C to 50°C was substantially greater for the DGETAM/CEUZ_5-10 phr systems than for the other systems. The DGETAM/CEUZ_5 phr system exhibited the highest storage modulus value (5.7 MPa at −130°C), which was 1.2 times higher than that of the DGETAM system (4.6 MPa at −130°C). This result may have been caused by the highly stacked LC domains via the self-assembly of the rigid mesogenic moieties. However, the peak heights of the γ- and β-relaxations in the DGETAM/CEUZ_5-10 phr systems were higher than those of the DGETAM/CEUZ_1-3 phr systems. These results suggest that the local thermal motion of the main chain segments near the highly stacked LC domains was not sufficiently suppressed.

To investigate the network structure of the cured systems in detail, we studied their mean free volume using PALS. PALS is widely known as a practical tool to analyze the nanoscale free volume structure of various materials. The mean free volume (V_f) of the polymer chains was estimated from the *o*-positronium (*o*-Ps) annihilation lifetime (τ_3) as a long-lived component. The temperature-dependency of V_f is presented in Figure I-2-5. We found that the V_f gradually increased with increasing temperature and further increased at higher temperatures. This behavior is attributed to the glass-transition behavior. Although there was no substantial difference in V_f among the samples at temperatures less than 50°C, at temperatures greater than 50°C, the DGETAM/CEUZ_5 phr system exhibited considerably higher V_f values than the other systems. The DGETAM/CEUZ_5 phr system exhibited a V_f (245°C) of 0.116 nm^3, which was 1.2 times higher than that of the DGETAM system (0.098 nm^3 at 245°C). Here, to estimate the glass-transition temperature based on V_f (T_{fg}), the V_f variation with changing temperature was split into two regions—the glassy and rubbery regions—and each dataset was fitted by a linear function using the least-squares method. The T_{fg} was then estimated from the intersection of the resultant two straight lines. As shown in Table 2, the T_{fg} of the cured

systems slightly decreased when the CEUZ content was less than 3 phr; however, the T_{fg} of the DGETAM/CEUZ_5 pht system (170°C) was substantially decreased by ~40 °C. Similar to the DMA results (Figure I-2-4), the PALS data demonstrate that the systems with greater CEUZ contents could not substantially restrain the thermal motion of the network polymer chains. This behavior was ascribed to a reduction in the number of crosslinking points in the mesogenic moiety.

The thermal expansion properties of the cured systems were also evaluated by TMA (Figure I-2-6.). Similar to the CTE of the DGETAM system, that of the DGETAM/CEUZ_1 phr system exhibited a slight increase. This T_g-less behavior can be achieved by the crosslinking-point formation in the rigid mesogenic moiety. By contrast, for the systems with greater CEUZ contents, the CTE substantially increased at ~100°C. As summarized in Table 2, the T_{fg} of these systems gradually decreased with increasing CEUZ content.

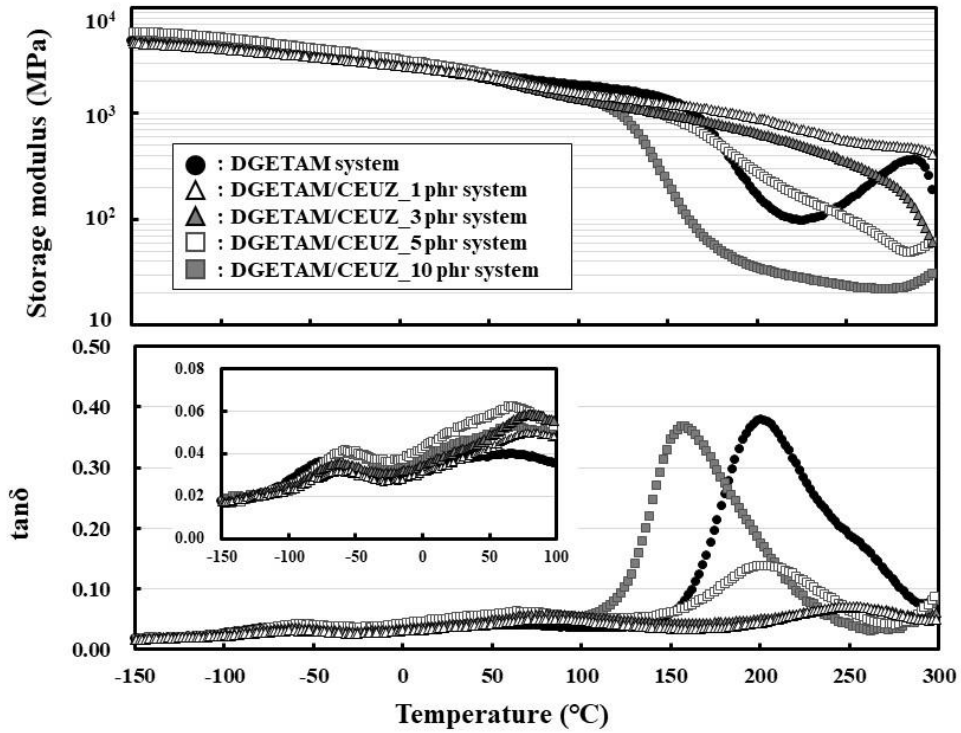

Figure I-2-4 Dynamic mechanical properties of DGETAM system and DGETAM/CEUZ_1-10 phr systems (1st run measurement).

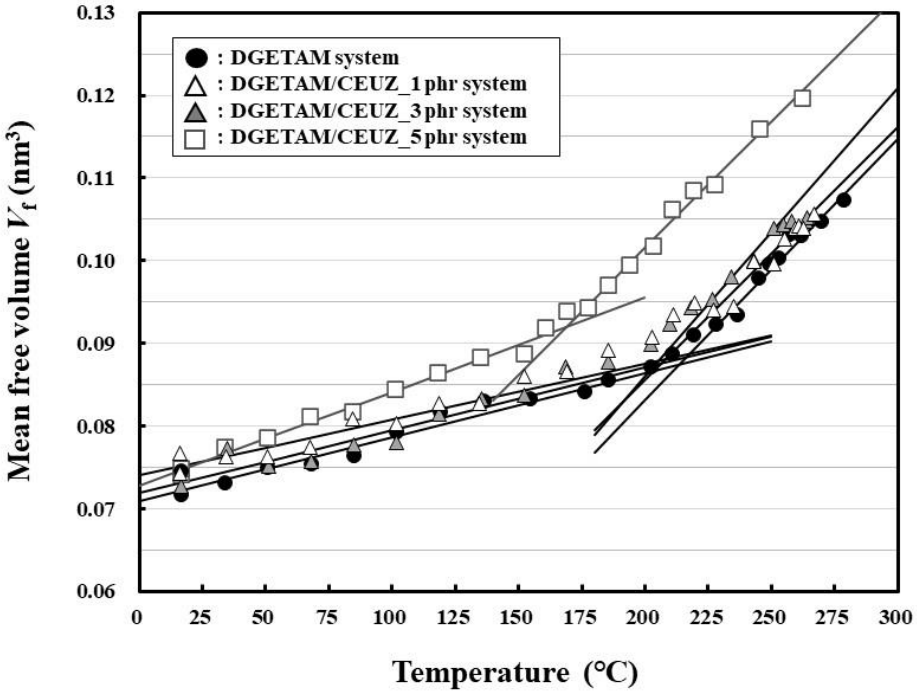

I-2-5 Temperature-dependency of mean free volume by PALS of DGETAM system and DGETAM/CEUZ_1-10 phr systems.

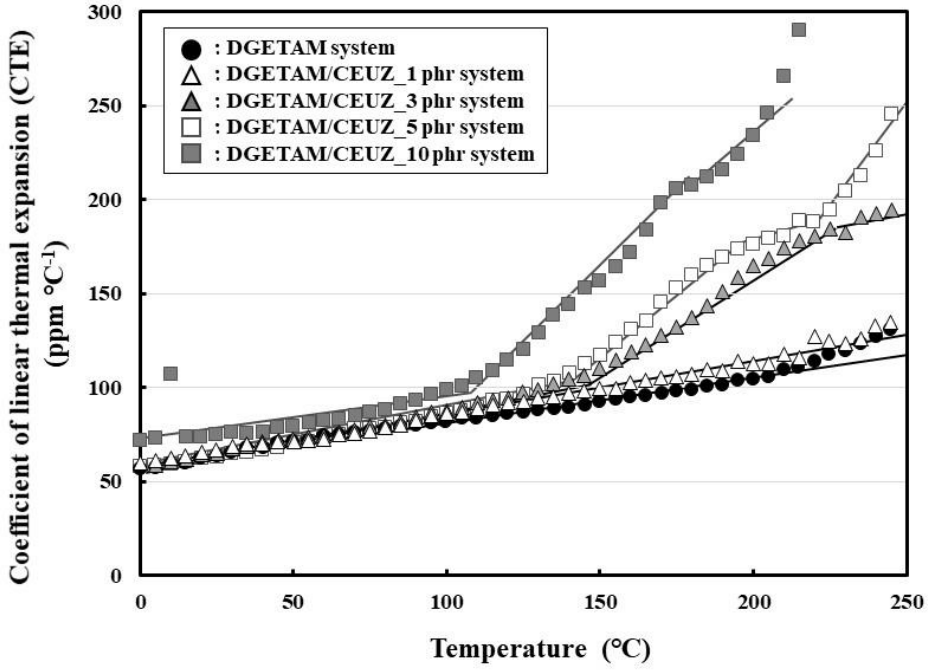

I-2-6 Temperature-dependency of coefficient of linear thermal expansion (CTE) of DGETAM system and DGETAM/CEUZ_1-10 phr systems (2nd run measurement).

I-2-4. CONCLUSIONS

In this chapter, novel T_g-less epoxy materials were successfully prepared by a Schiff base (CH=N)-derived self-polymerization of mesogenic epoxy in the presence of imidazole catalyst. The structure–property relationship of the imidazole-cured systems was investigated in detail. The results indicated that the crosslinking points in the rigid mesogenic moiety in the system with less imidazole could result in T_g-less behavior. By contrast, the system with a greater imidazole content proceeded with epoxy–imidazole adduct formation rather than with CH=N-derived self-polymerization. As a result, the CTE dramatically increased in the rubbery region and the dynamic mechanical property deteriorated. This behavior is attributed mainly to the decreased crosslinking points in the rigid mesogenic moiety and to the lower-density domain formed by the addition of excess imidazole.

I-2-5. REFERENCES

1. M. Harada, D. Morioka, M. Ochi, *Journal of Applied Polymer Science*, **2018**, DOI: 10.1002/app.46181
2. B.E. O'Rourke, N. Oshima, A. Kinomura, R. Suzuki, *JJAP Conference Proceedings*, 2, **2014**, 011304
3. J. V. Olsen, P. Kirkegaard, N. J. Pedersen, M. Eldrup, *Physica Status Solidi C*, **2007**, 4, 40043
4. M. Eldrup, D. Lightbody, J. N. Sherwood, *Chemical Physics*, **1981**, 63, 51-58
5. S. J. Tao, *Chemical Physics*, **1972**, 56, 5499-5510
6. M. Fedtke, V. Strehmel, *Polymer Bulletin*, **1989**, 21, 549-554
7. S. Heise, G. C. Martin, *Macromolecules*, **1989**, 22, 99-104
8. S. K. Ooi, W. D. Cook, G. P. Simon, C. H. Such, *Polymer*, **2000**, 41, 3639-3649
9. Y. R. Ham, S. H. Kim, Y. J. Shin, D. H. Lee, M. Yang, J. H. Min, J. S. Shin, *Journal of Industrial and Engineering Chemistry*, **2010**, 16, 556-559
10. L. Pauling, The Chemical Bond, *Cornell University Press*, New York, **1960**, p. 60, p. 119

Chapter 3.

Glass Transition Temperature and Packing Density of Schiff Base Type Mesogenic Epoxy/Imidazole Systems Cured at Different Temperatures

I-3-1. INTRODUCTION

Epoxy resins are generally used as the matrix resin of composite materials for IC packaging and printed circuit boards because of their excellent electrical insulation and adhesive properties. Nevertheless, However, the drawbacks of conventional epoxy resins such as diglycidyl ether of bisphenol A (DGEBA) are their relatively lower glass-transition temperatures (T_gs) of ~200°C than those of cyanate ester resins and polyimide resins. In addition, due to their lower thermal conductivity compared to that of inorganic fillers, effective heat transfer in the epoxy composite can be inhibited by thermal resistance at the interface between the filler surface and the matrix resin. To overcome these obstacles, mesogenic epoxy resins have recently attracted tremendous attention for their higher T_gs and excellent thermal conductivity [1-20]. Our latest studies reported the CH=N-derived self-polymerization mechanism of mesogenic epoxy resin and revealed that the crosslinking points in the rigid mesogenic moiety and to effectively suppress the chain thermal motion. Moreover, the CH=N and the imidazole-derived self-polymerizations were found to occur competitively and the ratio between these two reactions is dependent on the imidazole catalyst content.

In this chapter, Schiff base type mesogenic epoxy resins were cured by the same content of imidazole catalyst at different temperature conditions. The effect of curing temperatures on their T_gs and packing densities (mean free volume and free volume distribution) were investigated by DMA and PALS. The LC phase structures and thermal conductivities of cured systems were also studied in detail.

I-3-2. EXPERIMENTAL

I-3-2-1. Curing materials

The liquid crystalline (LC) epoxy (DGETAM; C 170 N 212, Mw = 456) was synthesized in-house.

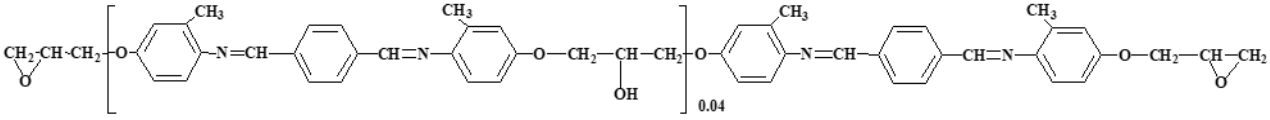

Diglycidyl ether of bisphenol A (DGEBA; JER 828EL, Mw = 370, epoxy equivalent: 185 g/eq.) was available from Mitsubishi Chemical Co., Ltd.

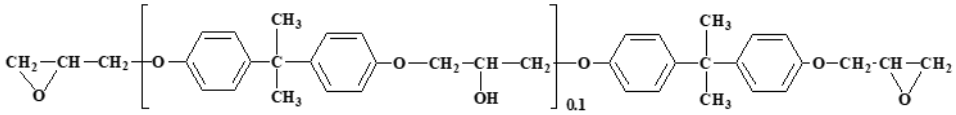

1-(2-Cyanoethyl)-2-undecylimidazole (CEUZ, Mw = 275, m.p. 49-54°C) was purchased from Tokyo Chemical Industry Co., Ltd.

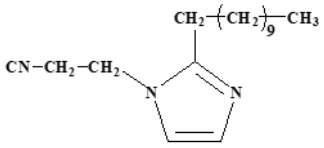

I-3-2-2. Curing method of the DGETAM/CEUZ_220°C systems

DGETAM in an aluminum cup (25×35×15 mm^3) completely melted on a heating plate at 190-200°C for 2 min and degassed under a vacuum for 5 min. DGETAM (1.20 g, 2.63 mmol) was mixed with 3 phr CEUZ (3.60×10^{-2} g, 0.13 mmol)) and stirred at 220-230°C for 1 min. Finally, it was cured at 220°C for 60 min in an oven and gradually cooled. The obtained sample was 25×35 mm^2 with a thickness of about 0.8 mm.

I-3-2-3. Curing method of the DGETAM/CEUZ_180°C systems

Similar to the DGETAM/CEUZ_220°C system, DGETAM (1.20 g, 2.63 mmol) was mixed with 3 phr CEUZ (3.60×10^{-2} g, 0.13 mmol)) and stirred at 190-200°C for 1 min. Subsequently, it was cured at 180°C for 1 h + 210°C for 0.5 h in an oven and gradually cooled. The obtained sample was 25×35 mm^2 with a thickness of about 0.8 mm.

I-3-2-4. Curing method of DGEBA/CEUZ_3 phr systems

DGEBA system was used as an exemplar network polymer containing no CH=N

group for comparison. DGEBA in an aluminum cup (45×45×25 mm^3) was degassed under a vacuum at 130°C for 10 min. Subsequently, DGEBA (8.0 g, 21.6 mmol) was mixed with 3 phr CEUZ (0.24 g, 0.87 mmol)) and stirred at 130°C for 1 min. Finally, it was cured in an oven and gradually cooled. Two kinds of curing conditions were applied; (i) 130°C for 2 h + 180°C for 2 h + 210°C for 1 h, (ii) 180°C for 2 h + 210°C for 1 h. The obtained sample was 45×45 mm^2 with a thickness of about 3 mm. These conditions were determined based by DSC (Figure I-3-1). The DSC thermogram of the DGEBA/CEUZ systems showed a broad exothermic peak at 110–170°C, assigning to the imidazole-derived polymerization.

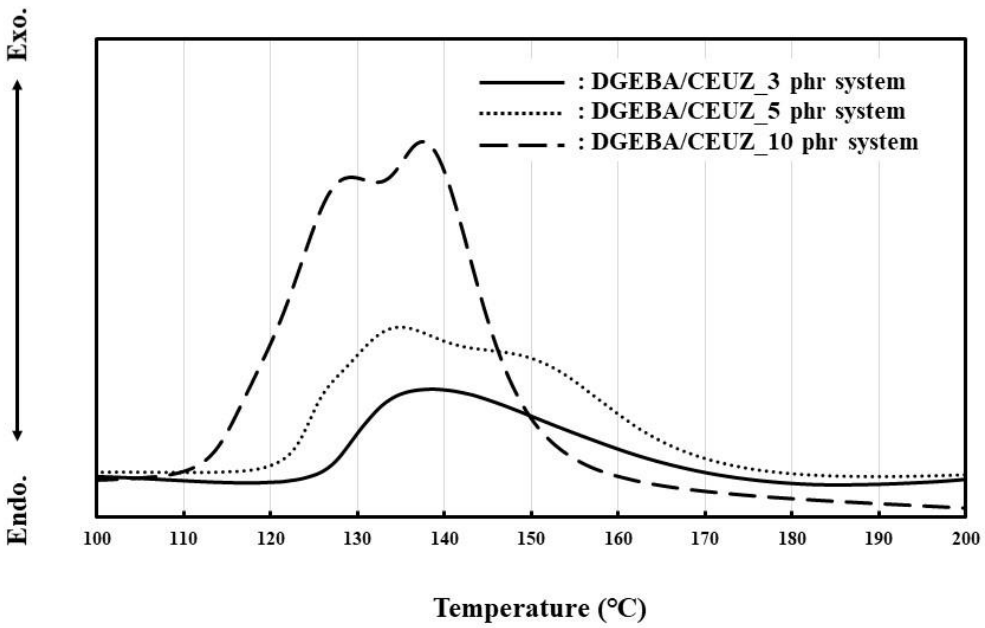

Figure I-3-1 DSC charts of DGEBA systems with various CEUZ (before curing).

I-3-2-5. Measurement and analysis

Curing behaviors of DGEBA/CEUZ systems were identified using a differential scanning calorimeter (DSC; DSC7020, Seiko Instruments Inc.) from 100°C to 200°C at a heating rate of 5°C/min. The sample (about 3 mg) was filled into an aluminum pan.

The chemical structure of cured systems was investigated using a Fourier transform infrared spectroscopy (FTIR; Spectrum 100, Perkin-Elmer Inc.). The sample was

incorporated into a KBr pellet (Merck) and molded by a tableting machine (Shimadzu Corp.). The resolution of the IR spectrum was 4 cm^{-1}, and the spectra were collected after 32 scans for each sample. The conversion of the epoxy group was estimated from the reduction rate of the peak area at 910 cm^{-1}. Here, the peak area at 1600 cm^{-1} assigned to the aromatic ring was used as an internal standard.

The dynamic mechanical analysis (DMA) of the cured system was conducted using a non-resonance forced vibration viscoelastometer (Rheogel-E4000, UBM Co.). A bar-shaped sample (4.0×30.0×0.4 mm^3) was tested in tension mode. The test condition was -150°C to 300°C at a heating rate of 5°C/min. The vibration frequency and amplitude were adjusted to 10 Hz and ± 5 μm, respectively.

The thermal decomposition behavior of epoxy monomers and cured systems was studied by thermogravimetric analysis (TGA; TG/DTA 6200, Seiko Instruments Inc.). The test condition was under N_2 atmosphere (gas flow rate: about 350 mL/min) from 100°C to 600°C at a heating rate of 25°C/min using an aluminum pan. The sample weight was about 5 mg.

The phase structure of the cured systems was observed using polarized optical microscopy under crossed Nicols (POM; BX53 LED-33P-OC, Olympus Corp.). The sample was polished with sandpaper and a buff polishing machine to prepare a film of approximately 30 μm in thickness.

The periodic arrangement structure of the network polymer chains of the cured systems was evaluated by X-ray diffractometry (XRD; RINT-Ultima III, Rigaku Co.). The d-spacing of the ordered structure was calculated using Bragg's formula ($n\lambda = 2d\sin\theta$). The XRD patterns were measured using CuKα (λ = 0.154 nm) radiation generated at 40 kV and 40 mA at a scan rate of 1.2°/s and a sample interval of 0.02°. A sample measuring 15×15×1.2 mm^3 was cut using a diamond cutter and polished with sandpaper and a buff polishing machine to obtain a flat, smooth surface.

The mean free volume and free volume distribution of cured systems at 20°C were studied by positron annihilation lifetime spectroscopy (PALS) using a bulk method. The positron source was sandwiched between two identical samples (15 × 15 × 1.9 mm). The time resolution was 207 ps full width at half-maximum (FWHM). The total count for positron annihilation events was 10^7 for the positron lifetime spectrum of each sample.

All PALS spectra were analyzed by the PALSfit program [21] and were decomposed into three lifetime components: τ_1, τ_2, τ_3 ($\tau_1 < \tau_2 < \tau_3$). The long-lived component τ_3 corresponds to the *o*-positronium (*o*-Ps) pick-off annihilation lifetime. The mean free volume radius (R) was estimated using a spherical infinite potential well model (Tao–Eldrup model, (Eq. I-3-1)) [22, 23]:

$$\tau_3 = \frac{1}{2}\left[1 - \frac{R}{R_0} + \frac{1}{2\pi}\sin\left(\frac{2\pi R}{R_0}\right)\right]^{-1} , \quad \text{Eq. I-3-1}$$

where $R_0 = R + \Delta R$ and ΔR is the thickness of an electron layer in the spherical potential well (ΔR = 0.166 nm).

The mean free volume (V_f) was determined using the equation (Eq. I-3-2):

$$V_f = \frac{4}{3}\pi R^3 , \quad \text{Eq. I-3-2}$$

Probability density function (PDF) of positron annihilation was determined by Laplace inverse transform program for CONTIN PALS-2 [24] to estimate the free volume distribution.

The temperature-dependency of mean free volumes of the cured system was studied by PALS using a slow positron beam [25] housed at the National Institute of Advanced Industrial Science and Technology (AIST). A sample with a size of 20×20×0.4 mm^3 was placed on a ceramic heater covered with a graphite sheet and heated for about 20 min at the corresponding temperature. The temperature was monitored within 1°C resolutions using a thermocouple attached to the heater and was converted to that of the sample's surface by the calibrated coefficient. Positron irradiation was carried out under vacuum (~10^{-3} Pa). The time resolution was 0.26 ns full width at half-maximum (FWHM), and the incident energy was set at 10 keV, which corresponds to a mean implantation depth of 1.2 μm from the sample's top surface with a material density of 1.2 g/cm^3 measured by a pycnometer method at 21-23°C. The total count for positron annihilation events was 2×10^6 for the positron lifetime spectrum of each sample.

The thermal conductivity (λ) at 25°C for the fully cured composite was determined by using the equation (Eq. I-3-3):

$$\lambda = \alpha\, C_p\, \rho , \quad \text{Eq. I-3-3}$$

where α is the thermal diffusivity, C_p is the specific heat and ρ is the density. The thermal diffusivity was determined using a laser flash analyzer (LFA 447, Netzsch Co.)

in accordance with the ASTM E1461-13 standard. A disk-shaped sample (diameter: 10 mm, thickness: 1 mm) was coated with a carbon layer (Graphite coat, Nihon Senpaku Co., Ltd., thickness: 15 ± 5 μm) on both the upper and lower surfaces after the sputtering process for a gold layer (thickness: 50 nm). The density of the fully cured composite was measured by a pycnometer method at 21°C. The specific heat was determined by DSC (DSC7020, Seiko Instruments Inc.) in the temperature range from 5°C to 100°C at a heating rate of 10°C/min.

I-3-3. RESULTS AND DISCUSSION

I-3-3-1 Dynamic mechanical properties of the DGETAM/CEUZ systems

The dynamic mechanical properties of the DGETAM/CEUZ systems and DGEBA/CEUZ systems cured at different temperatures were studied by DMA (Figure I-3-2). As summarized in Table I-3-1, the epoxy conversion of all cured systems was ~100%. According to the tanδ peak in the DMA thermogram, T_g of the DGEBA/CEUZ _180°C system (106°C) decreased by 30°C compared with that of the DGEBA/CEUZ _130°C system (136°C). Moreover, the DGEBA/CEUZ _180°C system also showed a lower storage modulus in a rubbery region than the DGEBA/CEUZ _130°C system. Generally, for imidazole-derived polymerization, epoxies first react with an imidazole compound, forming the epoxy-imidazole adduct. Afterward, the resulting alkoxide reacts with another epoxy, and the anionic polymerization generates a three-dimensional network structure. Additionally, it is expected that the gelation rate was accelerated at the higher curing temperature, leading to insufficient growth of polymer chains via anionic polymerization. Therefore, the DMA result indicated that the higher curing temperature could reduce the crosslinking density, deteriorating the material's thermomechanical property. However, the DGETAM/CEUZ system showed an opposite trend against the DGEBA/CEUZ system. The DGETAM/CEUZ _220°C system a very small and flat tanδ peak at ~250°C while the DGETAM/CEUZ _180°C system exhibited a clear T_g peak at 190°C. Furthermore, the DGETAM/CEUZ _220°C system maintained a higher storage modulus even above 200°C. This result indicated that the DGETAM/CEUZ _220°C system could effectively suppress the thermal motion of networked chains. On the other hand, the storage modulus in the glassy region of the DGETAM/CEUZ _180°C system

was significantly higher than that of the DGETAM/CEUZ _220°C system. This result implied a higher packing density of the DGETAM/CEUZ _180°C system. Given the above results, it is found that the curing temperature condition drastically changed the network structures of DGETAM/CEUZ systems.

Table I-3-1 Curing condition and conversion of epoxy groups of cured systems.

Curing system	CEUZ content (phr)	Curing condition	Epoxy conversion (%)*1
DGETAM/CEUZ_220°C system	3	220°C・1 h	99
DGETAM/CEUZ_180°C system	3	180°C・1 h + 210°C・0.5 h	99
DGEBA/CEUZ_180°C system	3	180°C・2 h + 210°C・1 h	97
DGEBA/CEUZ_180°C system	3	130°C・2 h + 180°C・2 h + 210°C・1 h	95

*1 : determined from the reduction rate of FT-IR spectrum of epoxy peak (910 cm^{-1})

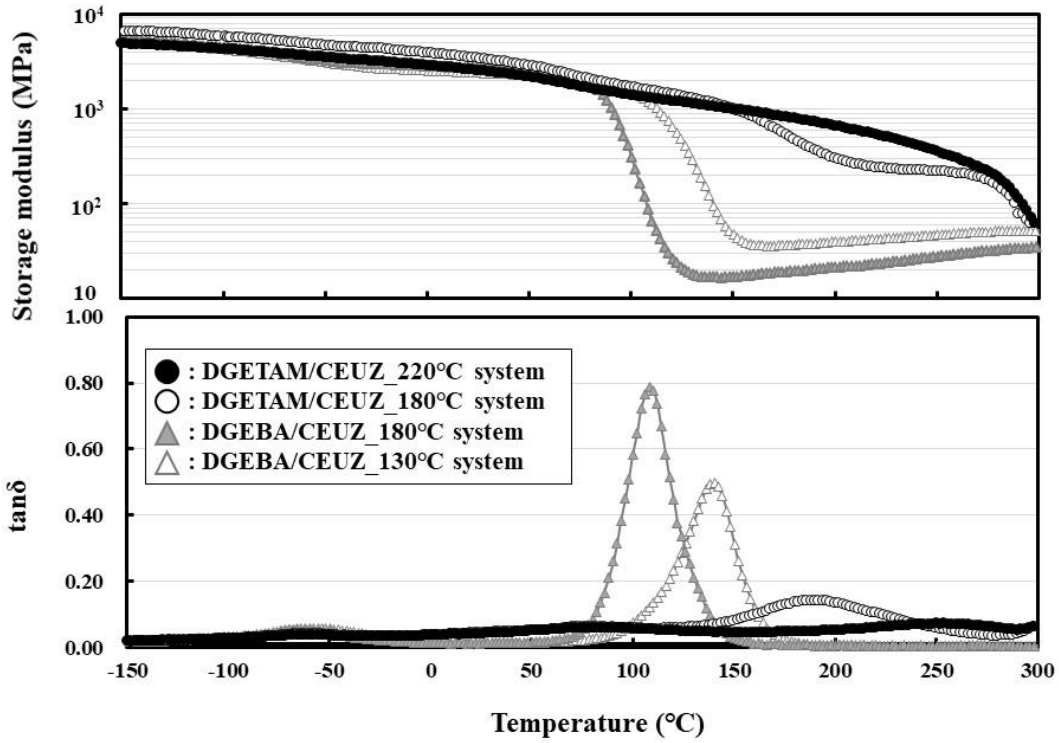

Figure I-3-2 Dynamic mechanical properties of DGETAM/CEUZ systems and DGEBA/CEUZ systems cured at different temperature.

I-3-3-2 Chemical structures of the DGETAM/CEUZ systems

To investigate the reason for this DMA result in detail, we analyzed the chemical structures of the cured systems. According to the DSC charts (Figure I-2-1) in Chapter 2, the DGETAM/CEUZ system exhibited two exothermic peaks at 140-160°C and 220–290°C, corresponding to the imidazole-derived and the CH=N-derived polymerizations, respectively. Therefore, we expected that the imidazole-derived polymerization could happen at a lower temperature compared to a CH=N-derived one (Scheme I-3-1). Additionally, the effect of curing temperatures and the CEUZ contents on the epoxy conversions were investigated (Figure I-3-3). At the CEUZ content greater than 3 phr, the epoxy conversion exhibits ~100%, in spite of curing temperatures. Nevertheless, the epoxy conversions were less than 90% when epoxies were cured by the lower temperature condition (180°C for 1 h + 210°C for 0.5 h) at the CEUZ content less than 1 phr. In particular, the epoxy conversion could not reach 80% under this temperature condition without CEUZ. These data suggested that the CH=N-derived polymerization is less likely to occur under the lower temperature condition compared to the higher temperature one (220°C for 1 h).

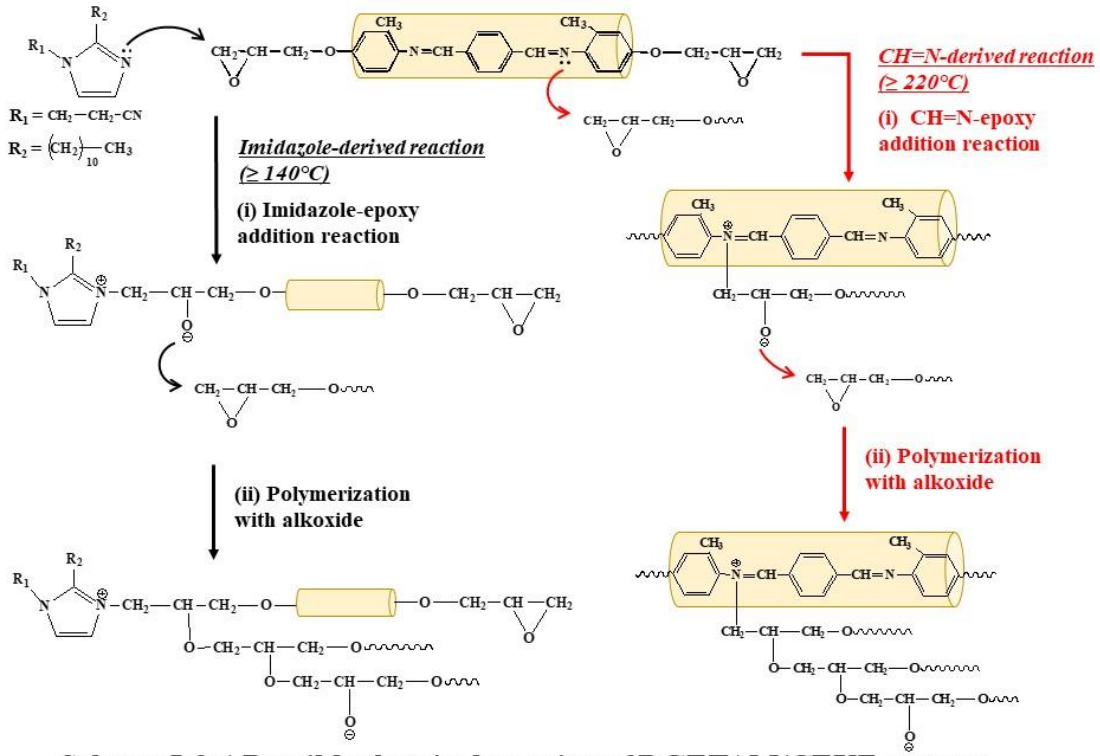

Scheme I-3-1 Possible chemical reaction of DGETAM/CEUZ systems

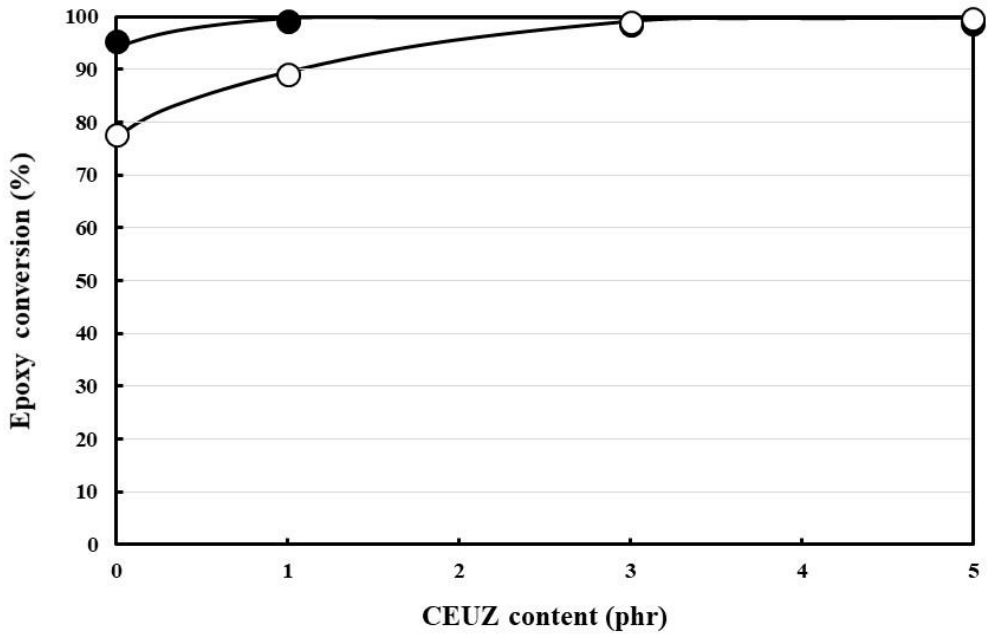

Fig. I-3-3 Conversion of epoxy groups of DGETAM system and DGETAM/CEUZ systems cured at different temperatures; (●) 220℃・1h, (○) 180℃・1 h + 210℃・0.5 h.

In addition, the chemical structure of the DGETAM/CEUZ systems was studied by FTIR spectroscopy (Figure I-3-4). Here, the DGETAM_220℃ system was cured at 220°C for 1 h in the absence of CEUZ and used for comparison. The absorption peak of the epoxy group (910 cm^{-1}) completely disappeared in all cured systems. Compared to the uncured DGETAM, the intensity of absorption peak of the CH=N group (1619 cm^{-1}) substantially decreased in the DGETAM_220℃ system. Table I-3-2 summarizes the peak area ratio of the CH=N group at 1620 cm^{-1} determined based on the peak area of the aromatic ring at 1500 cm^{-1}. As a result, the CH=N group ratio of the DGETAM _220°C system was significantly lower than the DGETAM/CEUZ system. This result suggested that CH=N groups were consumed during the CH=N-derived self-polymerization. Furthermore, the DGETAM/CEUZ_220°C system shows a slightly lower value than the DGETAM/CEUZ_180°C system. These results could be related to the ratio between the imidazole-derived and the CH=N-derived curing reactions. Namely, the DGETAM/CEUZ_220°C system could proceed with a CH=N-derived polymerization in

addition to the imidazole-derived ones, although the DGETAM/CEUZ_180°C system could mainly proceed with the imidazole-derived polymerization.

Moreover, the TGA chart under nitrogen atmospheres (Figure I-3-5) revealed that the curing temperature condition strongly influenced the thermal decomposition behavior of the DGETAM/CEUZ systems. As shown in Table I-3-2, the 5% weight loss temperatures (T_{d5}) of the DGETAM _220°C system (331°C) and the DGETAM/CEUZ_220°C system (338°C) decreased by about 20°C compared with that of the DGETAM/CEUZ_180°C system (353°C). These results indicate that the CH=N-derived polymerization can deteriorate the initial thermal degradation of the network polymer chains. This is attributed to the decreased C=N group with higher binding energy (615 kJ/mol) than that of the C–N group (292 kJ/mol) [25]. In addition, the char yield at 600°C of the DGETAM/CEUZ_180°C system (46%) was slightly higher than those of the DGETAM_220°C system (41%) and the DGETAM/CEUZ_220°C system (41%). These data suggested the char formation could easily happen in the DGETAM/CEUZ_180°C system because of its high packing density.

On the basis of the aforementioned results, we propose a model for the possible network structure of the DGETAM/CEUZ_220°C system and the DGETAM/CEUZ_180°C system (Scheme I-3-2). We expected that the DGETAM/CEUZ_220°C system could proceed with a CH=N-derived polymerization in addition to the imidazole-derived ones, forming the crosslinking points into the rigid mesogenic moiety. As a result, the DGETAM/CEUZ _220°C system could effectively suppress the thermal motion of networked chains, as shown in DMA result (Figure I-3-2).

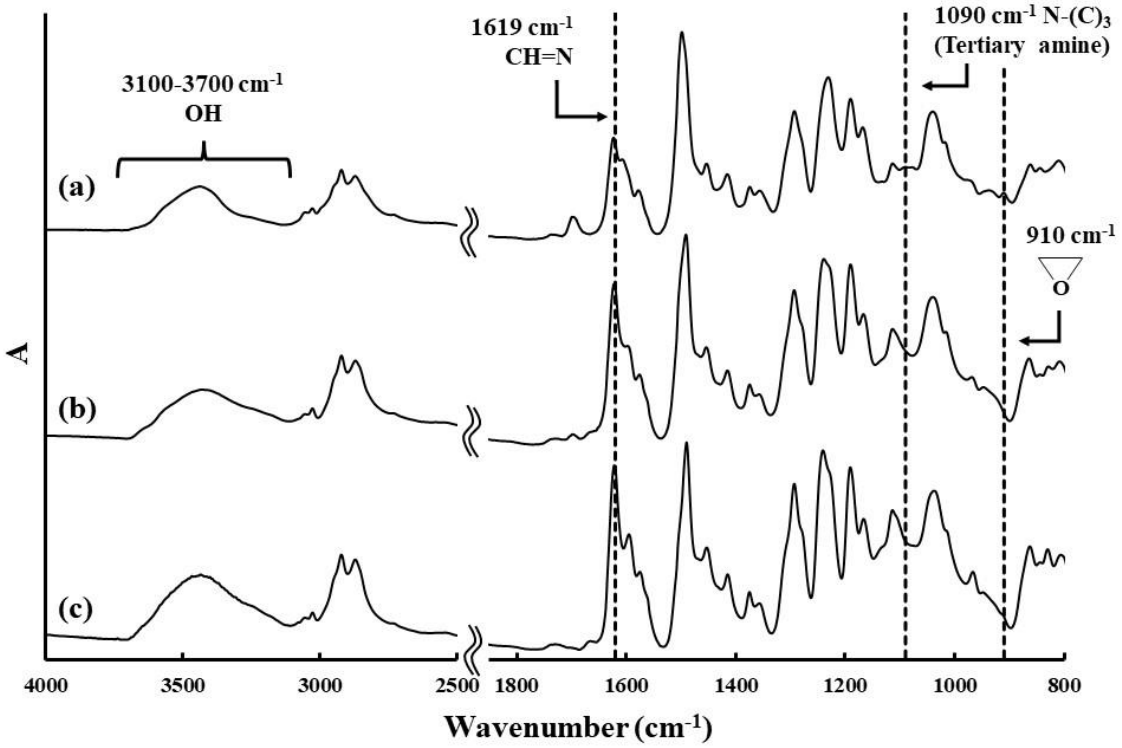

Figure I-3-4 FT-IR spectra of (a) DGETAM_220 °C system, (b) DGETAM/CEUZ_220°C system, and (c) DGETAM/CEUZ_180°C system.

Table I-3-2 CH=N group ratio and TGA data of DGETAM_220°C system and DGETAM/CEUZ systems cured at different temperature.

Curing system	CH=N group ratio*1	T_{d5} (°C) *2	Char yield at 600°C (%) *2
DGETAM_220°C system	0.1	331	41
DGETAM/CEUZ_220°C system	0.4	338	40
DGETAM/CEUZ_180°C system	0.7	353	46

*1 : CH=N peak area ratio (1620 cm^{-1}) based on the benzene peak area (1500 cm^{-1}) determined by FT-IR
*2 : determined from the TGA under N_2

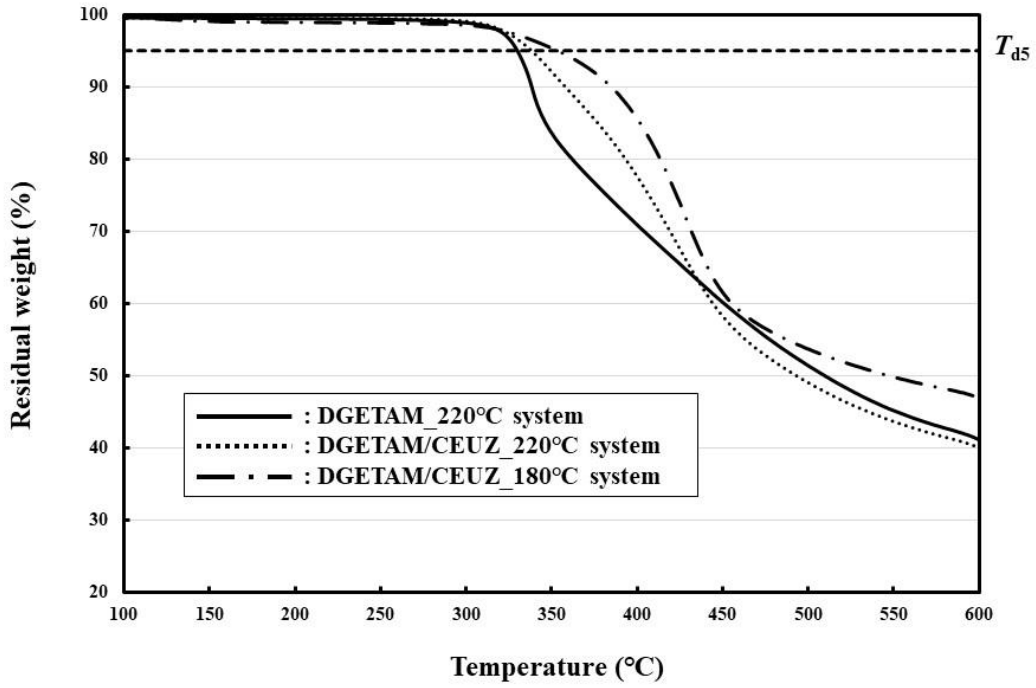

Figure I-3-5 TGA chart of DGETAM_220 ℃ system and DGETAM/CEUZ systems cured at different temperature (under N_2).

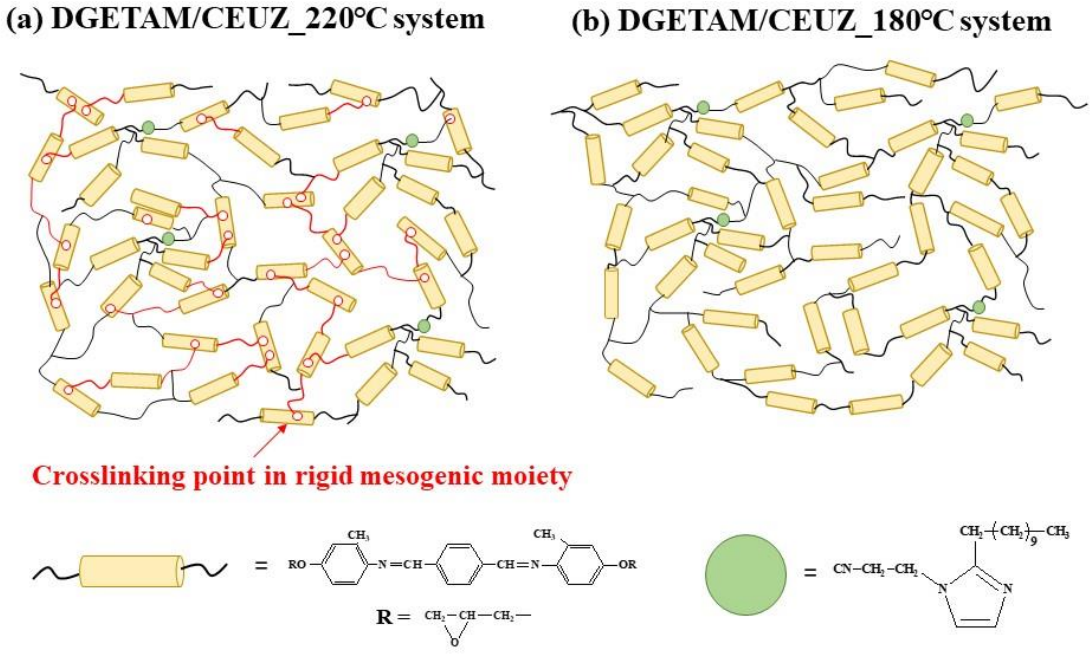

Scheme I-3-2 Proposed network structures of (a) DGETAM/CEUZ_220℃ system and (b) DGETAM/CEUZ_180℃ system.

I-3-3-3 Packing densities of the DGETAM/CEUZ systems

Optical photographs of the DGETAM_220°C system and the DGETAM/CEUZ systems are exhibited in Figure I-3-6. All the cured systems showed a red–brown appearance; however, the transparency in the DGETAM/CEUZ_180°C system remarkably decreased. In the POM image of the DGETAM/CEUZ_180°C system, birefringence patterns appeared throughout the observation regions, indicating the formation of an LC phase structure via self-assembly of mesogenic moieties. In contrast, a large number of small bright dotted patterns were clearly found in the DGETAM_220°C system and the DGETAM/CEUZ_220°C system. These data suggested that the higher temperature condition could reduce the orientation of mesogenic moieties. This is because the CH=N groups in mesogenic moieties were consumed during the CH=N-derived self-polymerization.

Moreover, the XRD patterns of all cured systems exhibited a halo around 2θ = 19°, corresponding to a plane space (d = 0.47 nm) of the network polymer chains (Figure I-3-7) [26]. Thus, it is considered that all cured systems formed the nematic phase structure of the mesogenic moieties. In addition, the DGETAM_220°C system shows a slightly broader halo compared to the DGETAM/CEUZ systems, meaning the reduction in packing density. This is related to the high bulkiness of the network polymer chains with the crosslinking points into the rigid mesogenic moiety.

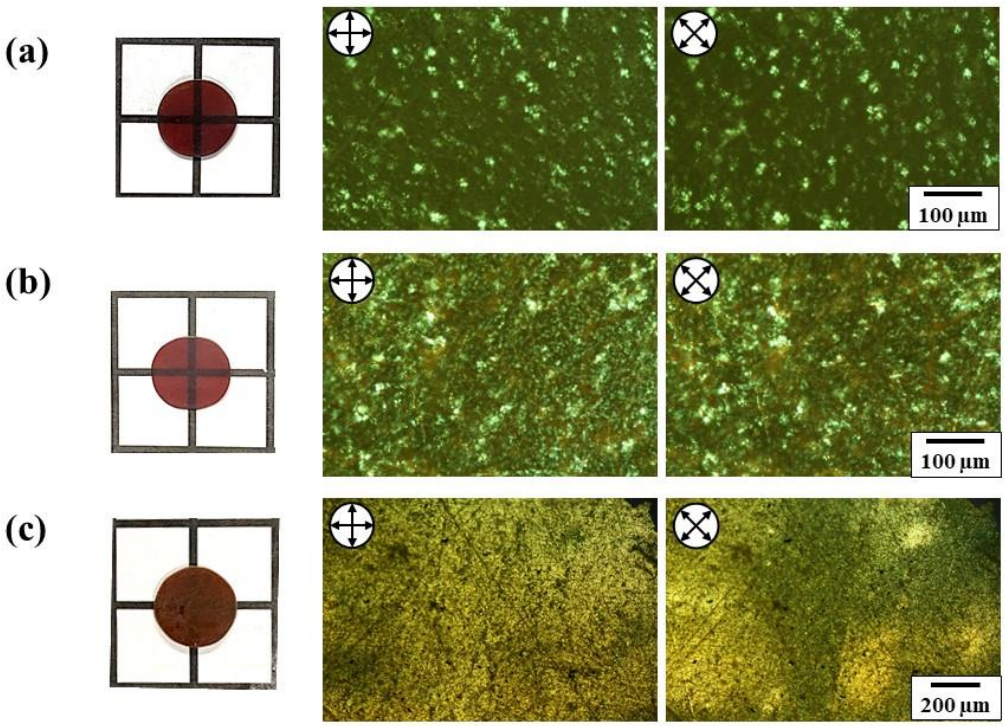

Figure I-3-6 Optical photographs and polarized optical micrographs of (a) DGETAM_220°C system, (b) DGETAM/CEUZ_220°C system, and (c) DGETAM/CEUZ_180°C system.

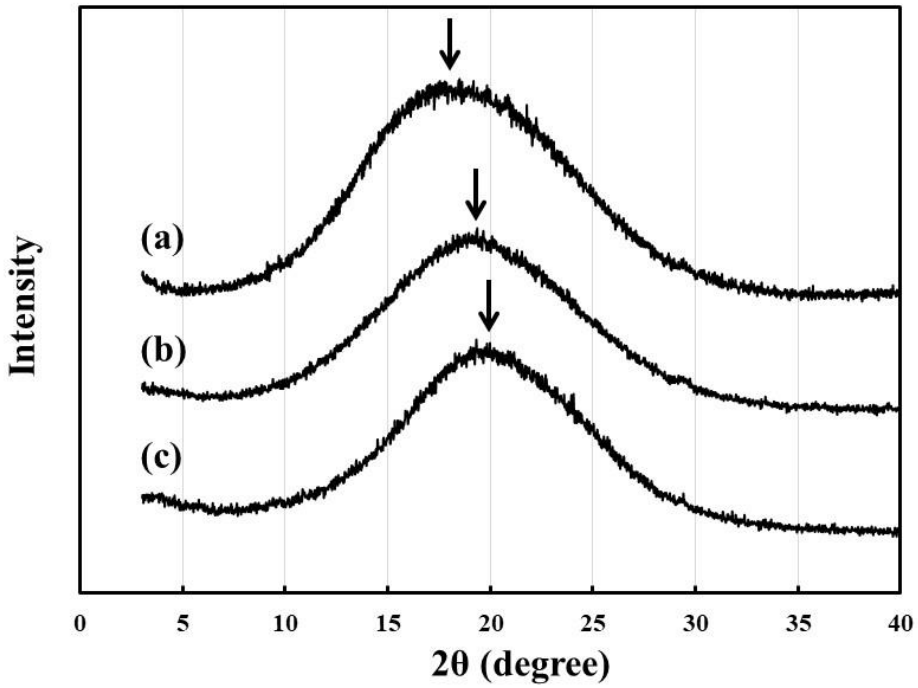

Figure I-3-7 XRD patterns of (a) DGETAM_220 °C system, (b) DGETAM/CEUZ_220°C system, and (c) DGETAM/CEUZ_180°C system.

To investigate the packing densities of the cured systems in detail, we studied the mean free volumes (V_f) and free volume distribution at 20°C using PALS (Table I-3-3). Here, DGEBA system was used as an exemplar network polymer for comparison. The DGETAM_220°C system shows a higher V_f (0.0806 nm^3) than the DGETAM/CEUZ systems and the DGEBA/CEUZ system. Similar to the XRD result (Figure I-3-7), this result could be caused by the bulky polymer chains with the crosslinking points into the rigid mesogenic moiety. Besides, the V_f of the DGETAM/CEUZ_220°C system (0.0780 nm^3) was slightly higher than that of the DGETAM/CEUZ_180°C system (0.0762 nm^3). This is because the DGETAM/CEUZ_220°C system could proceed with a CH=N-derived polymerization in addition to the imidazole-derived ones, forming the crosslinking points into the rigid mesogenic moiety. Moreover, the fractional free volume can be estimated from the *o*-Ps annihilation signal intensity (I_3). As a result, the I_3 of the DGETAM_220°C system was two times higher than the DGETAM/CEUZ systems, though there was no substantial difference between the DGETAM/CEUZ_220°C system and the DGETAM/CEUZ_180°C system. In addition, it can be seen from Figure I-3-8 that DGETAM_220°C system exhibited a very wide distribution of free volume compared to the other systems. Furthermore, the DGETAM/CEUZ_220°C system exhibited a high ratio of the relatively higher free volume than the DGETAM/CEUZ_180°C system. These results indicated that introducing the crosslinking points into the rigid mesogenic moiety increased the bulkiness of network polymer chains, reducing the packing density.

Table I-3-3 PALS data of DGETAM system, DGETAM/CEUZ systems, and DGEBA/CEUZ system.

Curing system	V_f at 20°C (nm^3) *1	I_3 at 20°C (%) *1	T_{fg} (°C) *2	$\alpha_{f(glassy)}$ (10^{-4}°C^{-1}) *2	$\alpha_{f(rubbery)}$ (10^{-4}°C^{-1}) *2
DGETAM_220°C system	0.0806±0.0005	20.5	214	8.8	36.1
DGETAM/CEUZ_220°C system	0.0780±0.0008	10.0	205	8.7	39.9
DGETAM/CEUZ_180°C system	0.0762±0.0008	10.5	149	10.8	39.2
DGEBA/CEUZ_130°C system	0.0788±0.0004	23.4			

*1 : measured by PALS (bulk method)
*2 : measured by PALS (slow beam method)

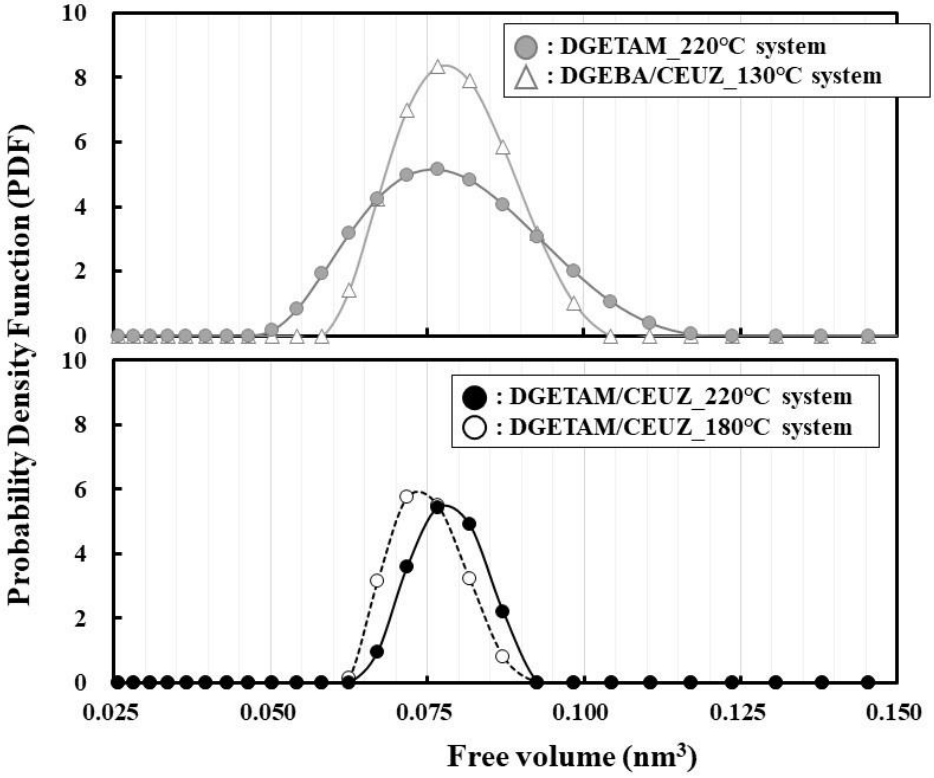

Figure I-3-8 Free volume distribution by PALS (Bulk method) of cured systems.

The temperature-dependency of mean free volume was also evaluated by PALS (Figure I-3-8). As a result, the V_f gradually increased with rising temperature and further increased at higher temperatures. This behavior can be attributed to the glass transition. Noticeably, at temperatures greater than 150°C, the DGETAM_220°C system and the DGETAM/CEUZ_220°C system showed considerably lower V_f values than the DGETAM/CEUZ_180°C system. Moreover, the glass-transition temperature based on the V_f (T_{fg}) variation was estimated from the intersection of the two lines of the glassy and rubbery regions. Each dataset was fitted by a linear function using the least-squares method. As summarized in Table I-3-3, T_{fg}s of the DGETAM_220°C system (214°C) was the maximum value. Besides, the DGETAM/CEUZ_220°C system (205°C) substantially increased by 56°C compared with that of the DGETAM/CEUZ_180°C system (149°C). Similar to the DMA results (Figure I-3-2), the PALS data demonstrate that the crosslinking points into the rigid mesogenic moiety could greatly restrain the micro-Brownian motion of networked chains. In addition, their coefficient of thermal expansion (CTE) based on the V_f variation in the glassy and rubbery regions ($\alpha_{f(glassy)}$ and $\alpha_{f(rubbery)}$)

was shown in n Table I-3-3. The $\alpha_{f(glassy)}$ of the DGETAM/CEUZ_220°C system was about 20% lower than that of the DGETAM/CEUZ_180°C system. From these results, it is considered that the DGETAM/CEUZ_220°C system can effectively inhibit the thermal motion of network polymer chains in the glassy region, despite its lower packing density than the DGETAM/CEUZ_180°C system with a high orientation of mesogenic moieties.

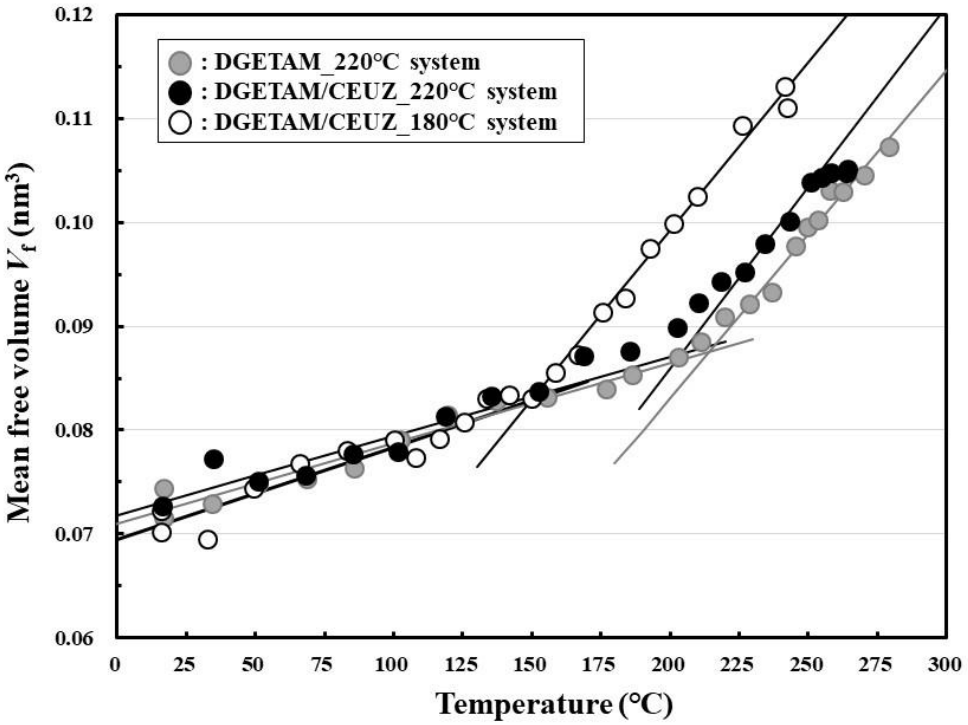

Figure I-3-8 Temperature-dependency of mean free volume V_f by PALS of DGETAM_220°C system and DGETAM/CEUZ systems cured at different temperature.

I-3-3-4 Thermal conductivities of the DGETAM/CEUZ systems

The thermal conductivity, thermal diffusivity, specific heat, and density of the cured systems are presented in Table I-3-4. Though there was no significant difference in specific heats and densities among the DGETAM systems, the thermal diffusivities differed unexpectedly. As a result, the thermal conductivities of the DGETAM_220°C system (0.28 W/(m·K)) and the DGETAM/CEUZ_220°C system (0.29 W/(m·K)) were about 1.3 times higher than that of the DGETAM/CEUZ_180°C system (0.23 W/(m·K)). Therefore, it is considered that these systems can effectively suppress the phonon

scattering in the materials, even though the POM images (Figure I-3-6) and PALS results (Table I-3-3) revealed their lower orientation of mesogenic moieties and relatively lower packing densities. Consequently, this result can be attributed to the higher crosslinking density related to introducing the crosslinking points into the rigid mesogenic moiety. In addition, the DGETAM_220°C system and the DGETAM/CEUZ_220°C system were about 1.5 times as high as the DGEBA/CEUZ_130°C system.

Table I-3-4 Thermal conductivity, thermal diffusivity, specific heat and density of DGETAM system, DGETAM/CEUZ systems, and DGEBA/CEUZ system.

Curing system	Specific heat (J/(g·K))	Density (g/cm^3)	Thermal diffusivity (mm^2/s)	Thermal conductivity (W/(m·K))
DGETAM_220°C system	1.23 ± 0.048	1.21 ± 0.003	0.187 ± 0.009	0.28 ± 0.01
DGETAM/CEUZ_220°C system	1.21 ± 0.001	1.20 ± 0.002	0.198 ± 0.014	0.29 ± 0.02
DGETAM/CEUZ_180°C system	1.22 ± 0.001	1.21 ± 0.005	0.155 ± 0.012	0.23 ± 0.02
DGEBA/CEUZ_130°C system	1.26 ± 0.017	1.17 ± 0.003	0.127 ± 0.008	0.19 ± 0.01

I-3-4. CONCLUSIONS

In this chapter, the effect of curing temperatures on their T_gs and packing densities were investigated by DMA and PALS. Schiff base type mesogenic epoxy resins were cured by the same content of imidazole catalyst at different temperatures. At lower temperatures, epoxy mainly proceeds with the imidazole-derived polymerization, forming a highly ordered nematic phase structure via self-assembly of mesogenic moieties. On the other hand, at higher temperatures, epoxy could proceed with a Schiff base-derived self-polymerization, in addition to the imidazole-derived ones. As a result, this cured system exhibited higher T_g and higher thermal conductivity than the lower temperature curing system although it showed relatively lower packing density. These results indicated that the crosslinking points into the rigid mesogenic moiety effectively suppressed network polymer chains' thermal motion.

I-3-5. REFERENCES

1. A. Shiota, C. K. Ober, *Journal of Polymer Science: Part A: Polymer Chemistry*, **1996**, 34, 1291-1303
2. Q. Lin, A. F. Yee, H. J. Sue, J. D. Earls, R. E. Hefner, Jr., J*ournal of Polymer Science: Part B : Polymer Physics*, **1997,** 35, 2363-2378
3. M. Ochi, Y. Shimizu, N. Nakanishi, Y. Murata, *Journal of Polymer Science: Part B: Polymer Physics*, **1997**, 35, 397-405
4. C. Ortiz, R. Kim, E. Rodighiero, C. K. Ober, E. J. Kramer, *Macromolecules*, **1998**, 31, 4074-4088
5. W. F. A. Su, K. C. Chen, S. Y. Tseng, *Journal of Applied Polymer Science*, **2000**, 78, 446-451
6. D. Ribera, A. Mantecon, A. Serra, *Journal of Polymer Science: Part A: Polymer Chemistry*, **2002**, 40, 3916-3926
7. M. Ochi, H. Takashima, *Polymer*, **2001**, 42, 2379-2385
8. M. Akatsuka, Y. Takezawa, *Journal of Applied Polymer Science*, **2003**, 89, 2464-2467
9. S. Song, H. Katagi, Y. Takezawa, *Polymer*, **2012**, 53, 4489-4492
10. H. Guo, J. Zheng, J. Gan, L. Liang, K. Wu, M. Lu, *Journal Materials. Science: Materials Electron*, **2016**, 27, 2754–2759
11. S. Kawamoto, H. Fujiwara, S. Nishimura, *International Journal of Hydrogen Energy*, **2016**, 41, 7500-7510
12. Y. Kim, H. Yeo, N. You, S. G. Jang, S. Ahn, K. Jeong, S. H. Lee, M. Goh, *Polymer Chemistry*, **2017**, 8, 2806-2814
13. I. Jeong, C. B. Kim, D. Kang, K. Jeong, S. G. Jang, N. You, S. Ahn, D. Lee, M. Goh, *Journal of Polymer Science: Part A: Polymer Chemistry*, **2019**, 57, 708-715
14. M. Harada, M. Ochi, M. Tobita, T. Kimura, T. Ishigaki, N. Shimoyama, H. Aoki, *Journal of Polymer Science: Part B: Polymer Physics*, **2003**, 41, 1739-1743
15. M. Harada, N. Hamaura, M. Ochi, Y. Agari, *Composites: Part B*, **2013**, 55, 306-313
16. S. Ota, K. Yamaguchi, M. Harada, *Journal of network polymer, Japan*, **2019**, 40, 278-286
17. T. Giang, J. Kim, *Journal of Industrial and Engineering Chemistry*, **2015**, 30, 77-84

18. S. Tanaka, F. Hojo, Y. Takezawa, K. Kanie, A. Muramatsu, *Polymer-Plastics Technology and Engineering*, **2018**, 57, 269-275
19. S. Tanaka, F. Hojo, Y. Takezawa, K. Kanie, A. Muramatsu, *ACS Omega*, **2018**, 3, 3562−3570
20. M. Harada, D. Morioka, M. Ochi, *Journal of Applied Polymer Science*, **2018**, DOI: 10.1002/app.46181
21. J. V. Olsen, P. Kirkegaard, N. J. Pedersen, M. Eldrup, *Physica Status Solidi C*, **2007**, 4, 40043
22. M. Eldrup, D. Lightbody, J. N. Sherwood, *Chemical Physics*, **1981**, 63, 51-58
23. S. J. Tao, *Chemical Physics*, **1972**, 56, 5499-5510
24. R. B. Gregory, *Journal of Applied Physics*, **1991**, 70, 4665
25. B.E. O'Rourke, N. Oshima, A. Kinomura, R. Suzuki, *JJAP Conference Proceedings*, 2, **2014**, 011304
26. L. Pauling, The Chemical Bond, *Cornell University Press*, New York, **1960**, p. 60, p. 119
27. M. Harada, M. Ochi, M. Tobita, T. Kimura, T. Ishigaki, N. Shimoyama, H. Aoki, *Journal of Polymer Science: Part B: Polymer Physics*, **2004**, 42, 758-7657

Part II

Thermal Conductivity and Liquid Crystalline Phase Structure of Schiff Base Type Mesogenic Epoxy Thermosets Cured by Binary Mixed Curing Agent

Chapter 4.

Thermal Conductivity and Liquid Crystalline Phase Structure of Schiff Base Type Mesogenic Epoxy Thermosets Cured by Binary Mixed Curing Agent

II-4-1. INTRODUCTION

The rapid development of high-performance electrical devices has resulted in a dramatic increase in heat generation over the past decade. Epoxy resins are generally used as the matrix resin of composite materials for IC packaging and printed circuit boards because of their excellent electrical insulation and adhesive properties. However, due to their lower thermal conductivity compared to that of inorganic fillers, effective heat transfer in the epoxy composite can be inhibited by thermal resistance at the interface between the filler surface and the matrix resin. Mesogenic epoxy resins have recently attracted tremendous attention for their unique and distinct properties. These resins can form a liquid crystalline (LC) phase structure via self-assembly of the mesogenic moieties under suitable curing conditions [1-7]. We previously investigated the relationship between the thermal conductivity and the LC phase structure including the LC domain size and the smectic phase formation [8-9].

Thus, in this chapter, Schiff base type mesogenic epoxy resin (DGETAM) was cured by the binary mixed curing agent with different chemical structures, *m*-phenylenediamine (*m*-PDA) and 4, 4'-bis (4-aminobenzoyloxy) dodecane (12BAB). The LC phase structures and thermal conductivities of the cured systems were investigated.

II-4-2. EXPERIMENTAL

II-4-2-1. Curing materials

The liquid crystalline (LC) epoxy (DGETAM; C 170 N 212, Mw = 456) was synthesized in-house.

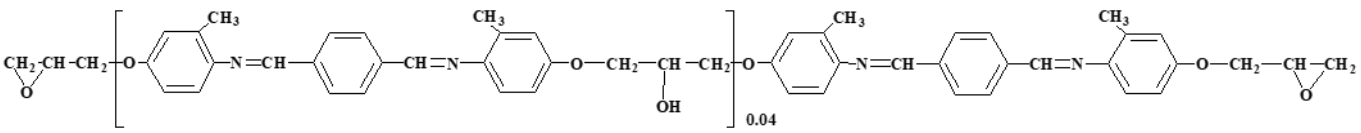

Diglycidyl ether of bisphenol A (DGEBA; JER 828EL, Mw = 370, epoxy

equivalent: 185 g/eq.) was available from Mitsubishi Chemical Co., Ltd.

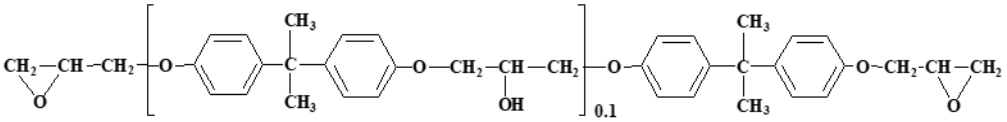

m-Phenylenediamine (*m*-PDA, m.p. 64°C, Mw = 108) was purchased from Fujifilm Wako Pure Chemical Co., Ltd.

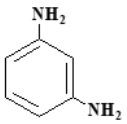

4,4'-Bis(4-aminobenzoyloxy) dodecane (12BAB, m.p. 134°C, Mw = 440) was synthesized in-house [31]. All the materials were used as received.

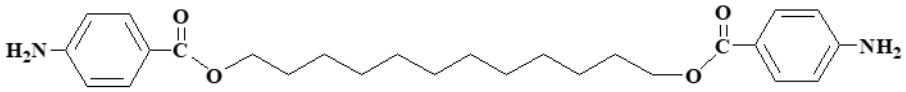

II-4-2-2. Curing method of DGETAM systems

DGETAM (0.60 g, 1.32 mmol) in an aluminum cup (coated by mold release agent, 20×20×20 mm^3) completely melted on a heating plate at 180°C. Table II-4-1 summarizes the composition ratio of the curing agent used in this study. A stoichiometric amount of the curing agent was added and stirred on a heating plate at 180°C. Finally, it was fully cured in an oven at 180°C for 2 h and then gradually cooled to ambient temperature.

Table II-4-1 Composition ratio of curing agents.

Curing system	*m*-PDA (mol%)	12BAB (mol%)
m-PDA system	100	0
12BAB_20 mol% system	80	20
12BAB_40 mol% system	60	40
12BAB system	0	100

II-4-2-3. Curing method of DGEBA systems

Similar to the DGETAM systems, DGEBA (0.60 g, 1.62 mmol) and a stoichiometric amount of the curing agent were mixed on a heating plate at 180°C. Finally, it was fully cured in an oven at 180°C for 2 h and then gradually cooled to ambient temperature.

II-4-2-4. Measurement and analysis

Curing behaviors of DGETAM systems were identified using a differential scanning calorimeter (DSC; DSC7020, Seiko Instruments Inc.) at various heating rates of 5, 10, 15, 20 K/min. The sample (about 3 mg) was filled into an aluminum pan. The apparent activation energies (E_a) were estimated by using a Kissinger equation (Eq. II-4-1) [10]

$$-E_a = R \cdot \frac{d\left[\ln\left(\frac{\beta}{T_p^2}\right)\right]}{d\left(\frac{1}{T_p}\right)} , \qquad \text{Eq. II-4-1}$$

Where R is the gas constant (8.3145 J/(K·mol)), β is the heating rate (5, 10, 15, 20 K/min), and T_p is the temperature of exothermic peak corresponding to the curing reaction.

Fourier transform infrared spectroscopy (FTIR; Spectrum 100, Perkin-Elmer Inc.) was used to investigate the chemical conversion of the epoxy resin. The sample was incorporated into a KBr pellet (Merck) and molded by a tableting machine (Shimadzu Co.). The resolution of the IR spectrum was 4 cm^{-1} and the spectra were collected after four scans. The chemical conversion of the epoxy resin was calculated from the reduction rate of the peak area at 910 cm^{-1} assigned to the epoxy group. Here, the peak area at 1600 cm^{-1} assigned to the aromatic ring was used as an internal standard.

The gelation degree of the cured systems was evaluated by the gel fraction measurement. The sample (about 0.5 g) in a cylindrical filter paper (No. 84, pore size : 8 μm, ADVANTEC TOYO KAISHA, LTD) was immersed in chloroform at room temperature for 6 h. Next, the sample were dried at 40°C for 2 h + 80°C for 3 h under vacuum pressure to remove the residual solvent. The gel fraction (X) was determined by using the equation (Eq. II-4-2):

$$X\,(\%) = m_2 / m_1 \times 100 \qquad \text{Eq. II-4-2}$$

Where m_1 is the sample's weight before solvent extraction (g), and m_2 is the sample's weight after solvent extraction (g).

The mesogenic group concentration of the cured system was estimated using

the equation (Eq. II-4-3):

Mesogenic group concentration(%)

$$= \frac{M_{\text{mesogen}}}{M_{\text{DGETAM}} + \{M_{m-\text{PDA}} \times \alpha + M_{12\text{BAB}} \times (1-\alpha)\} \times 0.5} \quad \text{Eq. II-4-3}$$

Here, the molecular weight of DGETAM, mesogenic moiety of DGETAM, *m*-PDA, and 12BAB are $M_{\text{DGETAM}} = 456$, $M_{\text{mesogen}} = 314$, $M_{m\text{-PDA}} = 108$, $M_{12\text{BAB}} = 440$. The equivalent ratio of the binary mixed curing agent was calculated based on the equation (Eq. II-4-4):

m-PDA : 12BAB = α:(1-α) Eq. II-4-4

Polarized optical microscopy under crossed Nicols (POM; BX53, Olympus Co.) was applied for the observation of the liquid crystalline phase structure in the cured systems. The sample was cut using a diamond cutter and polished with sandpaper to prepare a film of approximately 40 μm in thickness.

The dichroic map of the cured systems was drawn to observe a distribution of mesogenic orientation [11]. To determine the dichroic ratio (R), the polarized infrared (IR) spectrum was measured by a FT-IR imaging system (Frontier and Spotlight 400, Perkin-Elmer, Inc.) equipped with a wire grid polarizer. The resolution of the polarized IR spectrum was 2.0, 8.0 cm^{-1}. The spectra were collected after 4,16 scans. The thickness of the polished samples was approximately 30 μm. The pixel sizes were 50 μm, 6.25 μm. The R value was based on the peak area at 1620 cm^{-1} assigned to the stretching vibration of the C=N group since the long-axial direction of a mesogenic moiety in DGETAM is consistent with the direction of the C=N group. The *R* value was calculated from the equation (Eq. II-4-5):

$R = (A_{/\!/} - A_{\perp})/(A_{/\!/} + A_{\perp})$ Eq. II-4-5

where $A_{/\!/}$ and $A_{\perp}$ are parallel and perpendicular of polarized IR spectra, respectively. The area with *R* value (-0.05 to +0.05) was regarded as an amorphous region.

The periodic arrangement structure of the network polymer chains of the cured systems was evaluated by X-ray diffractometry (XRD; RINT-Ultima III, Rigaku Co.). The d-spacing of the ordered structure was calculated using Bragg's formula ($n\lambda = 2d\sin\theta$). The XRD patterns were measured using CuKα (λ = 0.154 nm) radiation generated at 40 kV and 40 mA at a scan rate of 1.2°/s and a sample interval of 0.02°. A

sample measuring 15×15×1.2 mm^3 was cut using a diamond cutter and polished with sandpaper and a buff polishing machine to obtain a flat, smooth surface.

The thermal conductivity (λ) at 25°C for the cured systems was determined by using the equation (Eq. II-4-6):

$$\lambda = \alpha\, C_p\, \rho\ , \qquad \text{Eq. II-4-6}$$

where α is the thermal diffusivity, C_p is the specific heat and ρ is the density. The thermal diffusivity was determined using a laser flash analyzer (LFA 447, Netzsch Co.) in accordance with the ASTM E1461-13 standard. A disk-shaped sample (diameter: 10 mm, thickness: 1 mm) was coated with a carbon layer (Graphite coat, Nihon Senpaku Co., Ltd., thickness: 15 ± 5 μm) on both the upper and lower surfaces after the sputtering process for a gold layer (thickness: 50 nm). The density of the cured systems was measured by a pycnometer method at 21°C. The specific heat was determined by DSC (DSC7020, Seiko Instruments Inc.) in the temperature range from 5°C to 100°C at a heating rate of 10°C/min.

A thermal conductive map showing thermal conductivity distribution in the cured systems was drawn by the periodic heating radiation-temperature measuring method. The phase gap between the heating and the measuring points in the plane of the sample (3.0×3.0×1.0 mm^3) was measured at 1 mm intervals and 900 points using a thermowave analyzer (TA, Bethel Inc.).

II-4-3. RESULTS AND DISCUSSION

II-4-3-1. Curing behaviors of the DGETAM systems

The effect of curing agents' chemical structures (*m*-PDA, 12BAB) on the curing behaviors of the DGETAM systems was studied by DSC (Table II-4-2). The DGETAM/12BAB system exhibited an exothermic peak at 200-250°C, corresponding to the curing reaction. This peak appeared at a higher temperature compared to that of the DGETAM/ *m*-PDA system at 140-180°C. In addition, the apparent activation energy (E_a) of the DGETAM/12BAB system (62.3 kJ/mol) was approximately 1.2 times higher than that of the DGETAM/ *m*-PDA system (51.8 kJ/mol). This result indicated that the 12BAB exhibited a lower curing reactivity compared to the *m*-PDA. In general, the curing reactivities of the amine-curing agents depend on the basicity of the amino group [12].

Therefore, it is considered that the 12BAB had the electron-withdrawing ester groups, decreasing the electron density of the neighboring aromatic ring.

The time evolution of the conversion of epoxy groups of the DGETAM systems during the isothermal curing process at 180°C was investigated by FT-IR (Figure II-4-1). The DGETAM/ *m*-PDA system showed an epoxy conversion of 91% at 5 min, while the DGETAM/12BAB system exhibited only 29% at the same time. Besides, the gel fractions at 6 min of the DGETAM/ *m*-PDA system and the DGETAM/12BAB system were 100% and 17%, respectively. Similar to the DSC result (Table II-4-2), these results suggested that the gelation reaction of the DGETAM/ *m*-PDA system occured faster than that of the DGETAM/12BAB system. Moreover, the epoxy conversions at 5 min of the binary mixed systems (DGETAM/*m*-PDA/12BAB_20 mol% system, DGETAM/*m*-PDA/12BAB_40 mol% system) were approximately 70-80% and gradually decreased with the increasing 12BAB content. This behavior can be attributed to the reduction in the curing reactivity by the addition of 12BAB. Nevertheless, DGETAM/*m*-PDA/12BAB_40 mol% system exhibited a gel fraction of 100% at 120 min. Given the above results, it is predicted that the addition of 12BAB could cause the distribution of curing rates in the system, prolonging the time to fix the network structure. In addition, the epoxy conversions of all cured systems were higher than 90%, irrespective of 12BAB content.

Table II-4-2 Apparent activation energies (E_a)and exothermic peak temperatures (T_p) of the DGETAM/*m*-PDA and DGETAM/12BAB systems.

Curing system	T_p (°C)				E_a (kJ / mol)
β (°C/min)	5	10	15	20	
DGETAM/*m*-PDA	144.0	159.9	172.7	180.6	51.8
DGETAM/12BAB	206.2	225.6	237.7	246.9	62.3

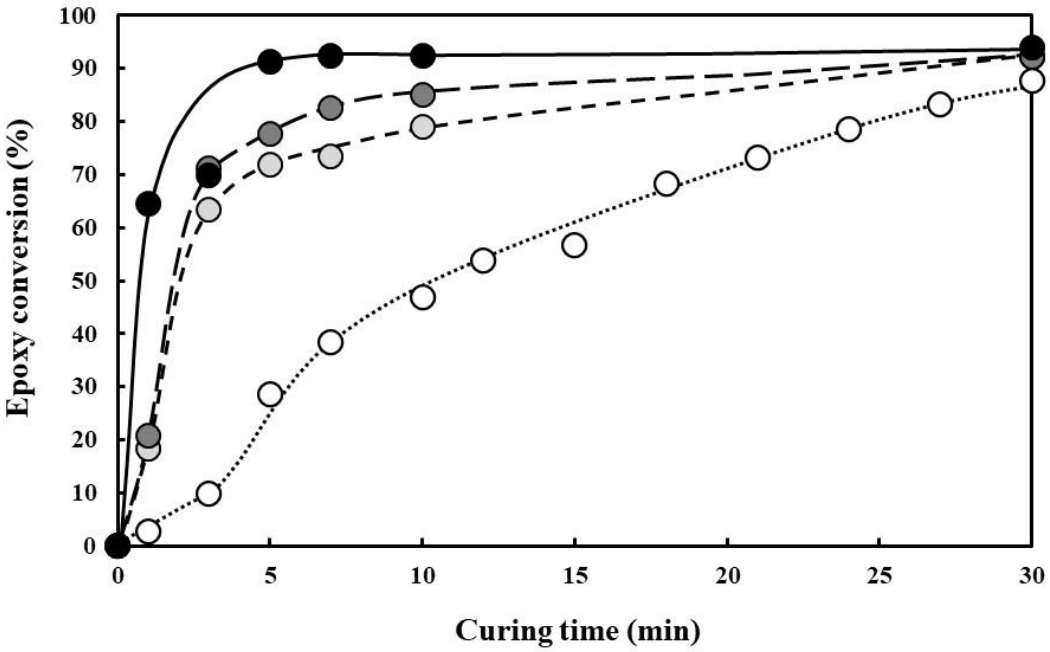

Figure II-4-1 Time dependence of epoxy conversion of the DGETAM systems (●: *m*-PDA, ● : *m*-PDA/12BAB_20 mol%, ○ : *m*-PDA/ 12BAB_40 mol%,○: 12BAB).

II-4-3-2. Liquid crystalline phase structures of the DGETAM system

The LC phase structure of the cured systems was analyzed by polarized optical microscopy (POM) (Figure II-4-2). As a result, birefringence patterns were found in the entire observation area of all cured systems, meaning the formation of the LC phase structure. In addition, some regions with a dark field changed to a bright field when the cross-nicols' angle changed from 0°to 45°. It is found that the DGETAM/ *m*-PDA system form larger LC domains (average size : ≤1 μm), while the DGETAM/*m*-PDA/12BAB_20 mol% system form small LC domains (average size : 100 μm). This data indicated the enlargement of LC domain size by using the binary mixed curing agent. However, the LC domain size decreased to ≤1 μm in the DGETAM/*m*-PDA/12BAB_40 mol% system. Moreover, the DGETAM/ 12BAB system increased the area of dark field regions. From these results, we expected that the DGETAM/ 12BAB system exhibited a lower orientation of mesogenic moieties compared to the other systems, and the 12BAB content greater than 40 mol% could inhibit the self-assembly of mesogenic moieties.

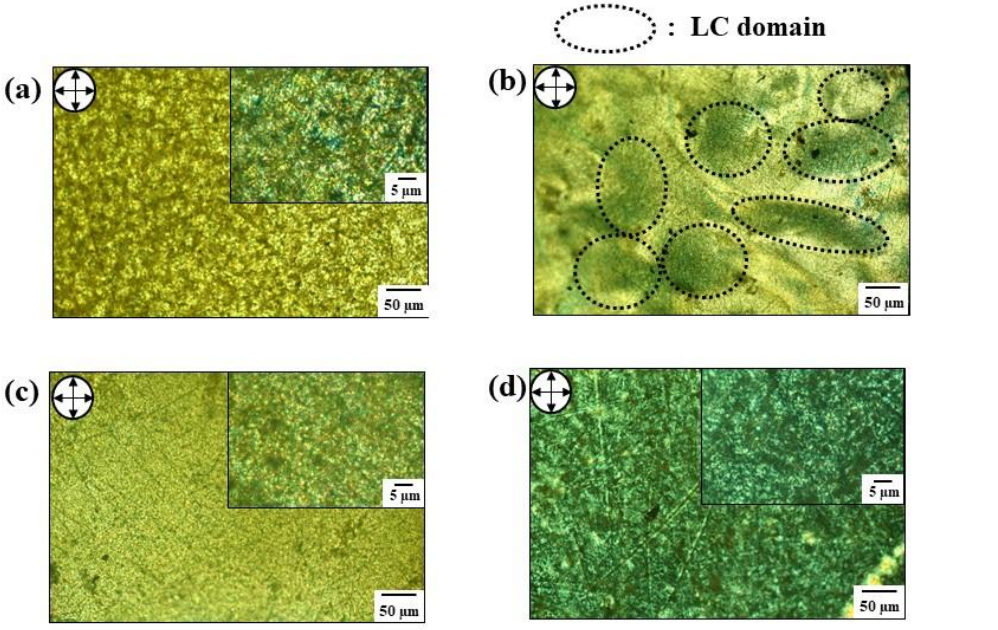

(Magnification ×200, Insert magnification : ×1000)

Figure II-4-2 POMs of the DGETAM systems: (a) *m*-PDA; (b) *m*-PDA/12BAB_20 mol%; (c) *m*-PDA/12BAB_40 mol%; (d) 12BAB.

The distribution of mesogenic orientation was studied by a dichroic map drawn by a polarized IR spectroscopy. Figure II-4-3 exhibits the dichroic ratio map, indicating the distribution of the long-axial direction of the mesogenic moiety in DGETAM. The average diameter of the LC domain structures was approximately 10 μm in the DGETAM/*m*-PDA system. However, the DGETAM/*m*-PDA/12BAB_20 mol% system exhibited a size distribution of LC domains between 50 μm to 150 μm. These results showed an almost similar trend to the POM images (Figure II-4-2). Therefore, it is discovered that the DGETAM/*m*-PDA/12BAB_20 mol% system formed larger LC domains than the other systems (Scheme II-4-1).

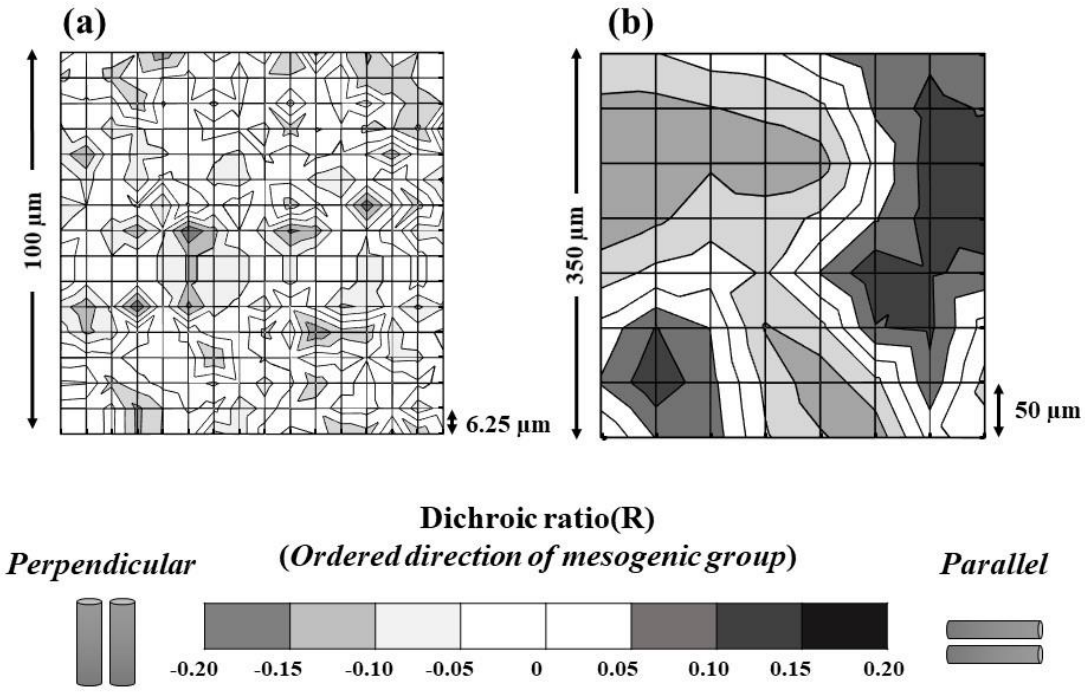

Figure II-4-3 Dichroic ratio maps of the DGETAM systems : (a) *m*-PDA; (b) *m*-PDA/12BAB_20mol%.

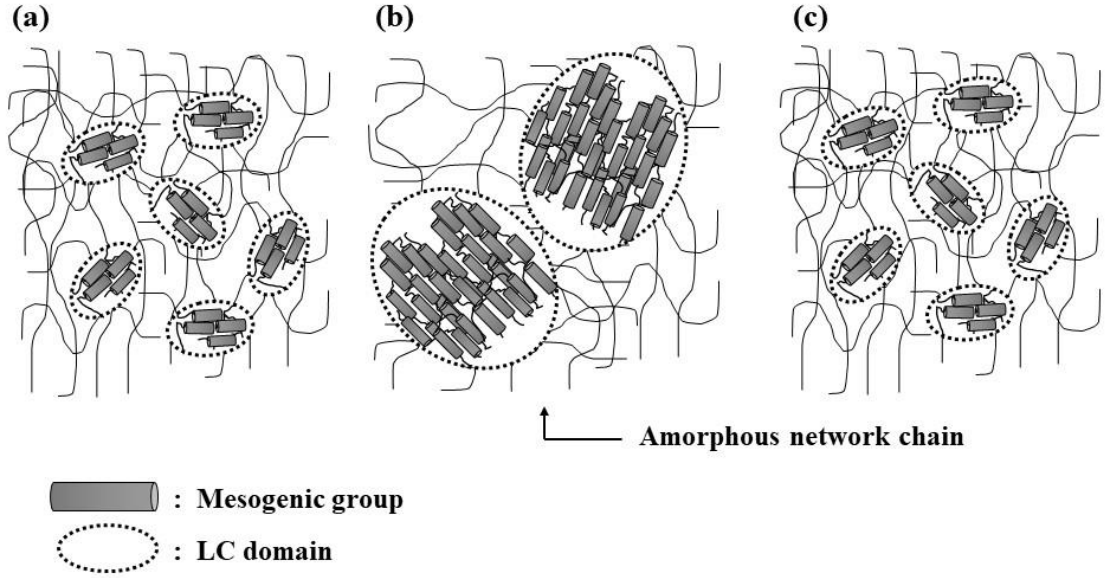

Scheme II-4-1 A schematic representation of the polydomain structure in DGETAM systems: (a) *m*-PDA; (b) *m*-PDA/12BAB_20 mol%; (c) *m*-PDA/12BAB_40 mol%.

Figure II-4-4 shows the XRD patterns of the DGETAM/*m*-PDA system, the DGETAM/*m*-PDA/12BAB_20 mol% system, and the DGETAM/*m*-PDA/12BAB_40 mol% system. A sharp peak at 2θ = 3° and a halo at 2θ = 19° were observed in all cured systems. These peaks corresponded to the smectic phase structure (2.9 nm) and the plane space (0.47 nm) of the mesogenic moieties, respectively [8](Scheme II-4-2). The ordered degree of the mesogenic network polymer chains was roughly estimated from the ratio of the smectic peak intensity at 2θ = 3° to the intensity of the halo at 2θ = 19° (I_{3°/I_{19°) since there was no big difference in the shape of halo among the samples. As a result, the DGETAM/*m*-PDA/12BAB_20 mol% system exhibited the highest value(I_{3°/I_{19°= 1.74), which was almost twice higher than the DGETAM/*m*-PDA system (I_{3°/I_{19°= 0.71) and the DGETAM/*m*-PDA/12BAB_40 mol% system(I_{3°/I_{19°= 0.53). Besides, the smectic peak completely disappeared in the DGETAM/ 12BAB system.

There are two possible reasons for this LC phase structure change in the isothermal curing systems; 1) mesogenic group concentration and 2) gelation rate. Due to the introducing flexible chains, the mesogenic group concentration of the

DGETAM/12BAB system (46%) was slightly lower than that of the DGETAM/ *m*-PDA system (62%). Furthermore, according to our previous study [13], the DGETAM/ *m*-PDA system was likely to form the smectic phase structure compared to the DGETAM/12BAB system because of the rigid and flat chemical structure. On the other hand, according to the DSC (Table II-4-2) and FT-IR (Figure II-4-1) results, it is considered that the addition of 12BAB could cause the distribution of curing rates in the system, prolonging the time to fix the network structure. Therefore, it is concluded that the DGETAM/*m*-PDA/12BAB_20 mol% system could decrease the gelation rate without reducing in the mesogenic group concentration, producing a highly ordered network structure with larger LC domain. From these results, we determined the DGETAM/*m*-PDA/12BAB_20 mol% system as an optimal composition ratio.

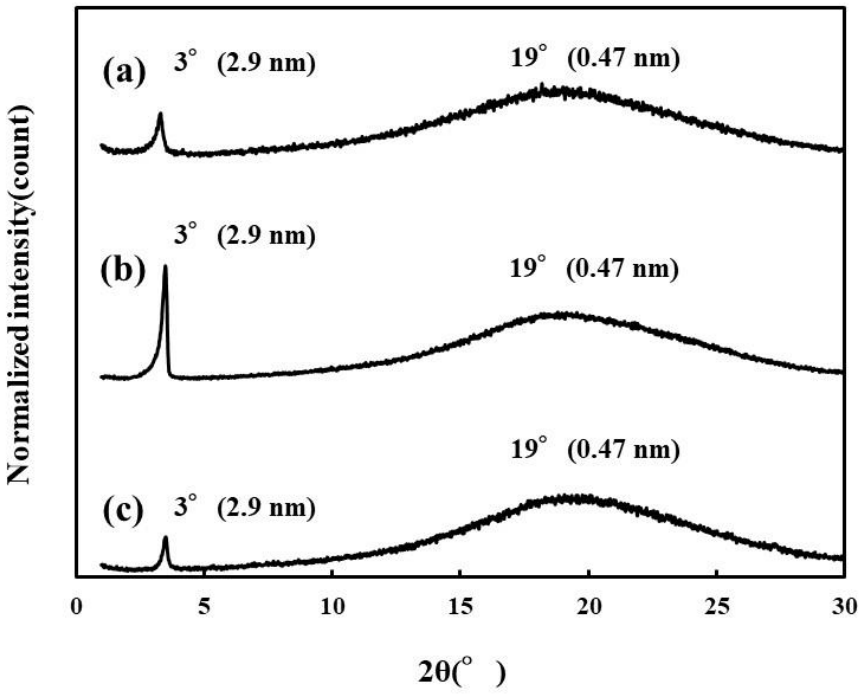

Figure II-4-4 XRD patterns of the DGETAM systems : (a) *m*-PDA; (b) *m*-PDA/12BAB_20mol%; (c) *m*-PDA/12BAB_40mol%.

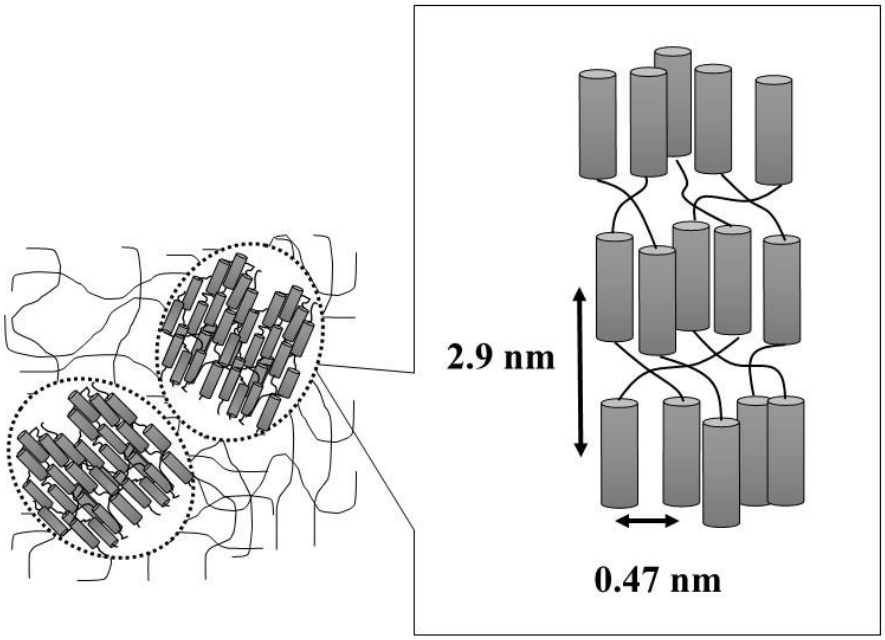

Scheme II-4-2 A schematic representation of smectic phase structure in the DGETAM system.

II-4-3-3. Thermal conductivities of the DGETAM system

The thermal conductivity of the cured systems was measured by a laser flash analyzer. Here, the DGEBA system was used as an exemplar network polymer containing no CH=N group for comparison. Table II-4-3 summarizes the thermal conductivity, thermal diffusivity, specific heat, and density of the DGETAM and DGEBA systems. As a result, the thermal conductivity of the DGETAM systems (0.27-0.31 W/(m·K)) was higher than that of the DGEBA systems (0.15-0.18 W/(m·K)). This is due to the introduction of a mesogenic structure that can provide effective phonon conductivity. Moreover, the DGETAM/*m*-PDA/12BAB_20 mol% system exhibited a slightly higher value compared to the other systems (0.27-0.30 W/(m·K)). This result can be derived from the enlarged LC domain size occurring the phonon conduction in the systems. However, there was no substantial difference in the thermal conductivities among the DGETAM systems, although the DGETAM/*m*-PDA/12BAB_20 mol% system formed a highly ordered network structure, as shown in the POM (Figure II-4-2), the dichroic map (Figure II-4-3), and the XRD (Figure II-4-4) results.

To investigate the reason, thermal conductivity distribution in the DGETAM/*m*-PDA/12BAB_20 mol% system was drawn by the periodic heating radiation-temperature measuring method. As shown in the Figure II-4-5, the DGETAM/*m*-PDA/12BAB_20 mol% system exhibited many of high thermal conductive regions compared to the other systems. In addition, the thermal conductive map indicated a clear distribution of thermal conductivity in the system (Figure II-4-6). It is expected that the locally high thermal conductive regions could be attributed to the ordered structures of mesogenic moieties. On the other hand, these results suggested that the locally low thermal conductive regions derived from the amorphous polymer chains may suppress the effective phonon conductivity in the whole material. Thus, such a thermal conductive distribution could inhibit the heat transport in the DGETAM/*m*-PDA/12BAB_20 mol% system, even though this system formed a highly ordered network structure with larger LC domains.

Table II-4-3 Thermal conductivity, thermal diffusivity, specific heat and density of the DGETAM and DGEBA systems.

Epoxy	*m*-PDA (mol%)	12BAB (mol%)	Specific heat (J/(g·K))	Density (g/cm^3)	Thermal diffusivity ($\times 10^{-3}$cm^2/s)	Thermal conductivity (W/(m·K))
DGETAM	100	0	1.09 ± 0.09	1.22 ± 0.005	2.00 ± 0.05	0.27 ± 0.02
	80	20	1.19 ± 0.02	1.22 ± 0.004	2.10 ± 0.09	0.31 ± 0.01
	60	40	1.19 ± 0.03	1.22 ± 0.001	2.05 ± 0.01	0.30 ± 0.01
	0	100	1.22	1.18 ± 0.006	1.86 ± 0.05	0.27 ± 0.01
DGEBA	100	0	0.91	1.20 ± 0.002	1.48 ± 0.01	0.16 ±0.001
	80	20	1.03	1.20 ± 0.001	1.45 ± 0.01	0.18 ± 0.001
	60	40	0.91	1.18 ± 0.001	1.43 ± 0.00	0.15 ± 0.000
	0	100	1.11	1.17 ± 0.004	1.41 ± 0.02	0.18 ± 0.003

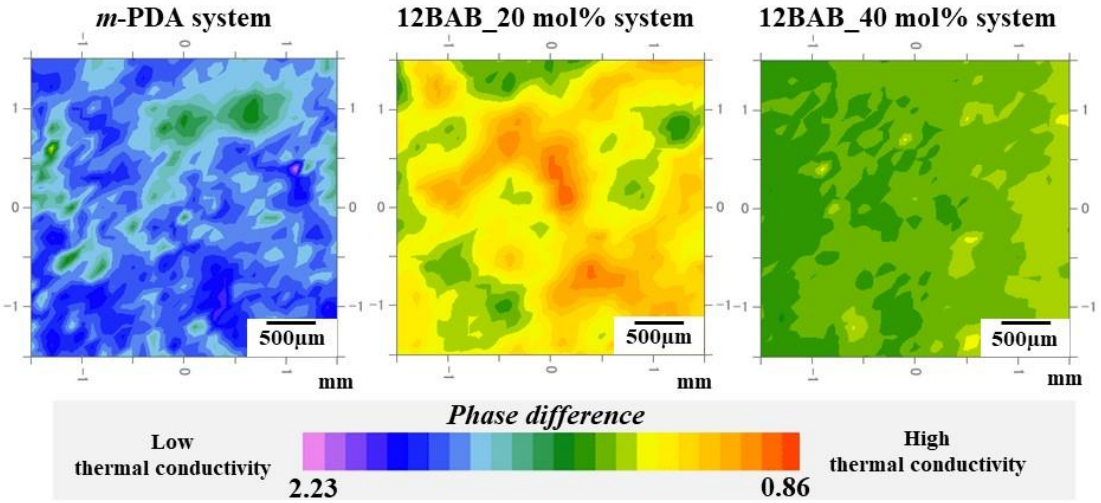

Figure II-4-5 Thermal conductive mapping (cycle heating method) of DGETAM systems.

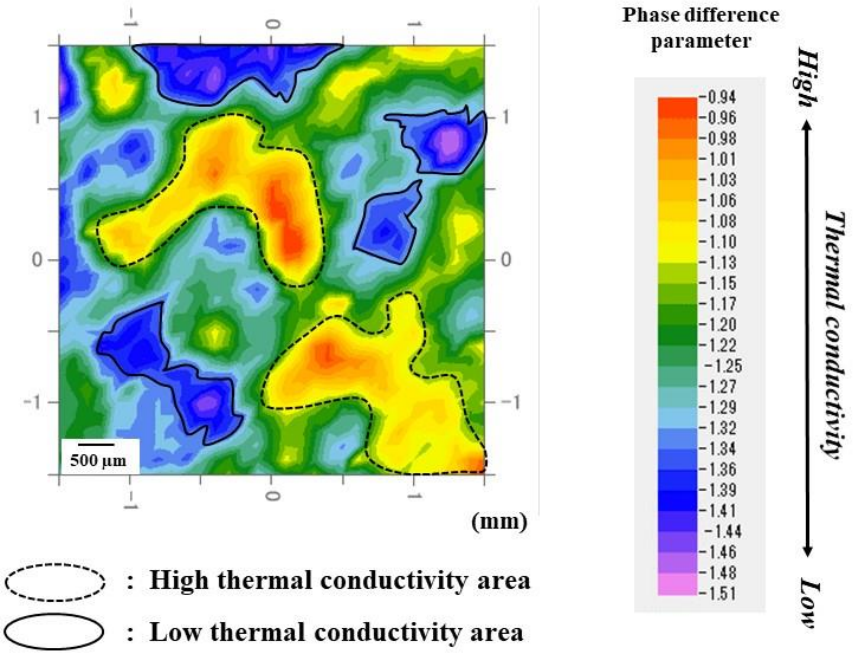

Figure II-4-6 Thermal conductive map of the DGETAM/*m*-PDA/12BAB_20 mol% system.

II-4-4. CONCLUSIONS

In this chapter, Schiff base type mesogenic epoxy resin (DGETAM) was cured by the binary mixed curing agent with different chemical structures, *m*-phenylenediamine (*m*-PDA) and 4, 4'-bis (4-aminobenzoyloxy) dodecane (12BAB). The optimal composition ratio in binary mixed curing agent to form highly ordered network structure was determined by polarized optical microscopy (POM), X-ray diffractometry (XRD), and a polarized IR mapping measurement. The results revealed that the DGETAM/*m*-PDA/12BAB_20 mol% system forms larger size of LC domain structure with a highly ordered smectic phase. According to the laser flash method, the thermal conductivity of DGETAM/*m*-PDA/12BAB_20 mol% system(0.31 W/(m・K)) is slightly higher compared to those of the other DGETAM and bisphenol A type epoxy (DGEBA) systems (0.27～0.30 (W/(m・K))). However, the thermal conductive map drawn by the periodic heating radiation-temperature measuring method indicated a clear thermal conductivity distribution in the DGETAM/*m*-PDA/12BAB_20 mol% system. These results suggest that the effective phonon conductivity may be suppressed by the locally low thermal conductive regions derived from the amorphous polymer chains, although this cured system formed a highly ordered network structure.

II-4-5. REFERENCES

1. A. Shiota, C. K. Ober, *Journal of Polymer Science Part A: Polymer Chemistry*, **1996**, 34, 1291-1303
2. C. Oritz, R. Kim, E. Rodighiero, C. K. Ober, E. J. Kramer, *Macromolecules*, **1998**, 31, 4074-4088
3. M. Ochi, Y. Shimizu, N. Nakanishi, Y. Murata, *Journal of Polymer Science Part B:Polymer Physics*, **1997**, 35, 397-405
4. M. Ochi, H. Takashima, *Polymer*, **2001**, 42, 2379-2385
5. D. Ribera, A. Mantecon, A. Serra, *Journal of Polymer Science Part A: Polymer Chemistry*, **2002**, 40, 3916-3926
6. M. Akatsuka, Y. Takezawa, *Journal of Applied Polymer Science*, **2003**, 89, 2464-2467
7. S. Song, H. Katagi, Y. Takezawa, *Polymer*, **2012**, 53, 4489-4492
8. M. Harada, M. Ochi, M. Tobita, T. Kimura, T. Ishigaki, N. Shimoyama, H. Aoki, *Journal of Polymer Science Part B: Polymer Physics*, **2003**, 41, 1739-1743
9. M. Harada, N. Hamaura, N. Ochi, Y. Agari, *Composites Part B : Engineering*, **2013**, 55, 306-313
10. H. E. Kissinger, *Journal of Research of the National Bureau of Standards*, **1956**, 57, 217-221
11. M. Harada, K. Sumitomo, Y. Nishimoto, M. Ochi, *Journal of Polymer Science, Part B: Polymer Physics*, **2009**, 47, 156-165
12. H. Yeo, *Polymer*, **2019**, 168, 209-217
13. M. Harada, J. Ando, S. Hattori, S. Sakurai, N. Sakamoto, T. Yamasaki, H. Masunaga, M. Ochi, *Polymer Journal*, **2013**, 45, 43-49

Part III

Thermal Conductivity and Liquid Crystalline Phase Structure of Schiff Base Type Mesogenic Epoxy /MgO Composites

Chapter 5.

Thermal Conductivity and Liquid Crystalline Phase Structure of Schiff Base Type Mesogenic Epoxy/MgO Composites

III-5-1. INTRODUCTION

Epoxy resin is one of the major crosslinking polymers and is widely used as a matrix resin of composites for IC packaging and printed circuit boards, because of its good electrical insulation, chemical resistance, and adhesive property. However, the drawbacks of the epoxy resin are its relatively lower thermal conductivity than that of an inorganic filler, and the fact that it causes the inhibition of the effective heat transport in the composite. One solution to this problem is the introduction of a rigid mesogenic moiety into the epoxy monomer [1-4]. In particular, a liquid crystalline (LC) epoxy resin containing a mesogenic moiety has recently gained attention because of its higher thermal conductivity than that of a non-mesogenic epoxy resin. The most prominent feature of the LC epoxy resin is the formation of a local self-assembled structure of network polymer chains [5-11]. Many studies investigated the relationship between the LC domain structure and the thermal conductivity of the LC epoxy resin [12-16].

Another solution to develop high thermal conductive epoxy composites is loading various inorganic fillers, such as boron nitride (BN), alumina (Al_2O_3), and aluminum nitride (AlN) into the epoxy matrix resin [17-19]. Nevertheless, it is more difficult and complicated to control the LC phase structure of the matrix resin in the presence of inorganic fillers. In general, the self-assembly behavior of LC molecules is strongly affected by interfacial interactions such as hydrogen bonding and dipole–dipole interactions between the filler surface and the mesogenic moieties [17-23]. For instance, Tanaka *et al.* reported that the alignment behavior of the mesogenic epoxy network polymer chains strongly depends on the hydrogen group concentration of the glass substrate surface [19]. Furthermore, it is well known that the hydroxyl group on the surface of a magnesium oxide (MgO) filler can improve the interfacial interaction between the filler and the polymer by the hydrogen bonding [24-26]. Moreover, Chandran *et al.* revealed that the doping of MgO nanoparticles remarkably changed the electro-

optical properties of the ferroelectric liquid crystals (FLCs), such as the optical tilt angle of the smectic phase structure, because of the electrostatic interactions between the MgO filler surfaces and the mesogenic moieties [27].

Thus, in this chapter, an MgO filler was dispersed in an LC epoxy resin to form a highly ordered network structure by the enhanced interfacial interaction between the filler surface and the mesogenic moieties. Magnesium oxide (MgO) is a promising thermal conductive filler because of its high thermal conductivity, nontoxicity, and unique dielectric property [28]. Our main aim is to improve the thermal conductivity of the LC epoxy composite by the synergistic effect of the high thermal conductive MgO filler and the highly ordered network polymer structure.

III-5-2. EXPERIMENTAL

III-5-2-1. Curing materials

The liquid crystalline (LC) epoxy (DGETAM; C 170 N 212, Mw = 456) was synthesized in-house.

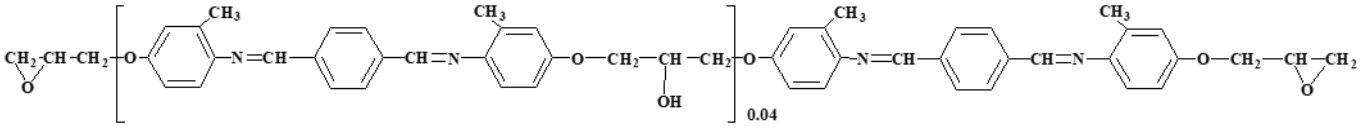

Diglycidyl ether of bisphenol A (DGEBA; JER 828EL, Mw = 370, epoxy equivalent: 185 g/eq.) was available from Mitsubishi Chemical Co., Ltd.

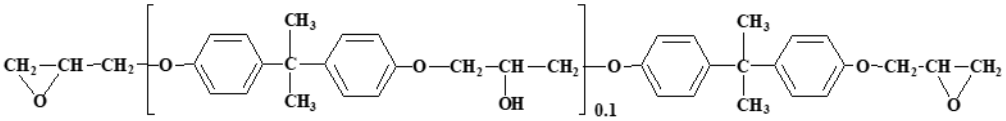

m-Phenylenediamine (*m*-PDA, m.p. 64°C, Mw = 108) was purchased from Fujifilm Wako Pure Chemical Co., Ltd.

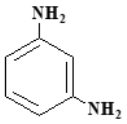

4,4’-Bis(4-aminobenzoyloxy) dodecane (12BAB, m.p. 134°C, Mw = 440) was synthesized in-house [31]. All the materials were used as received.

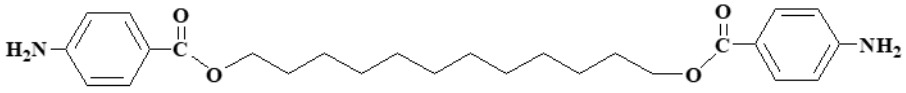

The MgO filler treated with an amino-silane coupling agent (RF50AC, average particle size: 40–70 μm (≤300 μm), density [28]: 3.6 g/cm^3, thermal conductivity: 42–60 W/(m·K) (Figure III-5-1)) was supplied by Ube Material Industries, Ltd.

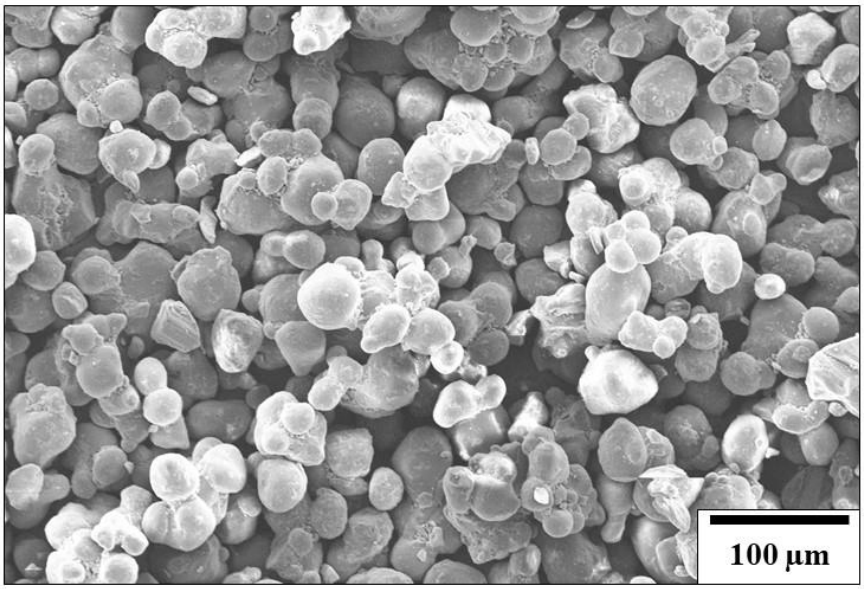

Figure III-5-1 SEM image of the MgO filler particles.

III-5-2-2. Curing method of DGETAM/MgO systems

As the MgO filler had a higher density than DGETAM, the pre-curing reaction of DGETAM was required to prevent the filler sedimentation. DGETAM and a stoichiometric amount of the binary mixed curing agent (optimizing composition ratio: *m*-PDA: 80 mol%, 12BAB: 20 mol%, see Part II) were dissolved in chloroform and pre-cured in an oil bath at 80°C for 45 min (epoxy conversion (FT–IR): 30%). The MgO filler (10–60 wt%) was uniformly dispersed in the mixture by a planetary centrifugal mixer at 2000 rpm for 5 min and then evaporated under vacuum to remove the solvent. After the obtained mixture was poured into an aluminum mold, then melted and stirred on a heating plate at 180°C. Finally, it was cured at 180°C for 2 h in an oven and gradually cooled to room temperature.

III-5-2-3. Curing method of DGEBA/MgO systems

For the uniform filler dispersion in the matrix resin, the mixture of DGEBA and MgO filler (10–60 wt%) was stirred on a heating plate at 180°C. A stoichiometric amount of the binary mixed curing agent was added and the obtained mixture was stirred for 8-10 min until the viscosity was sufficiently high to prevent filler sedimentation. Finally, it was cured at 180°C for 2 h in an oven and gradually cooled to room temperature. Both the DGETAM and the DGEBA composites showed approximately 90% epoxy conversion, which was confirmed by the FT–IR measurement.

III-5-2-4. Measurement and analysis

A scanning electron microscopy (SEM, JCM-6000, JEOL) was used to evaluate the filler dispersion in the composites. The observed surface was coated with a platinum layer (thickness : 20 nm) after the argon etching using by a cross-session polisher (IB-09010CP, JEOL).

The thermal conductivity (λ) at 25°C of the composite was determined by using the formula below :

$$\lambda = \alpha\, C_p\, \rho \qquad \text{Eq. III-5-1}$$

where, α is thermal diffusivity, C_p is specific heat and ρ is density. The thermal diffusivity was determined by the laser flash analysis (LFA 447, Netzsch Co.) in accordance with ASTM E1461-13 standard. The discotic shaped sample (diameter: 10 mm, thickness: 1 mm) was coated with a carbon layer (Graphite coat, Nihon Senpaku Co., Ltd., thickness : 15 ± 5 μm) each on upper/lower surfaces after the sputtering process of a gold layer (thickness : 50 nm), to avoid the direct transmission of the laser flash light through electrical insulating materials. The density measurement of the composite was conducted by a pycnometer method at 21°C. The specific heat was determined by a differential scanning calorimeter (DSC7020, Hitachi High-Tech Science Co.) in a temperature range from 5°C to 100°C at a heating rate of 10°C/min. Experimental thermal conductivity was compared with the value predicted using Bruggeman's theoretical model (Eq. III-5-2), where V_f is volume fraction of filler, k is thermal conductivity and the subscripts c, m, f refer to the composite, matrix resin and filler, respectively.

$$1 - V_f = \frac{k_f - k_c}{k_f - k_m}\left(\frac{k_m}{k_c}\right)^{1/3} \quad \text{Eq. III-5-2}$$

The LC phase structure of the composite was observed by using a polarized optical microscopy under the cross-nicols (BX53, OLYMPUS Co.) The thickness of the polished samples was approximately 40 μm.

The dichroic map of the composite was drawn to observe a distribution of mesogenic orientation [30]. To determine the dichroic ratio (R), the polarized infrared (IR) spectrum was measured by a FT-IR imaging system (Frontier and Spotlight 400, Perkin-Elmer, Inc.) equipped with a wire grid polarizer. The resolution of the polarized IR spectrum was 4 cm^{-1}. The spectra were collected after 64 scans. The thickness of the polished samples was approximately 40 μm. The observed area of the sample was 75×75 μm^2 (12×12 points, pixel size: 6.25 μm). The R value was based on the peak area at 1620 cm^{-1} assigned to the stretching vibration of the C=N group since the long-axial direction of a mesogenic moiety in DGETAM is consistent with the direction of the C=N group. The *R* value was calculated from the following equation below:

$R = (A_{/\!/} - A_{\perp})/(A_{/\!/} + A_{\perp})$ Eq. III-5-3

where $A_{/\!/}$ and $A_{\perp}$ are parallel and perpendicular of polarized IR spectra, respectively. The area with *R* value (-0.05 to +0.05) was regarded as an amorphous region.

The periodic arrangement structure of network polymer chains was evaluated by a reflection type X-ray diffractometer (RINT-Ultima III, Rigaku Co.) The d-spacing of the ordered structure was calculated using Bragg's formula ($n\lambda = 2d\sin\theta$). XRD patterns were measured by CuKα(λ = 0.154 nm) radiation generated at 40 kV and 40 mA with a scan rate of 1.2°/s and a sample interval of 0.02°.

III-5-3. RESULTS AND DISCUSSION

III-5-3-1. Thermal conductivity of DGETAM/MgO systems

The thermal conductivity of the DGETAM/MgO and the DGEBA/MgO systems was measured and is shown in Figure III-5-2. Table III-5-1 summarizes the thermal conductivity, thermal diffusivity, specific heat, and density of these composites. In the unloaded epoxy system, the thermal conductivity of the DGETAM system was 0.27

W/(m·K), which was approximately 1.3 times higher than that of the DGEBA system (0.21 W/(m·K)), as the introduction of a mesogenic structure can provide effective phonon conductivity. In addition, the thermal conductivity of both the DGETAM/MgO and the DGEBA/MgO systems increased with increasing filler content. This was because the MgO filler had higher thermal conductivity (42–60 W/(m·K)) than the neat resins. Clearly, the DGETAM/MgO system drastically increased with a filler content of more than 12 vol%. The maximum value of the DGETAM/MgO_33 vol% system (1.41W/(m·K)) was approximately 1.7 times higher than that of the DGEBA/MgO_32 vol% system (0.84 W/(m·K)). This result revealed that the incorporation of the MgO filler into the mesogenic epoxy resin was one of the most effective ways to improve the thermal conductivity of the epoxy composite. Furthermore, to investigate in detail the thermal conductive enhancement in these composites, the experimental thermal conductivities were compared with the corresponding values predicted using Bruggeman's theoretical model (k_m = 0.27 W/(m·K) for the DGETAM/MgO system, k_m = 0.21 W/(m·K) for the DGEBA/MgO system). In the non-mesogenic DGEBA/MgO system, the experimental thermal conductivity was almost consistent with the prediction line. However, the experimental value of the mesogenic DGETAM/MgO system always exceeded the prediction line, and the gap between the experimental and the theoretical values remarkably increased with an increase in the filler content.

To consider the reason for this significant enhancement of thermal conductivity in the DGETAM/MgO system, the filler dispersion was evaluated. Figure III-5-3 shows the scanning electron micrographs (SEMs) of the fracture surface after the argon etching in the DGETAM/MgO system. No obvious filler aggregation was found in the (a) and (b) DGETAM/MgO_12 vol% systems. In contrast, a partial aggregation of the MgO filler was observed in the (c) and (d) DGETAM/MgO_33 vol% systems. Although Bruggeman's theoretical model cannot be applied accurately to the high-loading composite including the filler aggregation, this is not a sufficient reason to explain such a significant improvement of the thermal conductivity in the DGETAM/MgO system, as shown in Figure III-5-2.

To investigate the enhancement of the thermal conductivity of the matrix resin as a function of the filler content, the experimental thermal conductivity of the

DGETAM/MgO system was compared with Bruggeman's theoretical prediction lines calculated using various values of the matrix resin's thermal conductivity (k_m) ranging from 0.27 W/(m·K) to 0.45 W/(m·K), as shown in Figure III-5-4. We found that the experimental thermal conductivity of the high-loading DGETAM/MgO system was consistent with the prediction lines of a higher k_m value. For example, the apparent thermal conductivity of the matrix resin in the DGETAM/MgO_33 vol% system was 0.45 W/(m·K), which was approximately 1.7 times higher than the experimental thermal conductivity of the neat DGETAM system (0.27 W/(m·K)). These data suggest that the thermal conductivity of the matrix resin gradually increased with an increase in the filler content. Consequently, this significant improvement of the thermal conductivity in the DGETAM/MgO composite must be affected by the thermal conductive enhancement of the matrix resin itself.

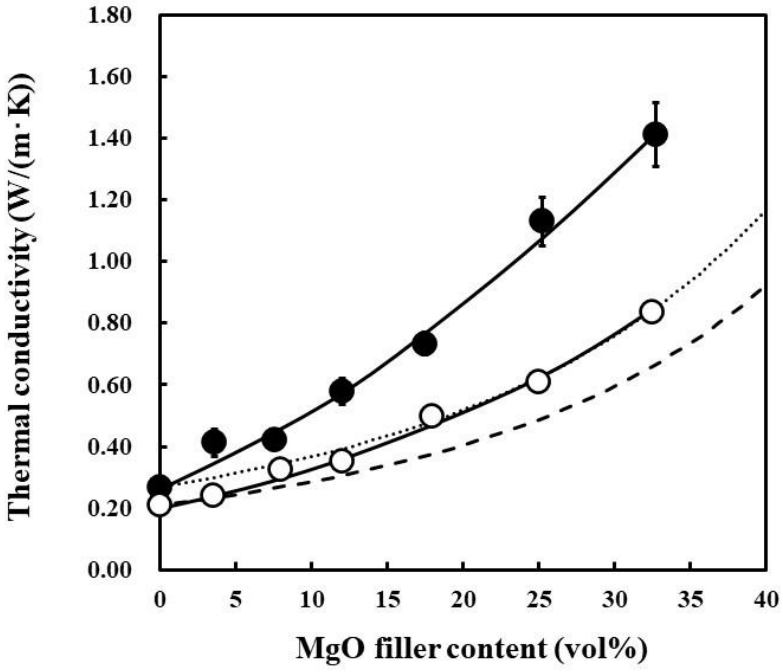

Figure III-5-2 Experimental thermal conductivity and Bruggeman's theoretical prediction of the composites(●: DGETAM/MgO system, ○:DGEBA/MgO system, Bruggeman's theory prediction ····· : k_m = 0.27 W/mK, – – – : k_m = 0.21 W/mK)

Table III-5-1 Thermal conductivity, thermal diffusivity, specific heat and density of the DGETAM/MgO and DGEBA/MgO systems.

Epoxy	MgO (wt%)	MgO (vol%)	Density (g/cm^3)	Specific heat (J/(g·K))	Thermal diffusivity (mm^2/s)	Thermal conductivity (W/(m·K))
DGETAM	0	0	1.21 ± 0.006	1.26 ± 0.01	0.18 ± 0.02	0.27 ± 0.02
	10	4	1.29 ± 0.004	1.25 ± 0.04	0.26 ± 0.03	0.41 ± 0.04
	20	8	1.37 ± 0.003	1.24 ± 0.01	0.25 ± 0.01	0.42 ± 0.01
	30	12	1.45 ± 0.006	1.18 ± 0.01	0.34 ± 0.03	0.58 ± 0.04
	40	17	1.57 ± 0.006	1.09 ± 0.05	0.43 ± 0.02	0.73 ± 0.04
	50	25	1.81 ± 0.002	1.13 ± 0.04	0.55 ± 0.04	1.13 ± 0.08
	60	33	1.96 ± 0.005	1.03 ± 0.01	0.70 ± 0.05	1.41 ± 0.10
DGEBA	0	0	1.20 ± 0.002	1.26 ± 0.002	0.14 ± 0.002	0.21 ± 0.003
	10	4	1.26 ± 0.004	1.24 ± 0.004	0.15 ± 0.007	0.24 ± 0.011
	20	8	1.39 ± 0.004	1.27 ± 0.004	0.19 ± 0.003	0.33 ± 0.006
	30	12	1.44 ± 0.008	1.18 ± 0.008	0.21 ± 0.008	0.35 ± 0.016
	40	18	1.64 ± 0.001	1.15 ± 0.001	0.26 ± 0.003	0.50 ± 0.007
	50	25	1.80 ± 0.002	1.08 ± 0.002	0.31 ± 0.011	0.61 ± 0.021
	60	32	1.95 ± 0.005	1.03 ± 0.005	0.42 ± 0.016	0.84 ± 0.030

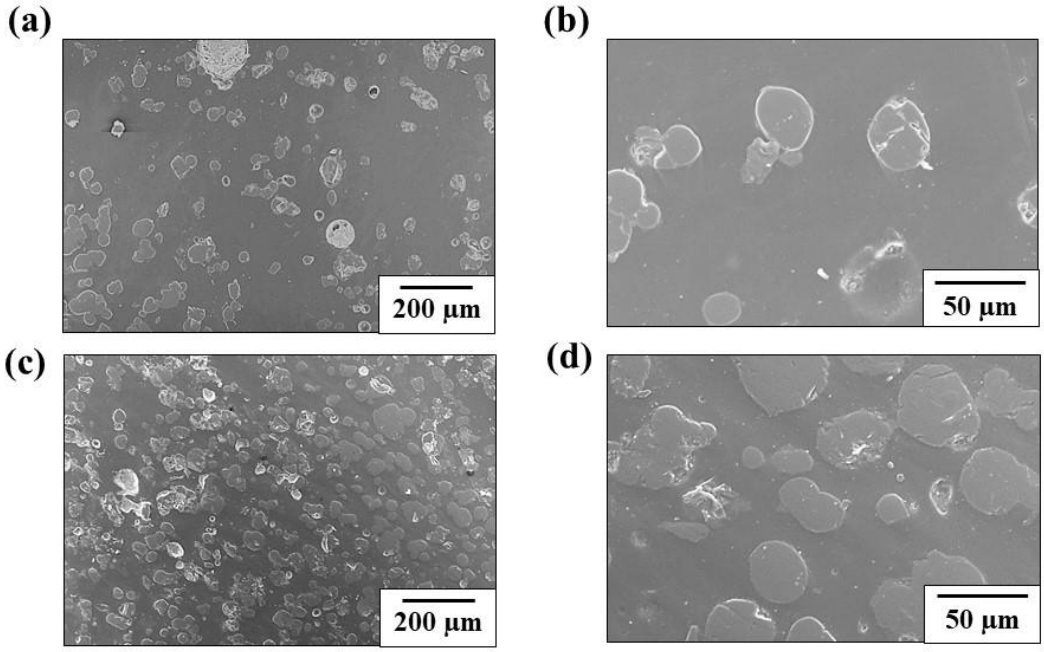

Figure III-5-3 Scanning electron micrographs of (a)(b) DGETAM/MgO_12 vol% system and (c)(d) DGETAM/MgO_33 vol% system.

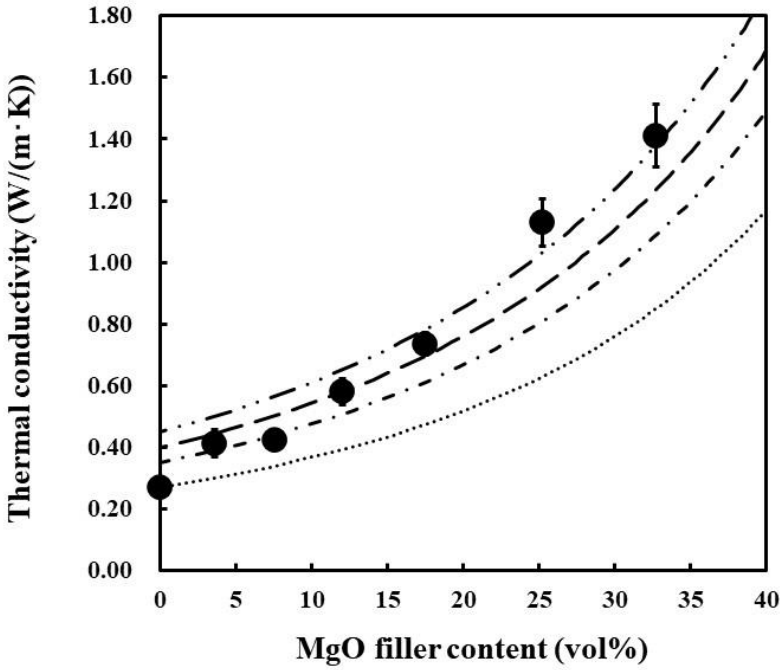

Figure III-5-4 Experimental thermal conductivity and Bruggeman's theoretical prediction of the DGETAM/MgO systems.
(····· : k_m = 0.27 W/mK, – · – · – : k_m = 0.35 W/mK
— — –: k_m = 0.40 W/mK, — · · — : k_m = 0.45 W/mK)

III-5-3-2. Analysis of LC phase structure and relationship to thermal conductivity

To consider the reason for this thermal conductive enhancement of the matrix resin in the DGETAM/MgO system, the LC phase structure of the composite was analyzed. Figure III-5-5 shows polarized optical micrographs (POMs) under the cross-nicols of the neat DGETAM system and the DGETAM/MgO system with various filler contents. A birefringence pattern was found in the entire observation area of the (a) and (d) neat DGETAM systems. Additionally, some regions with a dark field (marked by a black line circle) changed to a bright field when the angle of the cross-nicols changed from (a) 0°to (d) 45°, indicating the formation of the LC phase structure. In contrast, uniformly dispersed MgO filler and some holes (marked by a red line circle) were found in the (b) and (e) DGETAM/MgO_4 vol% systems, and (c) and (f) DGETAM/MgO_12 vol% systems. We considered that these small holes were generated by debonding the filler during the polishing process of the POM sample. Moreover, clear birefringence patterns were observed in the entire observation area excluding the MgO filler and the holes. The observation of the dark–bright inversion regions by changing the cross-nicols

from 0°to 45° (marked by a black line circle) confirmed, the coexistence of the LC domain structure and the MgO filler in all of the composites, even at a relatively higher content.

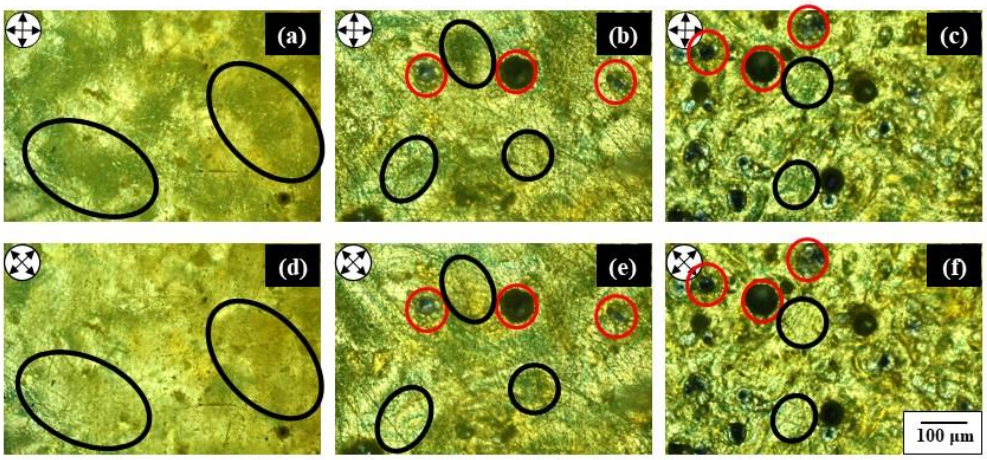

Figure III-5-5 Polarized optical micrographs (the cross nicols 0° and 45°)of (a)(d) neat DGETAM system, (b)(e) DGETAM/MgO_4 vol% system, (c)(f) DGETAM/MgO_12 vol% system.

To investigate thoroughly the segmental orientation of network polymer chains between MgO filler particles, the dichroic ratio map of the DGETAM/MgO_4 vol% system was drawn by using a polarized IR spectroscopy. Figure III-5-6(a) exhibits the dichroic ratio map, indicating the distribution of the long-axial direction of the mesogenic moiety in DGETAM. The observed matrix region (marked by a red square, as shown in Figure III-5-6(b)) was centered between two MgO particles with the inter-particle distance of 75 μm. In this map, many regions with positive or negative dichroic ratio (R) values were observed, suggesting the local formation of a self-assembled structure of the mesogenic moieties. In contrast, some of the regions with a nearly zero R value (−0.05 to +0.05) were regarded as an isotropic phase structure. The average diameter of the LC domain structures was approximately 10 μm in the DGETAM/MgO_ 4 vol%. Compared with the POM observation, as shown in Figure III-5-5(b) and, Figure III-5-5(e), we considered that the large-sized LC domain cluster was formed by the assembly of small LC domain structures. Scheme III-5-1 represents a schematic model of the network

polymer structure of the DGETAM/MgO composite, including a local arrangement of mesogenic groups in an amorphous network chain.

Figure III-5-7 shows the XRD patterns of the neat DGETAM and DGETAM/MgO systems. A sharp peak at 2θ = 3° and a halo at 2θ = 19° were observed for the (a) neat DGETAM system. These peaks corresponded to the smectic phase structure (2.9 nm) and the plane space (0.47 nm) of the mesogenic moieties, respectively [M. Harada, M. Ochi, M. Tobita, T. Kimura, T. Ishigaki, N. Shimoyama, H. Aoki, Journal of Polymer Science, Part B : *Polymer Physics*, **2004**, 42, 758-765]. This result indicated that the smectic phase structure was locally formed in the LC domain structure, as shown in Scheme III-5-2. For the (b) and, (c) DGETAM/MgO composites, similar XRD patterns were observed in the range between 2θ = 1° and 35°. Moreover, several sharp peaks in the range between 2θ = 35°and 100° were related to the rock-salt crystal structure of the MgO filler [28]. These results demonstrated that the formation of the smectic phase structure occurred even in the presence of the MgO filler.

To discuss the MgO loading effect on the LC phase structure of the DGETAM/MgO system, the ordered degree of the mesogenic network polymer chains was roughly estimated from the ratio of the smectic peak intensity at 2θ = 3° to the intensity of the halo at 2θ = 19° ($I_{3°}/I_{19°}$). As a result, (b)' DGETAM/MgO_12 vol% system and (c)' DGETAM/MgO_33 vol% system showed considerably higher ratio of the peak intensity ($I_{3°}/I_{19°}$ = 1.6 and 1.4, respectively), than the (a) neat DGETAM system ($I_{3°}/I_{19°}$ = 0.5). These data suggested that the ordered degree of mesogenic network polymer chains was significantly increased by the MgO loading. In our previous study [3], the LC phase structure of DGETAM composites loaded with pristine boron nitride (BN) fillers was also investigated. The XRD analysis indicated that the ordered degree of the DGETAM/BN system gradually decreased with increasing filler content and the smectic peak totally disappeared at high filler content of 30 vol%. This data suggests that self-assembly of the network polymer chains was inhibited by the pristine BN filler. Contrastingly, in the present study, the ordered degrees of the DGETAM/MgO system hardly decreased with increasing filler content from 12 vol% to 33 vol%, indicating the highly ordered network structure can form even in the high loading composite.

According to the past papers published by many of the other researchers, the LC

molecule alignment strongly depended on the surface free energy of the inorganic material. The following two factors could be considered for this promotion of the mesogenic polymer chain orientation in the DGETAM/MgO system. Firstly, the surface of magnesium oxide (MgO) generally contains hydroxyl groups generated from the heterolytic dissociation of water molecules [24-26]. Therefore, the smectic phase formation could be induced by the interfacial interaction of the mesogenic moieties with a hydroxyl group on the MgO filler surface. Secondary, the MgO filler used in this study was partially treated with an amino-silane coupling agent to improve the interfacial interaction between the filler surface and the matrix resin. Kubono *et al.* investigated whether the number and the position of polar functionalities, such as the amino and the hydroxyl groups influenced the thermoplastic LC molecule alignment. For instance, cyano-substituted biphenyl molecules can be adsorbed by an amino-coated glass substrate, resulting in a homeotropic alignment [22]. Namely, this phase structural change of the LC epoxy resin after the loading of the MgO filler could be derived from the strong interfacial interaction between the LC epoxy molecules and the amino groups on the MgO filler surface.

As mentioned in a previous section, the experimental thermal conductivity of the DGETAM/MgO system was considerably higher than the prediction line based on Bruggeman's theoretical model (Figure III-5-2). Furthermore, the apparent thermal conductivity of the matrix resin in the DGETAM/MgO system gradually increased from 0.27 to 0.45 W/(m·K) with an increase in the filler content (Figure III-5-4). Thus, we considered that this significant enhancement of the thermal conductivity in the DGETAM/MgO system could be influenced by the improvement of the matrix resin's thermal conductivity. A similar phenomenon has already been reported [31]. Yoshihira reported that the thermal conductivity of polyester matrix resin gradually increases from 0.52 to 1 W/(m·K) with an increase in the MgO filler content. This is attributed to the formation of a well-stacked lamellar structure of the mesogenic polyester resin between the MgO fillers at a high filler content, resulting in the formation of a more effective heat path. According to the XRD analysis of the LC phase structure in the DGETAM/MgO system, the promotion of the network polymer chain alignment in the LC epoxy resin was found by the loading of the MgO filler (Figure III-5-7). Therefore, the enhancement of

the thermal conductivity in the matrix resin was considered to be caused by the improvement of the mesogenic orientation due to the strong interaction between the MgO filler surface and the matrix resin.

A high thermal conductive composite was successfully developed by the introduction of an MgO filler into an LC epoxy resin. The thermal conductivity of the obtained LC epoxy composite was considerably higher than that of a non-mesogenic epoxy composite at the same filler content. Furthermore, the experimental thermal conductivity of the LC epoxy composite was significantly higher than the value predicted using Bruggeman's theoretical model. According to the LC phase analysis, this unexpected improvement of the thermal conductivity of the obtained LC epoxy composite could be affected by the enhancement of the thermal conductivity in the matrix resin, which was caused by the formation of a highly ordered smectic phase structure. This work provides an effective strategy for developing the high thermal conductive composite materials that can solve the issue of the thermal management of the high-performance electrical devices.

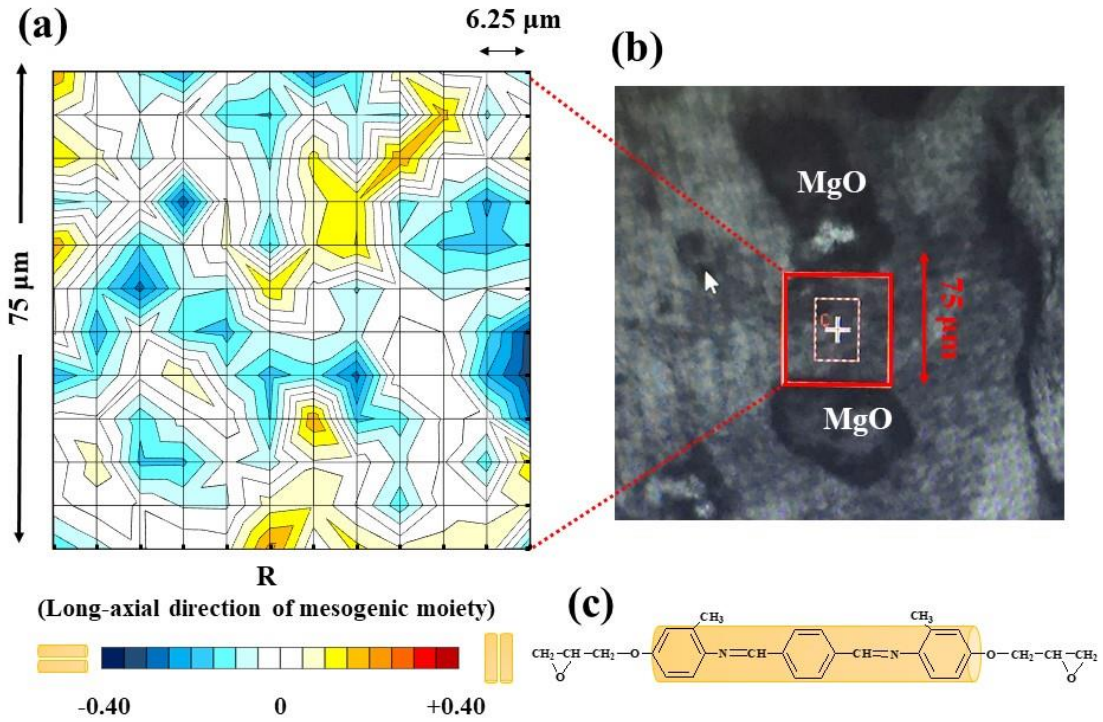

Figure III-5-6 (a) Dichroic ratio map, (b) optical micrograph of the DGETAM/MgO_4 vol% system and (c) chemical structure of the mesogenic moiety in DGETAM.

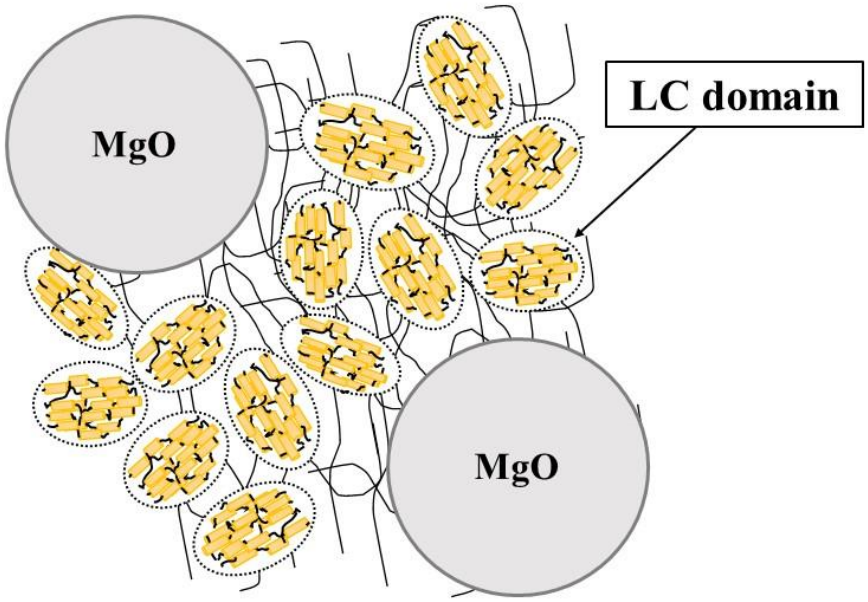

Scheme III-5-1 Schematic model of possible network structure in DGETAM/MgO composite.

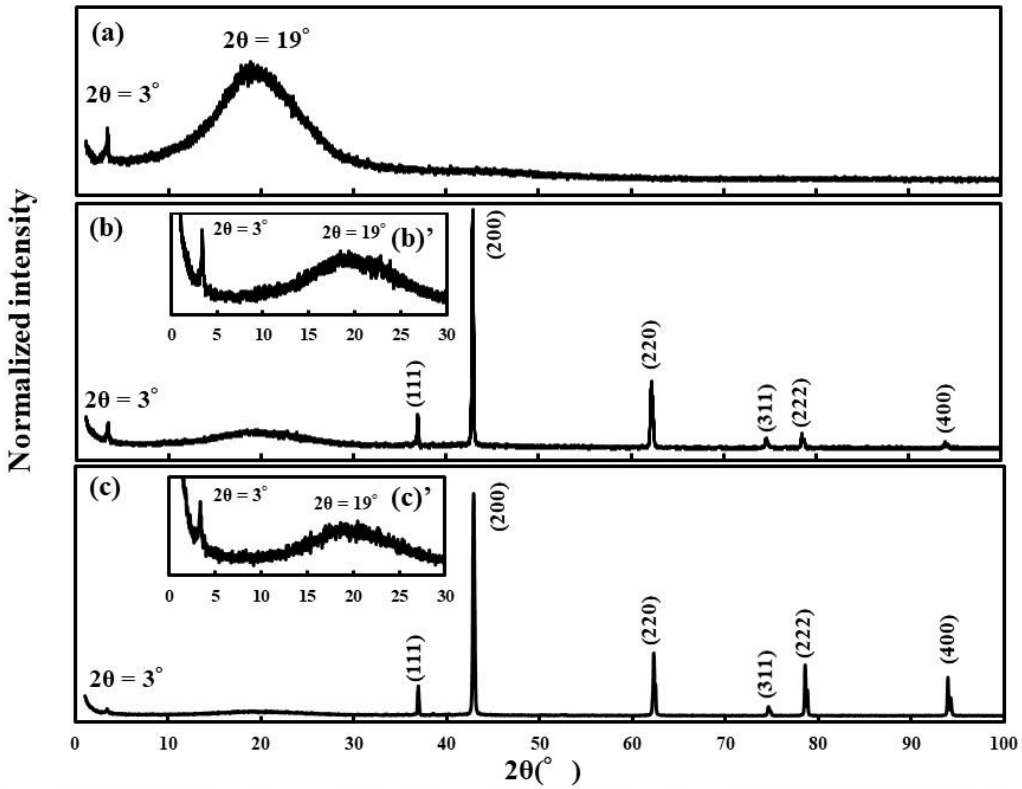

Figure III-5-7 XRD patterns of the (a) neat DGETAM system, (b)(b)' DGETAM/MgO_12 vol% system and (c)(c)'DGETAM/MgO_33 vol% system.

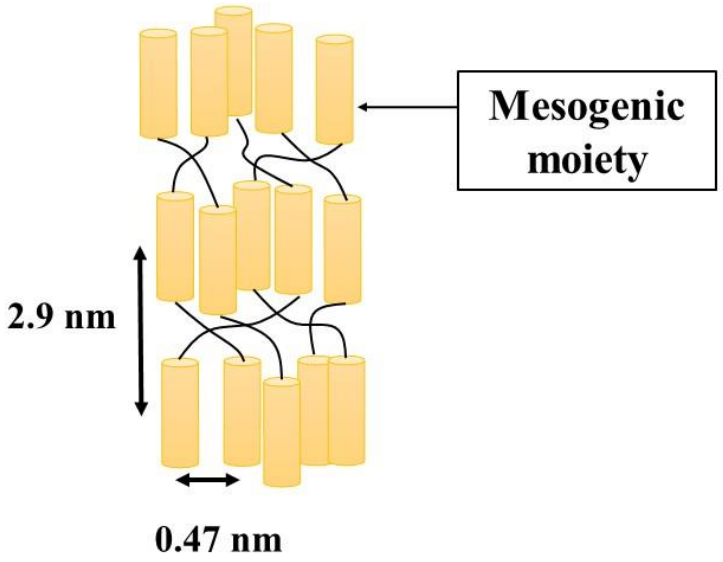

Scheme III-5-2 Schematic model of smectic phase structure.

III-5-4. CONCLUSIONS

In this chapter, a high thermal conductive composite was successfully developed by the introduction of an MgO filler into an LC epoxy resin. The thermal conductivity of the obtained LC epoxy composite was considerably higher than that of a non-mesogenic epoxy composite at the same filler content. Furthermore, the experimental thermal conductivity of the LC epoxy composite was significantly higher than the value predicted using Bruggeman's theoretical model. According to the LC phase analysis, this unexpected improvement of the thermal conductivity of the obtained LC epoxy composite could be affected by the enhancement of the thermal conductivity in the matrix resin, which was caused by the formation of a highly ordered smectic phase structure. This work provides an effective strategy for developing the high thermal conductive composite materials that can solve the issue of the thermal management of the high-performance electrical devices.

III-5-5. REFERENCES

1. M. Akatsuka, Y. Takezawa, *Journal of Applied Polymer Science*, **2003**, 89, 2464-2467
2. S. Song, H. Katagi, Y. Takezawa, *Polymer*, **2012**, 53, 4489-4492
3. M. Harada, N. Hamaura, M. Ochi, Y. Agari, *Composites: Part B*, **2013**, 55, 306-313
4. M. Harada, D. Morioka, M. Ochi, *Journal of Applied Polymer Science*, **2018**, doi:10.1002/APP.46181
5. A. Shiota, C. K. Ober, *Journal of Polymer Science, Part A: Polymer Chemistry*, **1996**, 34, 1291-1303
6. C. Ortiz, R. Kim, E. Rodighiero, C. K. Ober, E. J. Kramer, *Macromolecules*, **1998**, 31, 4074-4088
7. Q. Lin, A. F. Yee, H. J. Sue, J. D. Earls, R. E. Hefner, Jr., *Journal of Polymer Science, Part B : Polymer Physics*, **1997**, 35, 2363-2378
8. W. F. A. Su, K. C. Chen, S. Y. Tseng, *Journal of Applied Polymer Science*, **2000**, 78, 446-451
9. D. Ribera, A. Mantecon, A. Serra, *Journal of Polymer Science, Part A: Polymer Chemistry*, **2002**, 40, 3916-3926
10. M. Ochi, Y. Shimizu, N. Nakanishi, Y. Murata, *Journal of Polymer Science, Part B: Polymer Physics,* **1997**, 35, 397-405
11. M. Ochi, H. Takashima, *Polymer*, **2001**, 42, 2379-2385
12. S. Kawamoto, H. Fujiwara, S. Nishimura, *International Journal of Hydrogen Energy*, **2016**, 41, 7500-7510
13. I. Jeong, C. B. Kim, D. Kang, K. Jeong, S. G. Jang, N. You, S. Ahn, D. Lee, M. Goh, *Journal of Polymer Science, Part A: Polymer Chemistry*, **2019**, 57, 708-715
14. Y. Kim, H. Yeo, N. You, S. G. Jang, S. Ahn, K. Jeong, S. H. Lee, M. Goh, *Polymer Chemistry*, **2017**, 8, 2806-2814
15. H. Guo, J. Zheng, J. Gan, L. Liang, K. Wu, M. Lu, *J. Mater. Sci.: Mater. Electron*, **2016**, 27, 2754–2759
16. S. Ota, K. Yamaguchi, M. Harada, *Journal of network polymer*, *Japan*, **2019**, 40, 278-286
17. T. Giang, J. Kim, *Journal of Industrial and Engineering Chemistry*, **2015**, 30, 77-84

18. S. Tanaka, F. Hojo, Y. Takezawa, K. Kanie, A. Muramatsu, *Polymer-Plastics Technology and Engineering*, **2018**, 57, 269-275
19. S. Tanaka, F. Hojo, Y. Takezawa, K. Kanie, A. Muramatsu, *ACS Omega*, **2018**, 3, 3562−3570
20. T. Uchida, K. Ishikawa, M. Wada, *Molecular Crystals and Liquid Crystals*, **1980**, 60, 37-52
21. J. J. Mallon, P. M. Adams, *Molecular Crystals and Liquid Crystals Science and Technology*, **1992**, 213, 173-186
22. A. Kubono, H. Onoda, K. Inou, K. Tanaka, R. Akiyama, *Molecular Crystals and Liquid Crystals*, **2002**, 373, 127-141
23. J. Jang, J. Bae, S. Yoon, *Journal of Materials Chemistry*, **2003**, 13, 676-681
24. Y. Li, X. S. Sun, *Biomacromolecules*, **2010**, 11, 1847–1855
25. F. Du, H. Tang, D. Huang, *International Journal of Polymer Science*, **2013**, doi:10.1155/2013/541823
26. F. Du, W. Yang, F. Zhang, C. Tang, S. Liu, L. Yin, W. Law, *ACS Applied Materials and Interfaces*, **2015**, 7, 14397-14403
27. A. Chandran, J. Prakash, K. K. Naik, A. K. Srivastava, R. Dąbrowski, M. Czerwiński, A. M. Biradar, *J. Mater. Chem. C*, **2014**, 2, 1844-1853
28. J. Hornak, P. Trnka, P. Kadlec, O. Michal, V. Mentlík, P. Šutta, G. M. Csányi, Z. Á. Tamus, *Nanomaterials*, **2018**, 8, doi:10.3390/nano8060381
29. A. A. Wereszczak, T. G. Morrissey, C. N. Volante, P. J. Farris, Jr., R. J. Groele, R. H. Wiles, H. Wang, *IEEE Transactions on Components, Packaging and Manufacturing Technology*, **2013**, 3, 1994-2005
30. M. Harada, K. Sumitomo, Y. Nishimoto, M. Ochi, J*ournal of Polymer Science, Part B: Polymer Physics*, **2009,** 47, 156-165
31. S. Yoshihara, M.Tokita, T. Ezaki, M. Nakamura, M. Sakaguchi, K. Matsumoto, J. Watanabe, *Journal of Applied Polymer Science*, **2014**, doi: 10.1002/app.39896

Chapter 6.

The Effect of Filler Surface Treatment on Thermal Conductivity and Liquid Crystalline Phase Structure of Schiff Base type Mesogenic Epoxy/MgO Composites

III-6-1. INTRODUCTION

Mesogenic epoxy resins have recently attracted tremendous attention for their unique and distinct properties. These resins can form a liquid crystalline (LC) phase structure via self-assembly of the mesogenic moieties under suitable curing conditions [1-7]. Moreover, mesogenic epoxy resins exhibit higher thermal conductivity compared to those of conventional epoxy resins [8-13]. We previously investigated the relationship between the thermal conductivity and the LC phase structure including the LC domain size and the smectic phase formation [14-16]. Owing to such excellent thermal conductivity, various inorganic fillers have been dispersed in mesogenic epoxy resins to develop high thermal conductivity composites. [15, 17]. We also found that the thermal conductivity of a highly ordered LC epoxy/BN composite was 2.2 W/(m·K) at 30 vol% loading, which was dramatically higher than that of an isotropic system (1.5 W/(m·K)) at the same filler loading [15]. Generally, the self-orientation behavior of LC molecules is affected by the interfacial interactions between the surface of the inorganic materials and the mesogenic moieties [18, 19]. Tanaka *et al.* revealed that the surface free energy of a glass substrate influenced the ordered structure of a mesogenic epoxy resin [20]. In addition, Jang *et al.* showed that the ordered structure of a mesogenic epoxy resin can be induced by polar functional groups, such as hydroxyl and carboxyl groups on the carbon nanotube surface [21].

In this chapter, an MgO filler was used to form a highly ordered network structure of a mesogenic epoxy resin. To achieve this goal, we designed an optimal surface-treated layer of the MgO filler via surface adsorption of the mesogenic epoxies. Our main objective was to investigate the effect of the epoxy-adsorbed MgO filler on the network polymer structure and the thermal conductivity of the LC epoxy composites.

III-6-2. EXPERIMENTAL

III-6-2-1. Curing materials

The liquid crystalline (LC) epoxy (DGETAM; C 170 N 212, Mw = 456) was synthesized in-house.

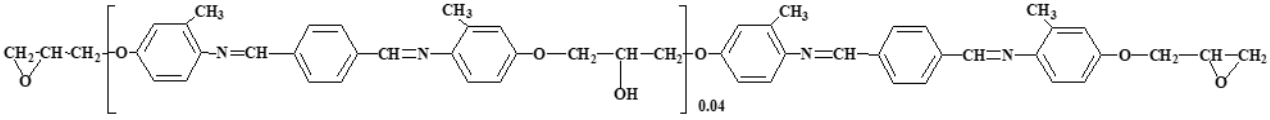

Diglycidyl ether of bisphenol A (DGEBA; JER 828EL, Mw = 370, epoxy equivalent: 185 g/eq.) was available from Mitsubishi Chemical Co., Ltd.

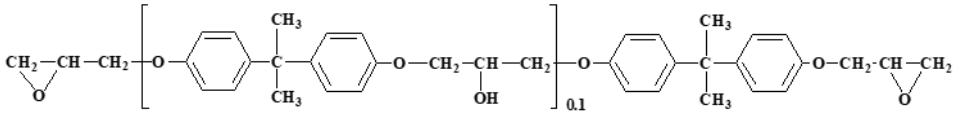

m-Phenylenediamine (*m*-PDA, m.p. 64°C, Mw = 108) was purchased from Fujifilm Wako Pure Chemical Co., Ltd.

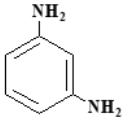

4,4'-Bis(4-aminobenzoyloxy) dodecane (12BAB, m.p. 134°C, Mw = 440) was synthesized in-house [31]. All the materials were used as received.

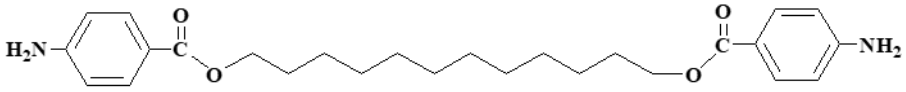

The MgO filler treated with an amino-silane coupling agent (RF50AC, average particle size: 40–70 μm (≤300 μm), density [22]: 3.6 g/cm^3, thermal conductivity: 42–60 W/(m·K) (see Figure III-5-1)) was supplied by Ube Material Industries, Ltd.

III-6-2-2. Preparation method for epoxy-adsorbed MgO fillers

As mentioned earlier, the MgO filler used in this study (MgO_$_{Amine}$) was treated with an amino-silane coupling agent. The MgO_$_{Amine}$ filler (9.00 g) and an epoxy monomer (3.00 g) (DGETAM or DGEBA) were mixed in an aluminum container (30×30×30 mm^3) and stirred on a heating plate under the following conditions: 180°C for 10 min + 200°C for 20 min + 215°C for 20 min. This heating temperature was selected based on the phase transition temperature of DGETAM, which was confirmed by

differential scanning calorimetry (DSC). This heating process was applied for the epoxy adsorption by the MgO_{Amine} filler. Subsequently, the obtained mixture was washed with chloroform (150 mL) in an oil bath at 80°C for 45 min to remove the excess amount of unreacted epoxy monomers. The epoxy-adsorbed MgO fillers (MgO_{DGETAM} and MgO_{DGEBA}) were dried at 80°C for 2 h under vacuum pressure to remove the residual solvent.

III-6-2-3. Curing method of DGETAM/MgO composites

As the MgO filler had a higher density than the DGETAM, pre-reaction of the DGETAM was required to prevent filler sedimentation. DGETAM (0.60 g, 1.32 mmol) and a stoichiometric amount of the curing agent (0.11 g, 0.658 mmol) were dissolved in chloroform (5 mL) and stirred in an oil bath at 80°C for 45 min to proceed with the pre-reaction. The composition ratio of the curing agent used in this study was determined based on our previous paper (*m*-PDA: 80 mol% (0.057 g, 0.526 mmol) see Part II), 12BAB: 20 mol% (0.058 g, 1.32×10^{-4} mol)). After the pre-reaction, the obtained solution was poured into a stainless-steel container and mixed with the MgO filler (10–60 wt%, 0.08–1.07 g) using a planetary centrifugal mixer (ARE-310, Thinky Corp.) at 2000 rpm for 5 min. Subsequently, the solution was evaporated under vacuum at ambient temperature for 2 h to remove the solvent. The obtained mixture was transferred to an aluminum mold ($20\times20\times20$ mm^3) and stirred on a heating plate at 180°C. Finally, it was fully cured in an oven at 180°C for 2 h and then gradually cooled to ambient temperature. A neat epoxy resin was also prepared by the same curing method as used for the 10–60 wt% loading composites.

For the high-loading system (70 wt%), the pre-reaction step was skipped because of the high viscosity of the composite. The MgO filler (1.67 g) and DGETAM (0.60 g, 1.32 mmol) were mixed in an aluminum mold ($20\times20\times20$ mm^3) and stirred on a heating plate at 190°C for 3 min to obtain a homogeneous mixture. Subsequently, it was mixed with a stoichiometric amount of the binary mixed curing agent (0.11 g, 0.658 mmol) and stirred until the viscosity was sufficiently high to prevent filler sedimentation. Finally, it was cured in an oven at 180°C for 2 h and then gradually cooled to ambient temperature. The obtained sample was 20×20 mm^2 with the thickness of 1.2-2.0 mm, depending on the

filler content.

III-6-2-4. Curing method of DGEBA/MgO composites

Non-mesogenic DGEBA (1.20 g, 3.24 mmol) and the MgO filler (3.46 g, 70 wt%) were mixed in an aluminum mold (40×20×20 mm^3) and stirred on a heating plate at 190°C for 3 min to obtain a homogeneous mixture. Subsequently, it was mixed with a stoichiometric amount of the binary mixed curing agent (*m*-PDA: 80 mol% (0.14 g, 1.29 mmol), 12BAB: 20 mol% (0.14 g, 0.324 mmol)) and stirred until the viscosity was sufficiently high to prevent filler sedimentation. Finally, it was cured in an oven at 180°C for 2 h and then gradually cooled to ambient temperature. The obtained sample was 40×20 mm^2 with a thickness of about 2.0 mm.

III-6-2-5. Measurement and analysis

Scanning electron microscopy (SEM; JCM-6000, Jeol) was used to observe the shape of the MgO filler and the filler dispersion of the fully cured composites. All samples were placed on carbon tape and coated with a platinum layer (thickness: 20 nm) on the upper surface to avoid an electrical charge forming on the insulating material surfaces and to increase the generation efficiency of secondary electrons. Prior to the platinum sputtering process, the surface of the fully cured composite was etched with argon gas using a cross-section polisher (IB-09010CP, Jeol).

X-ray photoelectron spectroscopy (XPS; ESCA-3400HSE, Shimadzu Corp.) was used for the characterization of the MgO filler surface. The XPS spectra were measured using MgKα radiation generated at 10 kV and 15 mA. All samples were placed on carbon tape. Here, the binding energy at 285 eV assigned to hydrocarbons was used as a reference for the energy calibration. The XPS spectra were analyzed by Gaussian function to investigate the chemical shift in detail.

Thermogravimetric analysis (TGA; TG/DTA 6200, Seiko Instruments Inc.) was used to estimate the amount of epoxy adsorption. The test conditions were under air atmosphere (gas flow rate: approximately 350 mL/min) from 30°C to 800°C at a heating rate of 10°C/min. The weight of the sample was 30 ± 5 mg for the MgO filler and 10 ± 2 mg for the epoxy monomer. An empty platinum pan was used as the reference.

Polarized optical microscopy under crossed Nicols (POM; BX53, Olympus Co.) was applied for the observation of the liquid crystalline phase structure in the fully cured composite. The sample was cut using a diamond cutter and polished with sandpaper to prepare a film of approximately 40 μm in thickness.

The periodic arrangement structure of the network polymer chains of the fully cured composite was evaluated by X-ray diffractometry (XRD; RINT-Ultima III, Rigaku Co.). The d-spacing of the ordered structure was calculated using Bragg's formula ($n\lambda = 2d\sin\theta$). The XRD patterns were measured using CuKα (λ = 0.154 nm) radiation generated at 40 kV and 40 mA at a scan rate of 1.2°/s and a sample interval of 0.02°. A sample measuring 15×15×1.2 mm^3 was cut using a diamond cutter and polished with sandpaper and a buff polishing machine to obtain a flat, smooth surface.

The free volume of the fully cured composite was studied by positron annihilation lifetime spectroscopy (PALS) by means of a slow positron beam [23] housed at the National Institute of Advanced Industrial Science and Technology (AIST). A sample measuring 10×10×1 mm^3 was placed on a Kapton polyimide sheet to avoid positron penetration of the metallic sample holder. Positron irradiation was carried out under vacuum (~10^{-4} Pa) at room temperature. The time resolution was 0.29 ns full width at half-maximum (FWHM) and the incident energy was set at 8 keV. The total count for positron annihilation events was 2×10^6 for the positron lifetime spectrum of each sample. All PALS spectra were analyzed using a resolution code [24] and decomposed into three lifetime components: τ_1, τ_2, τ_3 ($\tau_1 < \tau_2 < \tau_3$). The long-lived component τ_3 corresponds to the *o*-positronium (*o*-Ps) pick-off annihilation lifetime. The mean free volume radius (R) was estimated by using a spherical infinite potential well model (Tao–Eldrup model, (Eq. III-6-1) [25, 26]:

$$\tau_3 = \frac{1}{2}\left[1 - \frac{R}{R_0} + \frac{1}{2\pi}\sin\left(\frac{2\pi R}{R_0}\right)\right]^{-1} , \qquad \text{Eq. III-6-1}$$

where $R_0 = R + \Delta R$ and ΔR is the radius of the free electron cloud (ΔR = 0.166 nm).

The mean free volume (V_f) was determined using the equation (Eq. III-6-2):

$$V_f = \frac{4}{3}\pi R^3 , \qquad \text{Eq. III-6-2}$$

Fourier transform infrared spectroscopy (FTIR; Spectrum 100, Perkin-Elmer Inc.) was used to investigate the chemical conversion of the epoxy resin. The sample was

incorporated into a KBr pellet (Merck) and molded by a tableting machine (Shimadzu Co.). The resolution of the IR spectrum was 4 cm^{-1} and the spectra were collected after four scans. The chemical conversion of the epoxy resin was calculated from the reduction rate of the peak area at 910 cm^{-1} assigned to the epoxy group. Here, the peak area at 1600 cm^{-1} assigned to the aromatic ring was used as an internal standard.

A nonresonance forced vibration viscoelastometer (Rheogel-E4000, UBM Co.) was used for the dynamic mechanical analysis (DMA) of the fully cured composite. A bar-shaped sample measuring 4.0×30.0×0.4 mm^3 was tested in the tension mode. The test was carried out under the following conditions: −150°C to 80°C under a nitrogen atmosphere, followed by and then 80°C to 250°C under an air atmosphere at a heating rate of 2°C/min. The vibration frequency and amplitude were adjusted to 10 Hz and ±5 μm, respectively.

The thermal conductivity (λ) at 25°C for the fully cured composite was determined by using the equation (Eq. III-6-3):

$$\lambda = \alpha\, C_p\, \rho\ , \qquad \text{Eq. III-6-3}$$

where α is the thermal diffusivity, C_p is the specific heat and ρ is the density. The thermal diffusivity was determined using a laser flash analyzer (LFA 447, Netzsch Co.) in accordance with the ASTM E1461-13 standard. A disk-shaped sample (diameter: 10 mm, thickness: 1 mm) was coated with a carbon layer (Graphite coat, Nihon Senpaku Co., Ltd., thickness: 15 ± 5 μm) on both the upper and lower surfaces after the sputtering process for a gold layer (thickness: 50 nm). The density of the fully cured composite was measured by a pycnometer method at 21°C. The specific heat was determined by DSC (DSC7020, Seiko Instruments Inc.) in the temperature range from 5°C to 100°C at a heating rate of 10°C/min. The thermal conductivity was compared with the value predicted using Bruggeman's theoretical model (Eq. III-6-4), where X_f is the volume fraction of the MgO filler, k is the thermal conductivity, and the subscripts c, m, and f refer to the composite, the matrix resin (0.27 W/(m·K)) and the MgO filler(42 W/(m·K)), respectively. The value of X_f is calculated from the literature values of the MgO density (~3.6 g/cm^3 [22]).

$$1 - X_f = \frac{k_f - k_c}{k_f - k_m}\left(\frac{k_m}{k_c}\right)^{1/3} \qquad \text{Eq. III-6-4}$$

III-6-3. RESULTS AND DISCUSSION

III-6-3-1. Characterization of epoxy-adsorbed MgO fillers

Optical photographs of the various surface-treated MgO fillers and DGETAM are shown in Figure III-6-1. In contrast with the (a) MgO_$_{Amine}$ filler having a white color, the (b)MgO_$_{DGETAM}$ filler exhibited a pale-yellow appearance. This result suggests the possible surface adsorption of (c) DGETAM in the MgO_$_{DGETAM}$ filler. However, the color of the (d) MgO_$_{DGEBA}$ filler remained unchanged since DGEBA is a colorless viscous liquid. SEM images of the MgO fillers used in this study are presented in Figure III-6-2. The (a) MgO_$_{Amine}$ filler has a rounded shape and a wide particle-size distribution (approximately 20–90 μm). On the other hand, it seems that the (b) MgO_$_{DGETAM}$ filler and (c) MgO_$_{DGEBA}$ filler tend to form a cluster of small-sized particles.

A surface chemical analysis of the MgO fillers was conducted by XPS. Figure III-6-3. shows the O1s spectra and the fitting curves analyzed by Gaussian function. The O1s peak of the (a) MgO_$_{Amine}$ filler was observed at 532.4 eV, corresponding to the chemical structure of the silane coupling agent. In a comparison with the (a) MgO_$_{Amine}$ filler, the peaks of the (b) MgO_$_{DGETAM}$ filler and (c) MgO_$_{DGEBA}$ filler were shifted to a higher binding energy (533.0 and 532.7 eV, respectively). To investigate the chemical shift in detail, the O1s spectra were decomposed into the following five components: Si-O-Si (530.7 eV), C-O-H (531.5 eV), Si-OH (532.7 eV), and C-O-Si (534.1 eV) bonds [27], and a C-O-C bond (533.3 eV), which was determined based on the O1s spectrum of the DGETAM. In the (a) MgO_$_{Amine}$ filler, the peak at 533.3 eV corresponding to the C-O-C bond (indicated by a blue dotted line) was very low and broad. Contrastingly, in the (b) MgO_$_{DGETAM}$ filler and (c) MgO_$_{DGEBA}$ filler, the peak height of the C-O-C bond (533.3 eV) was higher than in the (a) MgO_$_{Amine}$ filler. In particular, the (b) MgO_$_{DGETAM}$ filler exhibited a significant higher C-O-C bond peak. This result demonstrates that the epoxies were successfully adsorbed onto the filler surface. Since the surface of the MgO_$_{Amine}$ filler contained an amino-silane coupling agent, this epoxy adsorption was considered to be a chemical adsorption by the covalent bonding between the epoxy group and the amino group of the amino-silane coupling agent. In addition, as mentioned in the Experimental, the excess amount of epoxy monomers was used for this adsorption treatment; consequently, it is expected that the unreacted epoxy groups possibly remained in the surface-treated layer, partially forming the covalent bonding between the surface-treated

layer and the matrix resin in the composites.

The amount of epoxy adsorption was evaluated by TGA under an air atmosphere. As shown in Figure III-6-4, a drastic weight reduction related to the pyrolysis of the epoxy monomers (DGETAM and DGEBA) occurred in the temperature range above 300°C. It can be seen from the enlarged view of the TGA chart that the residual weight of all the MgO fillers gradually decreased in three steps. The first step, below 300°C, is attributed to the desorption of the physically adsorbed water. The second step, from 300°C to 500°C, corresponds to the pyrolysis of the organic surface-treated layers. The final step, above 500°C, is derived from the desorption of the hydroxyl groups in the MgO lattice [28]. In addition, the MgO_{DGETAM} filler and MgO_{DGEBA} filler showed a higher weight loss compared to that of the MgO_{Amine} filler. Based on the weight loss of the MgO_{Amine} filler at 800°C, the amount of epoxy adsorption in the MgO_{DGETAM} filler and MgO_{DGEBA} filler was estimated at 0.18% and 0.09%, respectively.

The characteristics of the MgO fillers used in this study are summarized below;

(I) MgO_{Amine} : the MgO filler was surface-treated with an amino-silane coupling agent. It is considered that the amino-silane molecules were immobilized onto the MgO filler surfaces via a covalent bonding and a physically adsorption.

(II) MgO_{DGETAM} : as the further surface-treatment, mesogenic epoxy (DGETAM) was adsorbed onto the surface of MgO_{Amine} filler. It is expected that this epoxy adsorbed layer was prepared by a chemical adsorption treatment via the covalent bonding between the epoxies and the amino-silane coupling agent. Due to the excess amount of the epoxy monomers used in this adsorption treatments, there are possibly unreacted epoxy groups in the surface treated layer.

(III) MgO_{DGEBA} : non-mesogenic epoxy (DGEBA) was also adsorbed onto the surface of MgO_{Amine} filler for the comparative investigation of the mesogenic moiety effect of the MgO_{DGETAM} filler. It is believed that the DGEBA adsorbed layer was also formed by the covalent bonding between the epoxies and the amino-silane coupling agent.

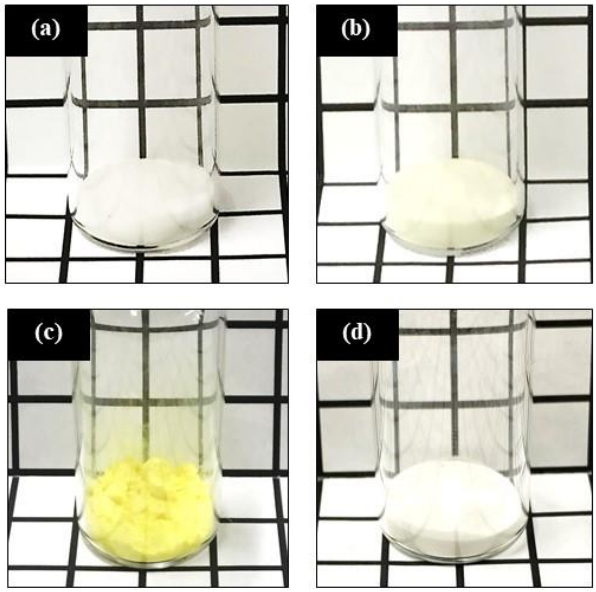

Figure III-6-1 Optical photographs of (a)MgO_$_{Amine}$ filler, (b)MgO_$_{DGETAM}$ filler, (c)DGETAM, and (d) MgO_$_{DGEBA}$ filler.

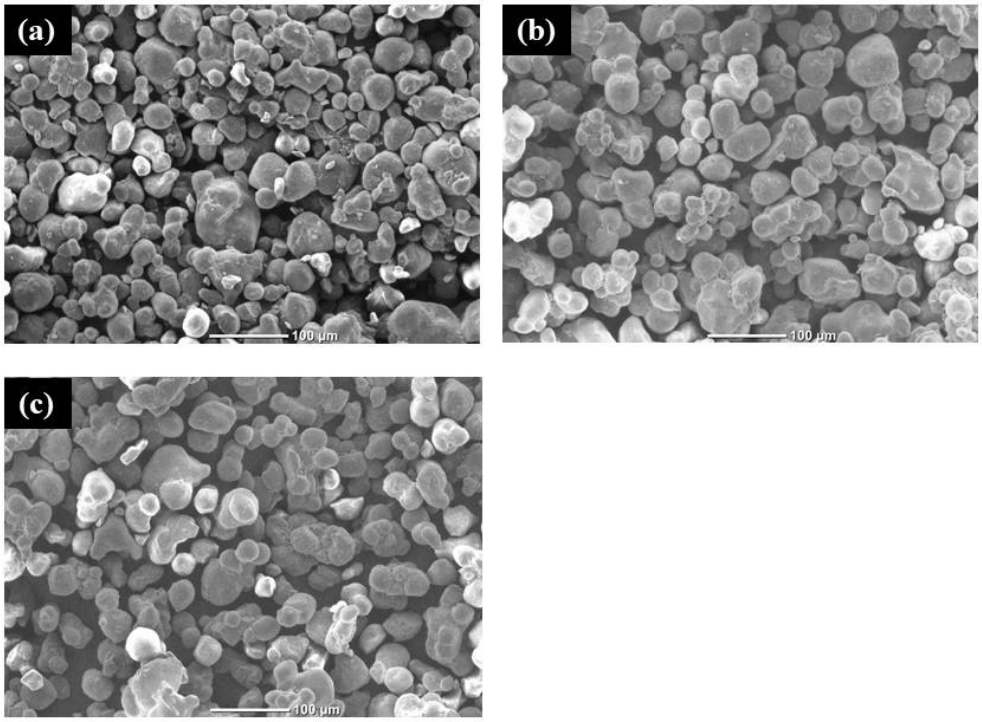

Figure III-6-2 Scanning electron micrographs of (a)MgO_$_{Amine}$ filler, (b)MgO_$_{DGETAM}$ filler, and (c)MgO_$_{DGEBA}$ filler.

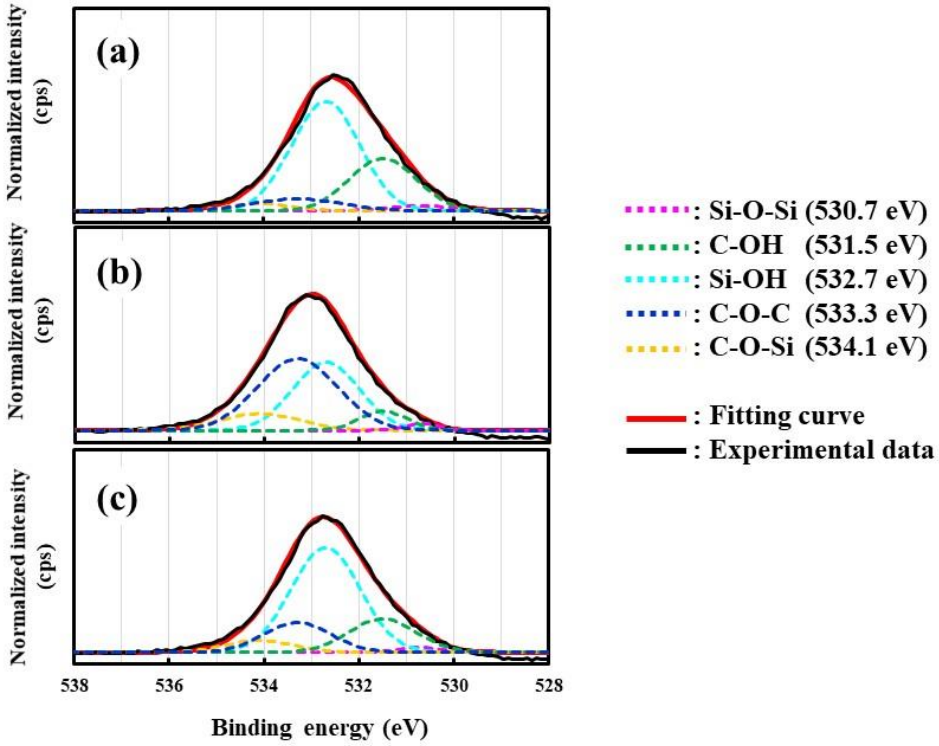

Figure III-6-3 O1s spectra and fitting curves of (a)MgO_Amine filler, (b)MgO_DGETAM filler, and (c)MgO_DGEBA filler.

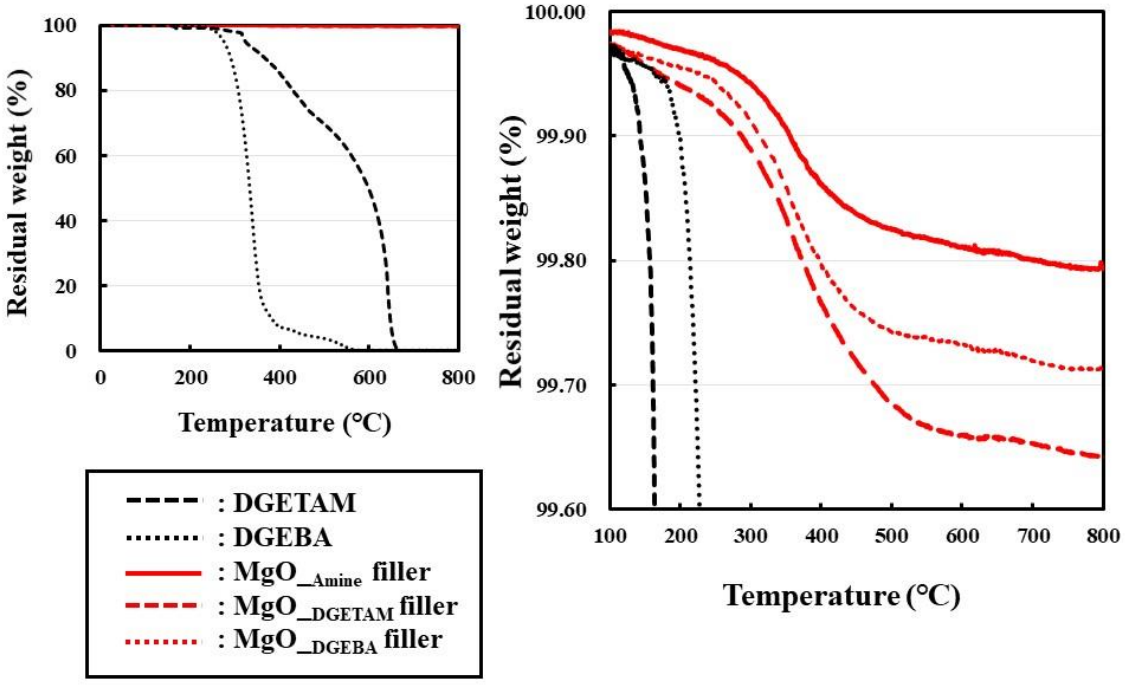

Figure III-6-4 Residual weight from TGA charts (under air atmosphere) of epoxy monomers and MgO fillers.

III-6-3-2. Liquid crystalline phase structure of DGETAM/MgO composites

The liquid crystalline (LC) phase structure of the DGETAM/MgO composite at 12-13 vol% was observed (Figure III-6-5). Birefringence patterns were clearly found throughout the observation regions of all the composites, indicating the formation of an LC phase structure in the matrix resin. Similar to the 12-13 vol % loading systems, it was confirmed that the LC phase structure was formed even in the high-loading systems up to 44-45 vol%. It was also found that the MgO fillers (indicated by black dotted circles) were uniformly dispersed in the matrix resin.

Figure III-6-6 shows the XRD patterns of the DGETAM/MgO composites with different filler content ((a)–(c) 12-13 vol% and (d)–(f) 44-45 vol%). All composites exhibited a sharp peak at $2\theta = 3°$, corresponding to the smectic phase structure (d = 2.9 nm) of the mesogenic moieties [29]. It was also confirmed that the enlarged view of the XRD patterns displayed a halo around $2\theta = 19°$, corresponding to a plane space (d = 0.47 nm) of the network polymer chains. Additionally, there was no clear difference in the peak intensity ($2\theta = 3°$) between the (a), (d) MgO_{Amine} system and (b), (e) MgO_{DGEBA} system. In contrast, the peak intensity ($2\theta = 3°$) of the (c), (f) MgO_{DGETAM} system was substantially higher than that in the other composites. This data suggests that the MgO_{DGETAM} system is likely to form a highly ordered network structure that includes a smectic phase, as illustrated in Scheme III-6-1. As mentioned in the Introduction, the ordered structure of the LC epoxy resin is affected by the interaction at the filler-matrix interface [20]. In our previous study, we investigated the LC phase structure of DGETAM composites loaded with pristine boron nitride (BN) fillers [15]. According to the XRD analysis, the peak intensity of the smectic phase structure gradually decreased with increasing filler content and the peak completely disappeared at 30 vol%. This data indicates that self-assembly of the network polymer chains was inhibited by the pristine BN filler. Therefore, we considered that this significant phase change in the MgO_{DGETAM} system can be attributed to the strong interaction at the filler-matrix interface, such as the π-π interaction of the mesogenic moieties between the matrix resin and the adsorbed epoxies on the MgO_{DGETAM} filler surface.

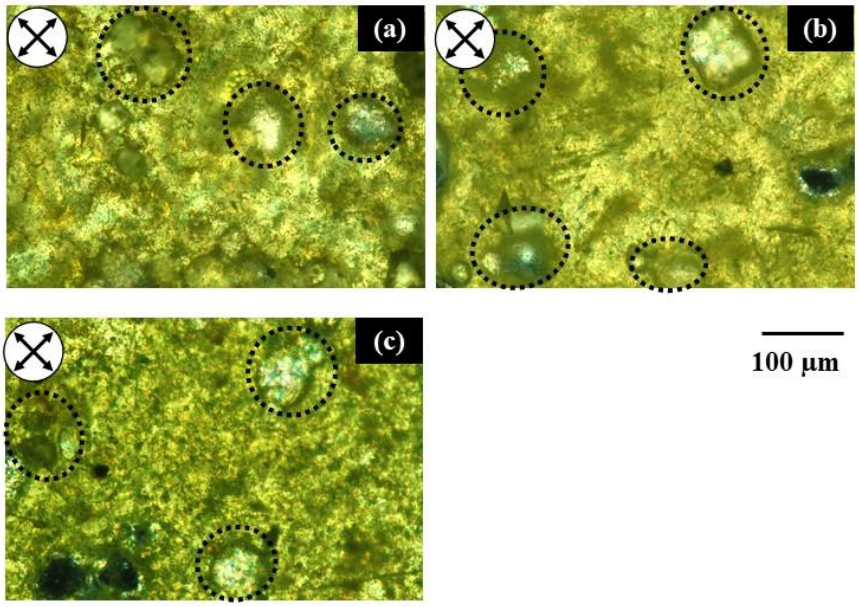

Fig. III-6-5 Polarized optical micrographs under crossed Nicols of DGETAM/MgO(12-13 vol%) composites; (a)MgO_Amine system, (b)MgO_DGETAM system, and (c)MgO_DGEBA system.

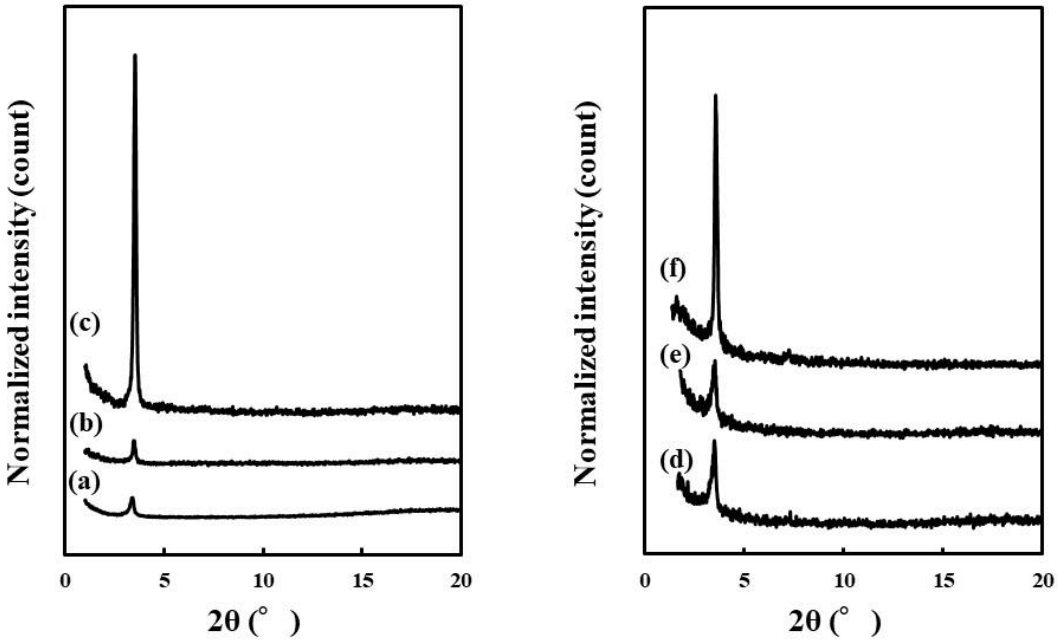

Figure III-6-6 XRD patterns of DGETAM/MgO composites with different filler content ((a-c)12-13 vol%, (d-f)44-45 vol%); (a, d)MgO_Amine system, (b, e)MgO_DGEBA system, and (c, f) MgO_DGETAM system.

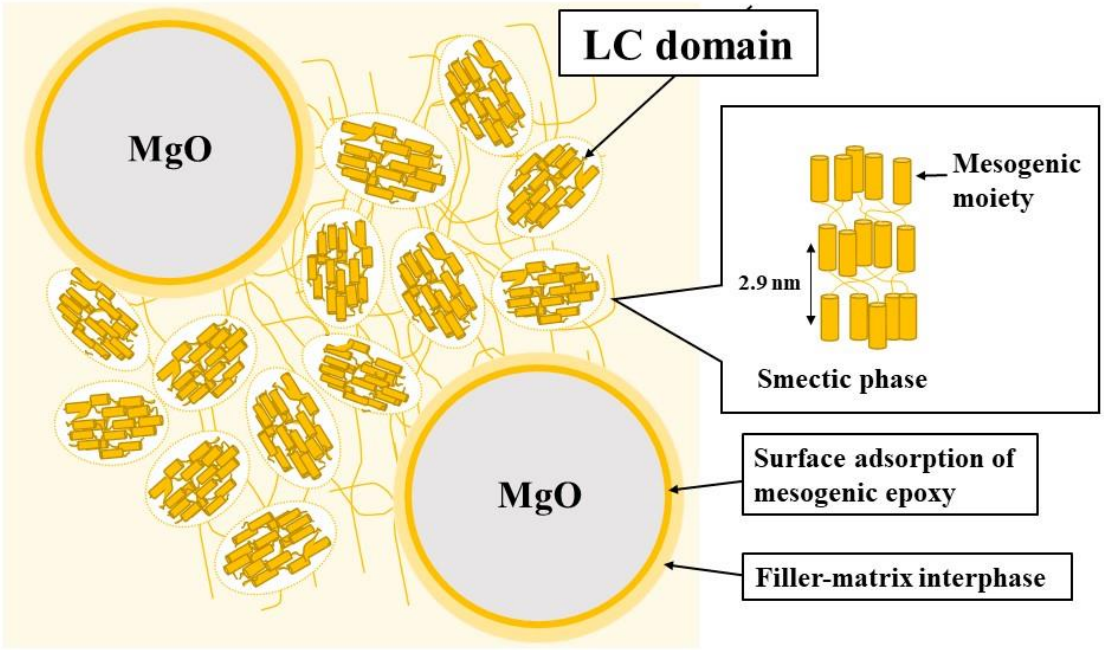

Scheme III-6-1 Schematic model of proposed network structure in DGETAM/MgO$_{_DGETAM}$ composite.

III-6-3-3. Free volume of the network polymer structure of DGETAM/MgO composites

The free volume of the DGETAM/MgO composite at 44-45 vol% was investigated by PALS to study the MgO$_{_DGETAM}$ filler loading effect on the network structure of the composite. It is well known that PALS is a useful tool for probing the nanoscale voids of various materials. In the case of polymer materials, the *o*-positronium (*o*-Ps) annihilation lifetime is generally proportional to the free volume of the polymer chains. Moreover, in the case of the DGETAM/MgO composite, the *o*-Ps annihilation lifetime can be determined by the free volume of the matrix resin since the MgO filler cannot form any positronia. Table III-6-1 summarizes the *o*-Ps annihilation lifetime (τ_3), the mean free volume radius (R_f), and the mean free volume (V_f) of the unloaded and 44-45 vol% loading systems. In a comparison with the unloaded system, the *o*-Ps annihilation lifetime (τ_3) was considerably increased by the MgO filler loading. Similar phenomena have been reported by other researchers [30, 31]. Zhou *et al.* revealed that the polymer chain motion of the matrix resin can be limited by the amine surface treatment of the

multiwalled carbon nanotubes (MWNT), leading to a reduction in the whole free volume of the epoxy composite [31]. Owing to the presence of the reactive functional groups on the MgO filler surface, such as amino groups and epoxy groups, the covalent bonding would be partially formed between the surface-treated layer and the matrix resin. Thus, this free volume change of the DGETAM/MgO composite is assumed to be due to the formation of a filler-matrix interphase (Scheme III-6-1). Namely, it is believed that the polymer chains were strongly stacked on the filler surface, limiting the mobility of the network polymer chains.

Moreover, τ_3 of the MgO_$_{DGETAM}$ system (1.917 ns) was obviously shorter than that of the MgO_$_{Amine}$ system (2.045 ns). According to the Tao–Eldrup model (Eq. III-6-1), the mean free volume radius (R_f) of the MgO_$_{DGETAM}$ system (0.2778 nm) was smaller than that of the MgO_$_{Amine}$ system (0.2896 nm). This data indicates that the MgO_$_{DGETAM}$ system has a smaller mean free volume (V_f) (0.0898 nm^3) compared to that of the MgO_$_{Amine}$ system (0.1017 nm^3). Additionally, the chemical conversions of the MgO_$_{Amine}$ system and MgO_$_{DGETAM}$ system were 97% and 93%, respectively. This result suggests that these composites were fully cured and had the similar crosslinking densities. More importantly, the XRD analysis (Figure III-6-6) implied that the highly ordered structural formation in the matrix resin of the MgO_$_{DGETAM}$ system could be induced by the strong π-π interaction of the mesogenic moieties between the matrix resin and the adsorbed epoxies. From this result, we assumed that the LC phase structure of the network polymer chains may influence the nano-scaled free volume structures of the matrix resin. Accordingly, it is speculated the ordered structure of the matrix resin can possibly affect the entire free volume of the composite. In other words, we considered that this decrease in the free volume of the MgO_$_{DGETAM}$ system could be caused by the formation of the highly ordered network structure in the matrix resin.

Table III-6-1 *o*-Positronium annihilation lifetime (τ_3), mean free volume radius (R_f), and mean free volume (V_f) of unloaded DGETAM system and DGETAM/MgO(44-45 vol%) composites; MgO_Amine system and MgO_DGETAM system.

Curing system	*o*-Positronium annihilation lifetime (τ_3, ns)	Mean free volume radius (R_f, nm)	Mean free volume (V_f, nm^3)
Unloaded system	1.695	0.2557	0.0700
MgO_Amine system (45 vol%)	2.045	0.2896	0.1017
MgO_DGETAM system (44 vol%)	1.917	0.2778	0.0898

III-6-4. Dynamic mechanical property and filler dispersibility of DGETAM/MgO composites

The dynamic mechanical properties of the DGETAM/MgO composites at 44-45 vol% also were studied by DMA (Figure III-6-7). It is interesting to note that the MgO_DGETAM system exhibited a higher storage modulus compared to that of the other composites in a wide temperature range from −150°C to 250°C. The storage modulus of the MgO_DGETAM system (16.7 GPa) at 25°C was approximately 1.4 times higher than that of the MgO_Amine system (11.6 GPa) and MgO_DGEBA system (11.8 GPa) even with almost the same content. Besides, the storage modulus of the MgO_DGETAM system decreased slightly in the temperature range above 230°C, which is attributed to the thermal decomposition of the network polymer chains. Although all the composites showed almost the same glass transition temperature (T_g) of around 180°C, the height of the tanδ peak decreased drastically in the MgO_DGETAM system. This data suggests the effective suppression of micro-Brownian motion of the network polymer chains. In addition, the SEM images of the fracture surface after the argon etching in the DGETAM/MgO composites at 44-45 vol% are shown in Figure III-6-8. Although the small amount of the MgO fillers were partially aggregated, there was no obvious filler aggregation in all the high-loading composites, despite the different surface treatments since the MgO_Amine filler has an intrinsic good compatibility with the matrix resin that can maintain a sufficient degree of the filler dispersion in the composite. More importantly,

the void region was not clearly observed at the filler-matrix interface. This is derived from both the covalent bonding and the strong molecular interaction between the surface-treated layer and the matrix resin. Considering the fact that the dynamic mechanical properties were not affected by the loading of the MgO_$_{DGEBA}$ filler, it is thought that the mobility of the network polymer chains in the MgO_$_{DGETAM}$ system could be strongly restricted by the π-π interaction of the mesogenic moieties between the matrix resin and the adsorbed epoxies.

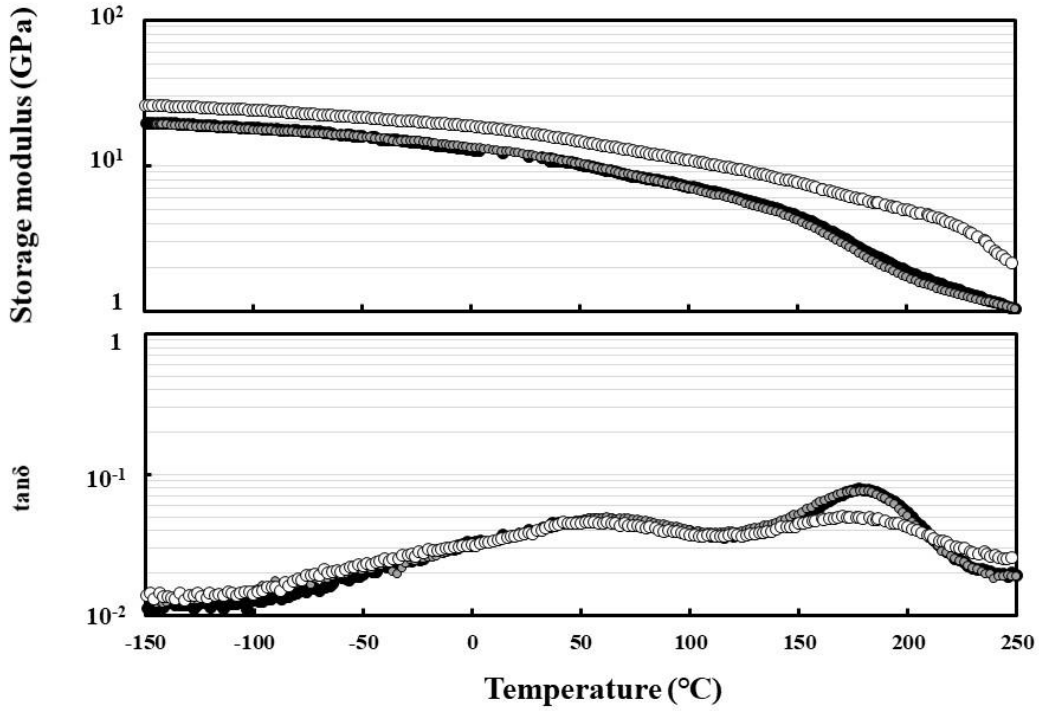

Figure III-6-7 Dynamic mechanical properties of DGETAM/MgO(44-45 vol%) composites; (●)MgO_$_{Amine}$ system, (◯)MgO_$_{DGETAM}$ system, and (◍)MgO_$_{DGEBA}$ system.

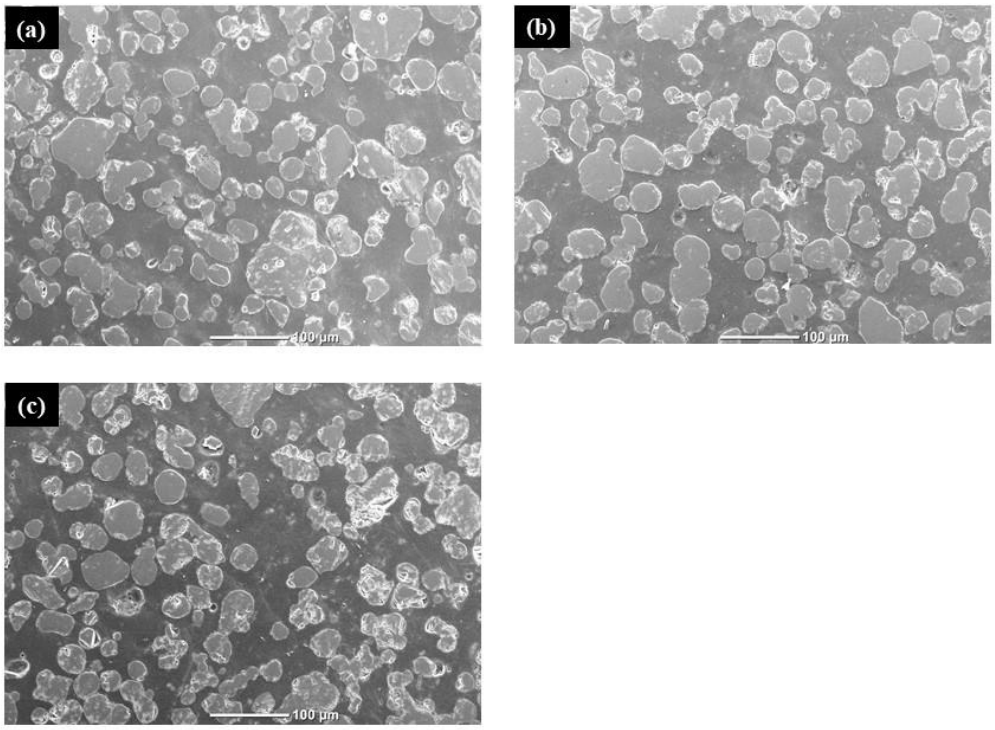

Figure III-6-8 Scanning electron micrographs of DGETAM/MgO(44-45 vol%) composites; (a)MgO$_{_Amine}$ system, (b)MgO$_{_DGETAM}$ system, and (c)MgO$_{_DGEBA}$ system.

III-6-3-5. Thermal conductivity of DGETAM/MgO composites

The thermal conductivity of the DGETAM composites as a function of the filler content is presented in Figure III-6-9. The thermal conductivity, thermal diffusivity, specific heat, and density of these composites were summarized in Table III-6-2. The thermal conductivity of all the composites gradually increased with the increase in filler content and always exceeded the value predicted using Bruggeman's theoretical mode (drawn by the broken line). This result indicates the effective enhancement of the thermal conductivity of the LC epoxy composite by the MgO filler loading. Above all, the MgO$_{_DGETAM}$ system shows the maximum value for the various filler content (13–44 vol%). The thermal conductivity of the MgO$_{_DGETAM}$ system (3.16 W/(m·K)) was nearly twice as high as that of the MgO$_{_Amine}$ system (1.93 W/(m·K)) at almost the same filler content of 44-45 vol%. Although the MgO$_{_Amine}$ system and MgO$_{_DGEBA}$ system exhibited almost the same values at a relatively low filler content below 25 vol%, the thermal conductivity of the MgO$_{_DGEBA}$ system (1.44 W/(m·K)) was slightly lower than the MgO$_{_Amine}$ system (1.93 W/(m·K)) at the high filler content (44-45 vol%.). These

results indicate that the surface-treated layer of the MgO filler strongly influenced the thermal conductivity of the high-loading composites. Considering the fact that there is no clear difference in the micro-scaled dispersion of the filler particles in all the high-loading composites (Figure III-6-8), there are two possible reasons for the determination of the thermal conductivity of the mesogenic epoxy composite: (1) the compatibility of the filler surface with the matrix resin, and (2) the formation of an ordered structure in the network polymer chains. As mentioned above, the SEM images of the composites at 44-45 vol% (Figure III-6-8) also confirmed that all composites had good bonding layers at filler-matrix interface, which is caused by the covalent bonding and strong molecular interaction.

Here, the non-mesogenic epoxy matrix (DGEBA) composites at 43 vol% was prepared and compared with the mesogenic DGETAM composite, as listed in Table 3. In the unloaded systems, the thermal conductivity of the non-mesogenic DGEBA system (0.21 W/(m·K)) was considerably lower than that of the mesogenic DGETAM system (0.27 W/(m·K)). This is because phonon scattering tends to be generated in the DGEBA system having an amorphous structure. Due to the lower thermal conductivity of the matrix resin, the high-loading DGEBA composites at 43 vol% showed relatively lower values than that of the DGETAM composites, regardless of the different surface treatments of the MgO fillers. In addition, the thermal conductivity of the DGEBA/MgO$_{_Amine}$ system (1.38 W/(m·K)) was somewhat higher than that of the DGEBA/MgO$_{_DGETAM}$ system (1.24 W/(m·K)) and DGEBA/MgO$_{_DGEBA}$ system (1.27 W/(m·K)). From these results, it is speculated that the phonon conductivity is probably inhibited by the surface adsorption of the epoxies, resulting in an increase in the thermal resistance at the filler-matrix interface. It is noteworthy that the thermal conductivity of the DGETAM composite was significantly improved by the MgO$_{_DGETAM}$ filler even having a mesogenic epoxy adsorbed layer. Consequently, it is considered that the thermal conductivity enhancement by the highly ordered structure of the network polymer chains (Figure III-6-6) can exceed the increment in thermal resistance caused by the filler surface treatment. Namely, this enhanced thermal conductivity of the DGETAM/MgO$_{_DGETAM}$ composite can be attributed to the highly ordered network structure of the mesogenic epoxy resin.

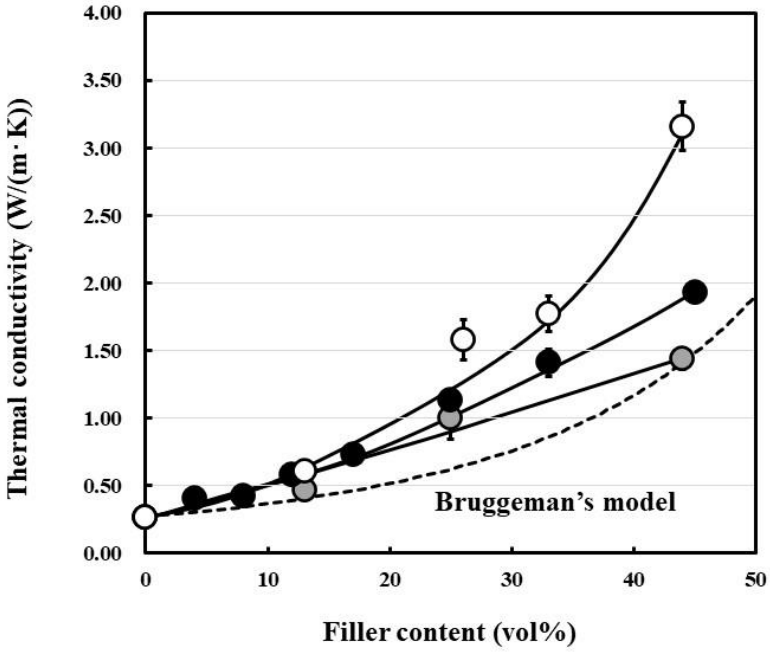

Figure III-6-9 Thermal conductivity of the of DGETAM/MgO composites; (●)MgO_Amine system, (○)MgO_DGETAM system, and (◍)MgO_DGEBA system.

Table III-6-2 Thermal conductivity, thermal diffusivity, specific heat and density of the MgO composites with different epoxy matrix.

Matrix resin	Filler	MgO (wt%)	MgO (vol%)	Density (g/cm^3)	Specific heat (J/(g·K))	Thermal diffusivity ($\times 10^{-3} cm^2/s$)	Thermal conductivity (W/(m·K))
DGETAM	Unloaded	0	0	1.21 ± 0.006	1.26 ± 0.01	0.18 ± 0.02	0.27 ± 0.02
	$MgO_{\_Amine}$	10	4	1.29 ± 0.004	1.25 ± 0.04	0.26 ± 0.03	0.41 ± 0.04
		20	8	1.37 ± 0.003	1.24 ± 0.01	0.25 ± 0.01	0.42 ± 0.01
		30	12	1.45 ± 0.006	1.18 ± 0.01	0.34 ± 0.03	0.58 ± 0.04
		40	17	1.57 ± 0.006	1.09 ± 0.05	0.43 ± 0.02	0.73 ± 0.04
		50	25	1.81 ± 0.002	1.13 ± 0.04	0.55 ± 0.04	1.13 ± 0.08
		60	33	1.96 ± 0.005	1.03 ± 0.01	0.70 ± 0.05	1.41 ± 0.10
		70	45	2.33 ± 0.006	0.99 ± 0.01	0.83 ± 0.02	1.93 ± 0.05
	$MgO_{\_DGETAM}$	30	13	1.53± 0.002	1.02 ± 0.035	0.39± 0.01	0.61 ± 0.02
		50	26	1.89± 0.001	1.07 ± 0.004	0.78± 0.08	1.58 ± 0.15
		60	33	2.00± 0.002	1.00 ± 0.004	0.88 ± 0.08	1.77 ± 0.13
		70	44	2.28± 0.007	1.02 ± 0.011	1.36± 0.08	3.16± 0.18
	$MgO_{\_DGEBA}$	30	13	1.53± 0.003	1.15 ± 0.06	0.27± 0.02	0.47 ± 0.04
		50	25	1.82± 0.002	1.05 ± 0.01	0.53 ± 0.09	1.00 ± 0.16
		70	44	2.25 ± 0.000	0.98 ± 0.01	0.65 ± 0.04	1.44 ± 0.08
DGEBA	Unloaded	0	0	1.20± 0.002	1.26 ± 0.01	0.14 ± 0.002	0.21 ± 0.003
	$MgO_{\_Amine}$	70	43	2.20± 0.008	1.01 ± 0.01	0.62 ± 0.02	1.38 ± 0.05
	$MgO_{\_DGETAM}$	70	43	2.21± 0.004	0.97 ± 0.001	0.58 ± 0.03	1.24 ± 0.06
	$MgO_{\_DGEBA}$	70	43	2.22± 0.002	0.97 ± 0.04	0.59 ± 0.04	1.27 ± 0.09

III-6-4. CONCLUSIONS

In this chapter, mesogenic epoxy (DGETAM) was successfully adsorbed onto the surface of the MgO treated with an amino-silane coupling agent ($MgO_{\_Amine}$). The epoxy-adsorbed MgO filler ($MgO_{\_DGETAM}$) filler was characterized by XPS and TGA and incorporated into the DGETAM to develop a high thermal conductivity composite. The effect of the $MgO_{\_DGETAM}$ filler on the network structure and the thermal conductivity of the liquid crystalline DGETAM composite was discussed. The formation of a highly ordered network structure including a smectic phase observed in the $MgO_{\_DGETAM}$ system, was derived from the strong π-π interaction of the mesogenic moieties between the matrix resin and the adsorbed epoxies. Additionally, the dynamic mechanical properties and thermal conductivity of the composite were dramatically improved by the $MgO_{\_DGETAM}$ filler. The thermal conductivity of the $MgO_{\_DGETAM}$ system (3.16 W/(m·K)) was almost twice as high as that of the $MgO_{\_Amine}$ system (1.93 W/(m·K)) at almost the same filler content of 44-45 vol%. This significant improvement in the thermal conductivity is attributed to the highly ordered structure of the network polymer chains.

III-6-5. REFERENCES

1. A. Shiota, C. K. Ober, *Journal of Polymer Science: Part A: Polymer Chemistry*, **1996**, 34, 1291-1303
2. Q. Lin, A. F. Yee, H. J. Sue, J. D. Earls, R. E. Hefner, Jr., *Journal of Polymer Science: Part B : Polymer Physics,* **1997**, 35, 2363-2378
3. M. Ochi, Y. Shimizu, N. Nakanishi, Y. Murata, *Journal of Polymer Science: Part B: Polymer Physics*, **1997**, 35, 397-405
4. C. Ortiz, R. Kim, E. Rodighiero, C. K. Ober, E. J. Kramer, *Macromolecules*, **1998**, 31, 4074-4088
5. W. F. A. Su, K. C. Chen, S. Y. Tseng, *Journal of Applied Polymer Science*, **2000**, 78, 446-451
6. D. Ribera, A. Mantecon, A. Serra, *Journal of Polymer Science: Part A: Polymer Chemistry*, **2002**, 40, 3916-3926
7. M. Ochi, H. Takashima, *Polymer*, **2001**, 42, 2379-2385
8. M. Akatsuka, Y. Takezawa, *Journal of Applied Polymer Science*, **2003**, 89, 2464-2467
9. S. Song, H. Katagi, Y. Takezawa, *Polymer*, **2012**, 53, 4489-4492
10. H. Guo, J. Zheng, J. Gan, L. Liang, K. Wu, M. Lu, *J. Mater. Sci.: Mater. Electron*, **2016**, 27, 2754–2759
11. S. Kawamoto, H. Fujiwara, S. Nishimura, *International Journal of Hydrogen Energy*, **2016**, 41, 7500-7510
12. Y. Kim, H. Yeo, N. You, S. G. Jang, S. Ahn, K. Jeong, S. H. Lee, M. Goh, *Polymer Chemistry*, **2017**, 8, 2806-2814
13. I. Jeong, C. B. Kim, D. Kang, K. Jeong, S. G. Jang, N. You, S. Ahn, D. Lee, M. Goh, *Journal of Polymer Science: Part A: Polymer Chemistry*, **2019**, 57, 708-715
14. M. Harada, M. Ochi, M. Tobita, T. Kimura, T. Ishigaki, N. Shimoyama, H. Aoki, *Journal of Polymer Science: Part B: Polymer Physics*, **2003**, 41, 1739-1743
15. M. Harada, N. Hamaura, M. Ochi, Y. Agari, *Composites: Part B*, **2013**, 55, 306-313
16. S. Ota, K. Yamaguchi, M. Harada, *Journal of network polymer, Japan*, **2019**, 40, 278-286
17. T. Giang, J. Kim, *Journal of Industrial and Engineering Chemistry*, **2015**, 30, 77-84

18. J. J. Mallon, P. M. Adams, *Molecular Crystals and Liquid Crystals Science and Technology*, **1992**, 213, 173-186
19. A. Kubono, H. Onoda, K. Inou, K. Tanaka, R. Akiyama, *Molecular Crystals and Liquid Crystals*, **2002**, 373, 127-141
20. S. Tanaka, F. Hojo, Y. Takezawa, K. Kanie, A. Muramatsu, *ACS Omega*, **2018**, 3, 3562−3570
21. J. Jang, J. Bae, S. Yoon, *Journal of Materials Chemistry*, **2003**, 13, 676-681
22. J. Hornak, P. Trnka, P. Kadlec, O. Michal, V. Mentlík, P. Šutta, G. M.Csányi, Z. Á. Tamus, *Nanomaterials*, **2018**, 8, 381, DOI:10.3390/nano8060381
23. B.E. O'Rourke, N. Oshima, A. Kinomura, R. Suzuki, *JJAP Conference Proceedings*, 2, **2014**, 011304
24. P. Kirkegaard, M. Eldrup, O. E. Mogensen, N. J, Pedersen, *Computer Physics Communications*, **1981**, 23, 307-335
25. M. Eldrup, D. Lightbody, J. N. Sherwood, *Chemical Physics*, **1981**, 63, 51-58
26. S. J. Tao, *Chemical Physics*, **1972**, 56, 5499-5510
27. H. Li, R. Wang, W. Liu, H. Hu, *Applied Surface Science*, **2008**, 255, 1894-1900
28. J.A. Wang, O. Novaro, X. Bokhimi, T. López, R. Gómez, J. Navarrete, M.E. Llanos, E. López-Salinas, *Materials Letters*, **1998**, 35, 317-323
29. M. Harada, M. Ochi, M. Tobita, T. Kimura, T. Ishigaki, N. Shimoyama, H. Aoki, *Journal of Polymer Science: Part B: Polymer Physics*, **2004**, 42, 758-765
30. P. Winberg, K. DeSitter, C. Dotremont, S. Mullens, I. F. J. Vankelecom, F. H. J. Maurer, *Macromolecules*, **2005**, 36, 3776-3782
31. W. Zhou, J. Wang, Z. Gong, J. Gong, N. Qi, B. Wang, *Applied Physics Letters*, **2009**, 84, 021904

CONCLUDING REMARKS

The series of studies aimed to improve the thermal property of epoxy thermosets. To achieve this goal, the studies focused on the characteristics of Schiff base-derived self-polymerization and liquid crystalline (LC) phase formation of mesogenic epoxy resins. In addition, our primary objectives are to demonstrate the structure-property relationship of epoxy thermosets by structural analysis from microscopic to nanoscopic.

Each chapter is summarized below;

In Part I (Chapter 1, 2, 3), the Schiff base-derived self-polymerization and the thermomechanical properties of mesogenic epoxy/imidazole cured systems were investigated.

Chapter 1.

Novel glass-transition-temperature-less (T_g-less) epoxy thermosets were developed by a non-catalytic method based on a Schiff base (CH=N)-derived self-polymerization of mesogenic epoxy. It was found that the epoxy–CH=N addition reaction formed a new tertiary amine, introducing a crosslinking point into the rigid mesogenic moiety. DMA of the cured system showed a slight α-relaxation in tanδ, and a high storage modulus was maintained at >250℃. Also, no drastic increase in the CTE related to the glass-transition behavior was observed in this cured system. The DMA and TMA results revealed that such a distinctive crosslinking structure could effectively suppress the thermal motion of networked chains, resulting in T_g-less behavior.

Chapter 2.

An imidazole catalyst was used to enhance the self-polymerization reactivity of Schiff base type mesogenic epoxy resin. The results suggested that the crosslinking points in the rigid mesogenic moiety could result in T_g-less behavior in the lower imidazole system, similar to the non-imidazole system. By contrast, the higher imidazole content system proceeded with epoxy–imidazole adduct formation rather than CH=N-derived self-polymerization. Consequently, the number of crosslinking points in the rigid mesogenic moiety significantly decreased, deteriorating the thermomechanical properties of final products. Moreover, it is found that the addition of excess imidazole forms the

lower-density domain.

Chapter 3.

Schiff base type mesogenic epoxy resins were cured by the same content of imidazole catalyst at different temperatures. At lower curing temperatures, epoxy mainly proceeds with the imidazole-derived polymerization, forming a highly ordered nematic phase structure via self-assembly of mesogenic moieties. On the other hand, at higher curing temperatures, epoxy could proceed with a CH=N-derived self-polymerization, in addition to the imidazole-derived ones. As a result, this cured system exhibited higher T_g than the lower temperature curing system although it showed relatively lower packing density. This result indicated that the crosslinking points into the rigid mesogenic moiety effectively suppressed network polymer chains' thermal motion.

In Part II (Chapter 4), the LC phase structure and thermal conductivity of mesogenic epoxy resins cured by binary mixed curing agents were investigated.

Chapter 4.

Schiff base type mesogenic epoxy resin (DGETAM) was cured by the binary mixed curing agent with different chemical structures, *m*-phenylenediamine (*m*-PDA) and 4, 4'-bis (4-aminobenzoyloxy) dodecane (12BAB). The results revealed that the DGETAM/*m*-PDA/12BAB_20 mol% system forms larger size of LC domain structure with a highly ordered smectic phase. According to the laser flash method, the thermal conductivity of DGETAM/*m*-PDA/12BAB_20 mol% system(0.31 W/(m･K)) is slightly higher compared to those of the other DGETAM and bisphenol A type epoxy (DGEBA) systems (0.27～0.30 (W/(m･K))). However, the thermal conductive map drawn by the periodic heating radiation-temperature measuring method indicated a clear thermal conductivity distribution in the DGETAM/*m*-PDA/12BAB_20 mol% system. These results suggest that the effective phonon conductivity may be suppressed by the locally low thermal conductive regions derived from the amorphous polymer chains, although this cured system formed a highly ordered network structure.

In Part III (Chapter 5, 6), the application as matrix resin and surface-treatment effect of mesogenic epoxy/magnesium oxide (MgO) composites were reported.

Chapter 5.

An MgO filler was incorporated into Schiff base type mesogenic epoxy resin (DGETAM). The thermal conductivity of the DGETAM/MgO composite was 1.41 W/(m·K) at 33 vol% content, which was remarkably higher than the value predicted using Bruggeman's model. An XRD analysis indicated the local formation of a highly ordered smectic phase structure, even in the high-loading composite. This result indicated the promotion of the self-assembly of the mesogenic network polymer chains by the MgO filler loading. We considered that this highly ordered structural formation can lead to an increase in the matrix resin's thermal conductivity, which can result in the effective enhancement of the thermal conductivity in the LC epoxy/MgO composite.

Chapter 6.

Mesogenic epoxies were adsorbed onto the surface of an MgO filler treated with an amino-silane coupling agent and the epoxy-adsorbed MgO filler was dispersed into the LC epoxy matrix resin to develop a high thermal conductivity composite. The thermal conductivity of the obtained composite (3.16 W/(m·K)) was remarkably higher than that of the nonadsorbed MgO system (1.93 W/(m·K)) at almost the same content of 44-45 vol%. This significant improvement of the thermal conductivity can be attributed to the highly ordered structural formation that was induced by the π-π interaction effect of the mesogenic moieties between the adsorbed epoxies and the matrix resin.

In conclusion, the most important findings were shortly summarized. These provided a novel approach to improve the thermal properties of the epoxy thermosets.

1. Introducing a crosslinking point into the rigid mesogenic moiety could effectively suppress the thermal motion of networked chains, resulting in T_g-less behavior. The T_g and packing density of the Schiff base type mesogenic epoxy/imidazole systems were changed by the control of curing temperatures.

2. The LC phase structures of mesogenic epoxy thermosets were controlled by the composition ratio of the binary mixed curing agents.
3. The MgO filler loading can cause the promotion of the self-assembly of the mesogenic network polymer chains, leading to the improvement of the matrix's thermal conductivity. Also, the highly ordered structural formation that was induced by the π-π interaction effect of the mesogenic moieties between the adsorbed epoxies and the matrix resin.

LIST OF PUBLICATIONS

[Dissertations]

Chapter 4:

“Phase Structure and Thermal Conductivity of Liquid Crystalline Epoxy Resins Cured with the Binary Mixed Curing Agents”

Journal of network polymer, Japan, **2019**, Vol. 40, pp. 278-286

Chapter 5:

“Thermal Conductivity Enhancement of Liquid Crystalline Epoxy/MgO Composites by Formation of Highly Ordered Network Structure”

Journal of Applied Polymer Science, **2020**, Vol.138, No.19, 50367

Chapter 6:

“Filler Surface Adsorption of Mesogenic Epoxy for LC Epoxy/MgO Composites with High Thermal Conductivity”

Composites Part C: Open Access, **2020**, Vol. 4, 100087

[Presentation in Symposium]

1. "The Effect of Curing Agent on Arrangement of Mesogenic Units and Thermal Conductivity of Liquid Epoxy Resin"
   66th Symposium on Macromolecules, *Preprints*, 1X11, p.41 (2017)

2. "Phase Structure and Thermal Conductivity of Liquid Crystalline Epoxy / BN Composites Cured with the Mixture of Curing Agents"
   67th SPSJ Annual Meeting, Preprints, 1K14, p.19 (2018)

3. "Thermal Conductivity of Liquid Crystalline Epoxy Composites Cured with the Optimal Mixture of Curing Agents"
   68th The Network Polymer Symposium Japan, Proceedings, Ippan 29, pp.65-66 (2018)

4. "LC Phase Structure and Thermal Conductivity of Liquid Crystalline Epoxy Resin Cured with the Binary Mixed Curing Agent"
   68th SPSJ Annual Meeting, Preprints, 2K27, p.20 (2019)

5. "Phase Structure and Thermal Conductivity of Liquid Crystalline Epoxy/ MgO Composites"
   68th Symposium on Macromolecules, *Preprints*, 3F11, p.21 (2019)

6. "The Effect of MgO Filler Surface-treatments on the Network Structure and Thermal Conductivity of Liquid Crystalline Epoxy Resin Composite"
   69th The Network Polymer Symposium Japan, Proceedings, Ippan 09, pp.17-18 (2019)

7. "Thermal Conductivity and Phase Structure of Liquid Crystalline Epoxy Resin/ MgO Filler Composites"

International Symposium on Advanced Power Packaging (2019)

8. "Development of T_g-less Materials via Self-polymerization of Mesogenic Epoxy Resins Containing Schiff Base Moieties"
   70th SPSJ Annual Meeting, Preprints, 1C27 (2021)

9. "Study of Thermal Latent Catalytic Effect on Free Volume Characteristics and Thermal Property of Schiff Base Containing Mesogenic Epoxy Resin for the Development of Novel T_g-less Material"
   3rd Virtual Edition of Polymers, Plastics and Composites (2021)

10. "Development of High Heat Resistant Epoxy Resin by Introducing Crosslinking Points into Rigid Mesogenic Moiety" *70th Symposium on Macromolecules*, *Preprints*, 2O16 (2021)

11. "Improvement of Epoxy Resins by Introducing Crosslinking Points into Rigid Mesogenic Moiety"
    70th The Network Polymer Symposium Japan, Proceedings, Ippan 29, pp.61-62 (2021)

ACKNOWLEDGEMENTS

The author gratefully acknowledges Professor Miyuki Harada, Faculty of Chemistry, Materials and Bioengineering, Kansai University, for supporting and discussing my research for a long period.

The author further acknowledges Professor Fumio Sanda and Professor Hiroto Kudo, Faculty of Chemistry, Materials and Bioengineering, Kansai University, for their good and helpful suggestions.

This research has been carried out in Applied Polymer Material Laboratory in Faculty of Chemistry, Materials and Bioengineering, Kansai University. The author wishes to express my sincere thanks to my co-workers, Mr. Ryo Nagatsuka, Mr. Kosuke Yamaguchi, Mr. Masahiro Murakami, Ms. Yuuka Fujiwara, Mr. Takuya Matsumoto, Mr. Masafumi Horimoto, Mr. Satoshi Yanaura, Mr. Yuusuke Akazaki, Ms. Shiori Asada, Mr. Tomoki Tsukuda, Mr. Takumi Hashizume, Mr. Ryusei Nakane, Mr. Maki Murai, and all other members (2016-2021) for supporting my research. I also thank Mr. Tatsuki Nagata, Mr. Taichi Sotani, and Mr. Masahide Goto for their helpful assistance and friendship.

The author wishes to express my deep appreciation to Professor Koji Michishio, National Institute of Advanced Industrial Science and Technology (AIST), for supporting the PALS experiment and analysis.

The author also acknowledges the Sasakawa Scientific Research Grant from The Japan Science Society for financial support of the PALS experiments.

Finally, the author would like to express my deepest thanks to my family for the encouragement and mental support.

March 2022

Saki OTA